A REDUCTION IN CARDIAC FUNCTION PRECEDES STRUCTURAL ADAPTATIONS IN EXPERIMENTAL SPINAL CORD INJURY

by

Mary Pauline Mona Fossey

B.Sc., The University of British Columbia, 2017

A THESIS SUBMITTED IN PARTIAL FULFILLMENT OF

THE REQUIREMENTS FOR THE DEGREE OF

MASTER OF SCIENCE

in

THE FACULTY OF GRADUATE AND POSTDOCTORAL STUDIES

(Kinesiology)

THE UNIVERSITY OF BRITISH COLUMBIA

(Vancouver)

December, 2019

The following individuals certify that they have read, and recommend to the Faculty of Graduate and Postdoctoral Studies for acceptance, a thesis entitled:

A reduction in cardiac function precedes structural adaptations in experimental spinal cord injury

submitted by Mary Pauline Mona Fossey in partial fulfillment of the requirements for
the degree of Master of Science
in Kinesiology

Examining Committee:

Christopher R. West, Department of Cellular and Physiology Sciences, Faculty of Medicine, UBCO
Supervisor

Matt S. Ramer, Department of Zoology, Faculty of Science, UBC
Supervisory Committee Member

David J. Granville, Department of Pathology and Laboratory Medicine, Faculty of Medicine, UBC
Supervisory Committee Member

Abstract

High-level spinal cord injury (SCI) causes the loss of descending sympathetic control to the heart which, in addition to other secondary consequences (i.e., changes in physical activity and metabolism), leads to premature onset and increased risk for cardiovascular disease. Our research team reported that chronic high-level experimental SCI is associated with systolic dysfunction, cardiomyocyte atrophy and up-regulation of the two main proteolytic pathways in cardiac tissue. How such events manifest over time post-injury is presently unknown. Therefore, the aim of this thesis was to investigate the temporal effects of high-thoracic SCI on cardiac function, structure and proteolysis. To achieve so, we used a pre-clinical rodent model which underwent complete transection SCI at the third thoracic spinal level (T3-SCI). Rats were terminated at different time-points along the acute timeline: 12 hours, 1 day, 3 days, 5 days and 7 days post-SCI. SHAM rats were used as controls and underwent dorsal durotomy with no SCI. Echocardiography was performed on the 7-day SCI and SHAM groups pre-surgery and on days 1, 2, 4 and 6 post-surgery to assess temporal changes in cardiac volumes and function. At termination time-points, left-ventricle (LV) catheterization was performed to assess cardiac function in all groups except in the 12-hour T3-SCI group. Additionally, cardiac tissue was collected for histological and gene expression analysis to quantify cardiomyocyte dimensions and the regulation of proteolytic pathways, respectively. We found a significant reduction in load-dependent and -independent systolic function with ventricular-arterial uncoupling as early as 1 day post-SCI which persisted into the chronic setting, but no changes in diastolic function. These results indicate a rapid onset of cardiac dysfunction following T3-SCI, implying that loss of cardiac sympathetic control and cardiac unloading are key determinants in reduced systolic performance post-SCI. Furthermore, in T3-SCI cardiac tissue, we report elevated gene expression of targets involved with the ubiquitin proteasome system, one of the two main proteolytic pathways. Although no significant

cardiomyocyte atrophy was observed, our results suggest that the molecular events ultimately causing chronic cardiac atrophy are initiated acutely post-SCI. Together, our findings imply that reduced cardiac function precedes structural remodelling following high-thoracic SCI.

Lay summary

Following high-level spinal cord injury, the brain signals sent down the spinal cord can no longer reach the heart. This lack of signalling negatively impacts heart function, reduces heart size and induces a wide range of complications, which can lead to increased risk for, and premature onset of, heart disease. Multiple studies have reported impairments in heart function and structure with associated protein breakdown following chronic spinal cord injury. However, the sequence and timeline of these changes are unknown. To study the changes in the heart across time after spinal cord injury, we collected heart data at different time-points using a rodent model. We report that, acutely following spinal cord injury, heart function was decreased, markers of protein breakdown were increased but there were no changes in heart structure within the first week, implying that the reduction in heart function occurs before the reduction in heart size.

Preface

All experimental protocols conducted for this thesis were reviewed and approved by the University of British Columbia (UBC) Animal Care Committee (A18-0344) and strictly followed the guidelines implemented by the Canadian Council for Animal Care. All data was collected and analyzed by Mary P.M. Fossey and members of the West lab at International Collaboration on Repair Discoveries (ICORD). No data from this thesis have been previously published.

I was the lead investigator for this project. My responsibilities included concept development, animal care, surgical assistance, *in vivo* and *ex vivo* data collection, tissue collection, analysis of physiological and molecular data, interpretation of results and writing of this manuscript. Dr. Malihe-Sadat Poormasjedi-Meibod was involved in concept development, performed all animal terminal procedures (echocardiography and catheterization) and trained me on all molecular techniques. Erin Erskine was involved in the organization of this project, performed all SHAM and spinal surgeries and further trained me on all animal care procedures. Brian Hayes aided with animal care and surgical assistance, and partly trained me on analysing physiological data. Dr. Matt S. Ramer and Dr. David J. Granville provided insight for concept development, thesis revisions and additional expertise.

Dr. Christopher R. West was the supervisory author for this project. Dr. West was involved with concept formation and development, trained me on analysing physiological data, aided with data collection, analysis and interpretation, and provided thesis revisions.

Table of contents

List of tables

List of figures

List of abbreviations

Ab – antibody
ACE – angiotensin converting enzyme
Ach – acetylcholine
Akt – protein kinase B
AMPK – AMP-activated protein kinase
ANGI – angiotensin I
ANGII – angiotensin II
ANOVA – analysis of variance
ANP – atrial natriuretic peptide
ANS – autonomic nervous system
Ao – angiotensinogen
AT1 – angiotensin II receptor 1
AT2 – angiotensin II receptor 2
ATG – autophagy related protein
ATG7 – autophagy related 7
ATG12 – autophagy related 12
ATG16L – ATG16-like protein
AV – atrioventricular
BECN1 – beclin 1
Bnip3 – BCL2/adenovirus E1B 19 kDa protein-interacting protein 3
BSA – bovine serum albumen
C# – cervical segment
cDNA – complementary DNA
CO – cardiac output
CON – control
CSA – cross-sectional area
CVD – cardiovascular disease
DBP – diastolic blood pressure
dP/dt_{max} – maximal rate of systolic pressure increment
$-dP/dt_{min}$ – maximal rate of diastolic pressure decrement
Ea – arterial elastance
Ea/ESPVR – ventricular vascular coupling ratio
EDPVR – end-diastolic pressure-volume relationship
EDV – end-diastolic volume
Ees – end-systolic elastance
EF – ejection fraction
eIF3f – eukaryotic translation initiation factor 3 subunit f
ESPVR – end-systolic pressure-volume relationship
ESV – end-systolic volume
FA – fascia adherens
FIP200 – FAK family kinase-interacting protein of 200 kDa
FoxO – forkhead box O

FoxO3 – forkhead box O3
FS – fractional shortening
HR – heart rate
ICORD – International Collaboration on Repair Discoveries
IML – intermediolateral nucleus
IVC – inferior vena cava
L# – lumbar segment
LC3 – microtubule-associated protein 1 light chain 3
LV – left-ventricle
MAFbx – muscle atrophy F-box
MAP – mean arterial pressure
MRI – magnetic resonance imaging
mRNA – messenger RNA
mTOR – mammalian target of rapamycin
MuRF1 – muscle RING-finger protein 1
MyoD – myoblast determination protein 1
NDS – normal donkey serum
NE – norepinephrine
NF-κB – nuclear factor kappa B
NT – neurotransmitter
NTS – nucleus of tractus solitarius
PBS – phosphate-buffered saline
PBS-T – phosphate-buffered saline with Triton
Pdev – developed pressure
Ped – end-diastolic pressure
Pes – end-systolic pressure
PI3K – phosphoinositide 3-kinase
PI3P – phosphatidylinositol 3-phosphate
Pmax – maximum pressure
PRSW – preload recruitable stroke work
PSLAX – parasternal long axis
PSNS – parasympathetic nervous system
PINK1-PRKN – PTEN-induced kinase 1 & Parkin complex
PV – pressure-volume
p52 – sporozoite surface protein P36p
qPCR - qualitative polymerase chain reaction
RAAS – renin-angiotensin-aldosterone system
RBP – renin binding protein
RV – right ventricle
RVLM – rostral ventral lateral medulla
S# – sacral segment
SA – sinoatrial
SBP – systolic blood pressure
SC – spinal cord
SCI – spinal cord injury

SE – standard error of the mean
SNS – sympathetic nervous system
SPN – sympathetic preganglionic neuron
SV – stroke volume
SW – stroke work
T# – thoracic segment
TGF-β – transforming growth factor beta
TNF – tumor necrosis factor
TNFα – tumor necrosis factor α
TPR – total peripheral resistance
TRAF6 – TNF receptor associated factor 6
TRIM32 – E3 ubiquitin-protein ligase TRIM32
TWEAK – TNF-like weak inducer of apoptosis
Ub – ubiquitin
UBC – the University of British Columbia
ULK1 – serine/threonine-protein kinase ULK1
UPS – ubiquitin proteasome system
USP14 – ubiquitin carboxyl-terminal hydrolase 14
USP19 – ubiquitin carboxyl-terminal hydrolase 19
Vps – phosphatidylinositol 3-kinase
WGA – wheat germ agglutinin
6-OH-DOPA – 6-hydroxy-dopamine

Acknowledgments

First of all, I would like to express my deepest and sincerest gratitude to my supervisor Dr. Christopher R. West for his exceptional mentorship, clear guidance and continuous support. Without your patience and expertise, this thesis would have not been possible. Thanks to you, I have learned so many skills which will surely last for the entirety of my scientific career. I am and was very fortunate to have had you as a mentor. I do not think I could have wished for a better supervisor. Thank you for this opportunity which allowed me to work with an outstanding team on a project which has further expanded my passion for science.

Secondly, I would like to express special thanks to Dr. Malihe-Sadat Poormasjedi-Meibod, Brian Hayes and Erin Erskine for their crucial help. Mali, your mentorship and passion for quality science has immensely guided me throughout this degree. You have taught me so much; I am truly grateful. Brian and Erin, your friendship, generous help and support throughout this project were invaluable and I could have not dreamed of better teammates.

Thirdly, I have profound appreciation for my committee members Dr. Matt S. Ramer and Dr. David J. Granville for their expertise, valuable insight and contributions.

Next, I would like to acknowledge with my sincerest thanks all members of my lab, the West lab (particularly Dr. Alexandra M. Williams, Dr. Guillermo A. Alanis and Cameron M. Gee), for their essential assistance, caring encouragement and never-ending positive attitude.

Finally, I would like to thank ICORD and UBC for their financial assistance and high-quality facilities.

Dedication

To my family.

Chapter 1. Literature review

1.1 Cardiac anatomy

1.1.1 Gross anatomy of the cardiovascular system

The cardiovascular system consists of three main components: 1) a fluid, 2) a pump to propel the fluid, and 3) an extensive network of vessels to transport and deliver the fluid around the body.[1,2] In mammals, the heart serves as the muscular pump and is formed of four chambers: two atria and two ventricles.[2,3] The blood functions to deliver nutrients and oxygen, collect wastes and carbon dioxide, transport communicating molecules, such as hormones and cytokines, and finally, protect all tissues with a myriad of different immune cells.[2]

1.1.1.1 Basic structure of the heart

The heart is enveloped by the pericardium, which is a fibrous sheet that encloses the heart in a liquid-producing frictionless chamber.[2] The pericardium is located within the thoracic cavity, more specifically in the middle mediastinum, ventral and slightly lateral to the spinal cord (SC).[2] The heart is protected by the ribs, the sternum, the vertebral column and surrounding adipose tissue.[2]

The heart is divided into two sides by an interatrial and interventricular septum.[2] The right-side of the heart pumps deoxygenated blood from all parts of the body to the lungs, and the left-side pumps freshly oxygenated blood from the lungs to the rest of the body.[1] When blood enters the heart, it first pools into an atrium then gets ejected into a secondary chamber with a larger lumen and thicker muscular wall, a ventricle.[2] Both sides of the heart contain an atrium and a ventricle.[1–3] Both atria and both ventricles contract in synchrony with each other, respectively, and contract to produce the unidirectional flow of blood.[2]

1.1.1.2 The systemic and pulmonary circuits

The heart pumps blood into two different circuits: the systemic and the pulmonary circuits.[1,2] Deoxygenated blood from all organ systems of the body travels back to the right side of the heart through the superior vena cava (blood flowing from the head, upper limbs and chest area) and inferior vena cava (blood flowing from the abdomen, pelvic area and lower limbs) to pool into the right atrium.[2,3] Right atrial contraction and subsequent ventricular contraction will propel venous blood to continue its path into the pulmonary system.[1,2] Blood enters the pulmonary trunk which later divides into the right and left pulmonary arteries to reach each respective lung.[2,3] In the capillary beds surrounding lung tissue, the blood comes into close contact with the air inhaled in the alveoli. As the blood has low levels of oxygen and is saturated with carbon dioxide, gaseous exchange of both gases occurs easily by diffusion across the moist one-cell-thick barrier.[3] Once oxygenated, blood will flow back to the left side of the heart through the pulmonary veins and enter the left atrium.[3] The atrium contracts and the ventricle consecutively; this sends the blood into the systemic circuit, which provides oxygen to the entire body.[1,3] As the left side of the heart has the goal to replenish all tissues from the body with freshly oxygenated blood, the muscle wall of the LV is thicker than the right (RV) as the left-side is required to produce more pressure to propel the blood at all extremities of the body.[1] Once exchange of oxygen has occurred in the systemic capillaries, the blood will travel back to the right side of the heart through the major veins and exit the systemic circuit. One important aspect to take note of is that both sides of the heart contract in synchrony, meaning both atria will contract simultaneously, as will the ventricles few milliseconds later.[1]

1.1.2 Layers of cardiac tissue

The layers of the heart are continuous and homologous to the layers, also known as tunics, of blood vessels.[3] Comparable to the vessel tunics, the heart has three layers of tissue: the *endocardium*,

homologous to the tunica intima, the cardiac *myocardium*, homologous to the tunica media, and the *epicardium*, homologous to the tunica adventitia.[1–3] All three layers are present in the free walls of the heart, which are defined to be the walls of the heart which are not in contact with the septa.[2] However, the septa between the chambers do not contain epicardium but rather one layer of myocardium surrounded by two layers of endocardium, as cardiac lumen are found on each side.[2] There exists subtle differences in layer thickness in different chambers, for example, the myocardium located in the atria is thinner compared to the one in the ventricles, this difference are be due to distinct force generation requirements.[2]

1.1.2.1 Epicardium

The epicardium is the most outer layer of the heart and forms part of the visceral layer of the pericardium.[3] The pericardium is a fibro-elastic membranous sac surrounding the heart, which consists with two membranous layers: the parietal and visceral layers, a pericardial space and a fibrous outer layer.[1,3] The serous surfaces secrete a lubricating liquid in the pericardial cavity to reduce friction between the heart with its surrounding tissue during contraction.[1–3] The epicardium consists of an epithelial layer and a subepicardial layer with loose connective tissue containing adipocytes, serving as shock absorbers, and infiltrating coronary blood vessels, lymph vessels and nerve supply for the heart itself.[1,3]

1.1.2.2 Endocardium

The endocardium, the inner lining of the heart, has direct contact with the blood in the lumen of the cardiac chambers.[1,3] The apical most layer consists of a single squamous epithelium, also known as the vascular endothelium.[1–3] Underneath the endothelium, there is a subendocardial layer, which can range from loose to dense connective tissue.[1] The subendocardium mostly contains a combination of scattered fibroblast, blood and nerve supply, smooth muscle cells and some specialized cardiac muscle cells, which form fibers of the conducting system of the heart (i.e., Purkinje fibers).[1–3] As the tissue grows

deeper towards and transitions to myocardium, the connective tissue seems to accumulate more collagen and elastic fibers.[1–3] Ventricular endocardium has trabeculae which creates texture to the lining.[1] Papillary muscles are expansions of trabeculae into the lumen, which serve as attachments for chordae tendineae, important for valve function.[1]

1.1.2.3 Myocardium

The myocardium is the middlemost and thickest layer of the cardiac wall.[1,3] It mostly consists of concentric bundles and sheets of cardiac muscle cells, also known as cardiomyocytes, which surround, in a circular fashion, all chambers of the heart.[1,3] The myocardium is a complex tissue with numerous cardiomyocytes, which are surrounded by an extracellular matrix for structural integrity.[4,5] The matrix around the muscle cells is composed of fibroblasts, intricate blood and nerve supply.[4,5] As the myocardium is the most energy demanding tissue in the entire body, it is richly vascularized.[6] It has been found that each cardiomyocyte in the myocardium has direct contact with at least one capillary vessel.[6]

Not surprisingly, the thickness of the myocardium differs between chambers due to their function and their target circuit.[1,2] While the ventricular myocardium is thicker than the atrial myocardium, the left ventricle prevails compared to the right ventricle as it pumps to the all extremities of the body.[1]

Cardiomyocytes (cardiac muscle cells) are the main effectors of the heart; there are many different types of cardiomyocytes, which all differ slightly in their function.[3] Some serve to contract in synchrony to generate force and propel the blood out of the chamber, others control the generation and frequency of electrical stimuli.[3] The sheets of cardiac muscle all have different orientations for the directionality of contraction and expulsion of blood.[3] The cellular characteristics of cardiomyocytes will be described in further detail when discussing the microscopic anatomy of cardiac muscle.

1.1.3 Cardiac muscle

Cardiac muscle is an involuntary striated muscle, which serves to generate mechanical force and ensure a constant heartbeat.[1–3] The functional units are the cardiomyocytes.[1–3] Contractile cardiomyocytes are branched tubular cells, which can connect to multiple neighbouring muscle cells to form parallel arrangements of cells, called laminae.[2,3] These laminae have distinct directionality depending on its location and function in the myocardium.[2,3] As cardiac muscle is the most energy demanding tissue in the entire body,[1] sheets of connective tissue lie between laminae with extensive blood and nerve supply resulting in all cardiomyocytes to be in close proximity to capillaries and nerve terminals.[3]

1.1.3.1 Cardiomyocytes

Cardiomyocytes present in the atria are smaller than their ventricular counterparts.[3] The different morphologies are correlated to the force of contraction they are required to exert to propel the blood to its next destination.[3] Even within one lamina, mature cardiomyocytes vary in shape and in size ranging from 10-35 μm in diameter and 80-120 μm in length.[1,7,8] Cells can attach to multiple different neighbouring cells through intercalated discs; this branching pattern facilitates the propagation of electrical impulses throughout the tissue.[1] Intracellularly their contents can differ depending on the species of interest, and the location in the heart.[9] Despite differences in organelle quantity, all regular cardiomyocytes have a nucleus, cytoskeleton for maintaining cell structure, and active Golgi and endoplasmic complexes.[2] Although the common cardiomyocyte only possesses one euchromatic centered nucleus, few can be doubly nucleated.[1] There are abundant contractile units, myofibrils, which lie parallel to the direction of stimuli.[2] Cardiomyocytes contain an active endoplasmic reticulum, specifically called sarcoplasmic reticulum and a plasma membrane, called sarcolemma.[1] Due to the extensive demand for ATP for contraction, large mitochondria with deep cristae (for increased surface

area) are present in large numbers in cardiomyocytes and make up 36% of the cell, compared to 5% in skeletal muscle fibers.[1,10] Most of the mitochondria can be located densely packed near the nucleus and between the longitudinally oriented myofibrils.[1,2,11,12] To aid the high energy demand, cardiomyocytes additionally store large quantities of glycogen and lipid droplets, which, similar to mitochondria, are located close to the nucleus and myofibrils.[2] These serve for energy back up in case of low oxygen levels.[1,2]

1.1.3.2 Cardiomyocyte contractile apparatus, T-tubules and the sarcoplasmic reticulum

Cardiomyocytes have similar longitudinal myofibrils to skeletal muscle cells.[1,2] Cardiac sarcomeres are made up of the same proteins as skeletal muscle: alternating thin (~1.0 μm long) and thick filaments (~1.6 μm long), predominantly composed of actin and myosin, respectively.[2] All filaments are anchored to the Z-line by multiple proteins, including α-actinin.[13,14] The contractile proteins make up more than 55% of the cytoplasm in cardiomyocytes.[15,16]

T-tubules are extensions of the plasma membrane that project into the deeper parts of a muscle cell to come into close contact with the contractile apparatus and the endoplasmic reticulum.[1,3] This organized arrangement and coming together of membranes are located in close proximity to Z-lines and serve to accelerate depolarization-induced calcium release.[1,3] As the electrical stimuli travel down the t-tubule, channels in the plasma membrane open to allow a net influx of calcium ions into the cytoplasm of the cardiac muscle cell.[3] Once a high concentration of calcium ions is detected in the cytoplasm, ryanodine receptors on the sarcoplasmic membrane will open to generate a greater influx of calcium ion into the cytoplasm.[3] Thanks to both of these ion influxes, the contractile apparatus is activated causing cells to contract, generating the gross contraction of the cardiac chamber.[3]

1.2 The innervation of the heart, its conducting system and the cardiac cycle

1.2.1 Autonomic nervous system

Cardiac muscle is known to contract rhythmically and spontaneously, meaning there is no conscious decision or need for innervation to stimulate a contraction and generate a heartbeat.[1,2] It has been shown *in vitro*, that embryonic cardiac muscle cells contract spontaneously with no direct stimulation: proving that heartbeat is spontaneous.[2] However, heartbeat frequency (chronotropism) and contractility (ionotropism) can be adjusted by the autonomic nervous system (ANS) depending on the metabolic needs.[2,17] In addition, the ANS can change the conductivity (dromotropism) and excitability (bathmotropism) of the cardiomyocytes, and the vascular tone of the myocardial capillaries and coronary vessels.[17] The ANS is composed of complimentary branches: the parasympathetic (PSNS) and sympathetic nervous systems (SNS), which act in opposite ways to maintain homeostasis.[17,18] The vagus and the glossopharyngeal cranial nerves relay sensory afferent information from chemoreceptors, baroreceptors, mechanoreceptors and metaboreceptors located in the vasculature and the sinuses to the nucleus of tractus solitarius (NTS) in the medulla oblongata.[19,20]

1.2.1.1 Parasympathetic nervous system

The PSNS is activated during situations of "rest and digest", when the body requires blood flow directed to the viscera (splanchnic area) as opposed to skeletal muscle.[17] Additionally, the PSNS is known to decrease heart rate (HR) and decrease contractility of the heart.[17] Cardiac afferent vagal neurons get stimulated by stretch receptors in the carotid sinuses and aortic arch when blood pressure is high, to decrease in HR and hypotensive cardiac reflexes.[17,21,22] In the case of low blood pressure, stretch receptors will ultimately cause an increase in HR by inhibiting PSNS.[17]

Anatomical, physiological and pharmacological data have shown that the PSNS receives input from cranial and sacral nerves.[17,23] Part of the parasympathetic outflow can occur through multiple cranial

nerves although only two innervate the cardiovascular system (the vagus and glossopharyngeal nerve).[17,19] The rest of the parasympathetic outflow is located in the sacral area (predominantly S2-S3 compared to S1 and S4) to innervate the urogenital system and the rectum.[17]

Parasympathetic preganglionic neurons, originating from the dorsal motor nucleus of the vagus and the nucleus ambiguous of the medulla oblongata, exit the vagal nerve and innervate many organs in the thorax and abdomen, including the heart (Figure 1.1.).[17,19] Postsynaptic nerve terminals from both branches of the ANS terminate in the sinoatrial (SA) and atrioventricular (AV) nodes in the right atrium of the heart (Figure 1.1.); additionally, some branches continue to run along the coronary arteries.[2,19] At the target organ, for example the heart, the parasympathetic neurotransmitter (NT) released to decrease HR and decrease contractility is acetylcholine (ACh).[17] This NT binds and activates nicotinic (muscular and nervous) and muscarinic receptors (i.e., M1 to M5) on the surface of the organ.[17,24] Muscarinic receptor M2, if activated, will decrease cardiac contractility and conduction velocity mostly in the atria.[17] Although, there are less M2 receptors in the ventricles, if the stimuli is sufficiently strong, it can decrease contractility by 20%.[17] M3 receptors serve to mildly dilate the coronary vasculature.[17]

1.2.1.2 Sympathetic nervous system

The SNS will be activated in moments of "fight or flight" when cardiac output (CO; volume of blood pumped out of the heart in 60 seconds) must be increased, for example, during stress or exercise.[17] To increase CO, the SNS will increase the frequency of depolarization in the SA node located in the right atrium to increase HR, and will increase the frequency of myocardial contraction to increase stroke volume (SV; volume of blood pumped out of the heart per beat) as CO=SV*HR.[17] Additional excitatory effects of the SNS include: increased conduction velocity and decreased refractory period in the nerves innervating the heart.[17]

Although multiple regions of the brain are involved in sympathetic input (i.e., paraventricular nucleus in the hypothalamus, the rostral ventromedial medulla, the A5 region of the brainstem and the caudal raphe nuclei), the majority of the sympathetic premotor neurons which innervate the heart and vessels are located in the rostral ventral lateral medulla (RVLM) of the medulla oblongata.[19] These bulbospinal premotor sympathetic neurons originate in the rostral ventral lateral medulla (RVLM) in the brainstem and descend the SC to synapse with sympathetic preganglionic neuron (SPN) in the gray commissure around the central canal, in the intermediolateral nucleus region of the grey matter (IML) and between these two regions in segments T1-L2 (Figure 1.1.).[17,19,20] Nerves innervating the cardiovascular system (heart and vessels) and the heart specifically will exit at T1-L2 and T1-T5 (Figure 1.1.), respectively.[17] SPNs will enter the ventral root, follow the white rami communicantes into a sympathetic ganglion, which is part of the sympathetic chain.[17] SPNs can go up and down the sympathetic chain to reach other anterior and posterior ganglia; there are 3 cervical, 11 thoracic, 4 lumbar and finally 4-5 sacral ganglia.[17] In the sympathetic chain ganglion, the SPN will release ACh to stimulate the postganglionic neuron.[17,25] The postganglionic neuron will exit the sympathetic chain through the grey rami communicantes to then innervate the target organ, where it will release norepinephrine (NE) to activate adrenergic receptors.[17] There are two types of adrenergic receptors: α (i.e., α_1, α_2 and subtypes) and β (β_1, β_2, β_3 and subtypes) adrenergic receptors.[17,26,27] In terms of cardiac functions, α_1 and α_2 mostly constrict coronary vasculature, whereas β_1 and β_2 (3:1 ratio) induce all physiological changes previously mentioned in this paragraph (i.e., increased ionotropy, dromotropy and bathmotropy).[17] β_2 is found to be distributed primarily in all chambers of the heart, while the presence of β_3 in the heart is yet to be clarified.[17]

The postganglionic neurons exit the ganglia and innervate different parts of the heart via the cardiac nerves.[17] There are eight ganglia on each side of the heart: superior, middle and inferior (stellate)

cervical ganglia, and first five thoracic ganglia (Figure 1.1.).[17–19] Sensory nerve endings can be located in the subendocardium, and at conjunctions of different vessels and chambers.[17] These will sense cardiac sensory information which will be sent to the NTS then to the higher sensory processing centers located in the diencephalon.[17,28]

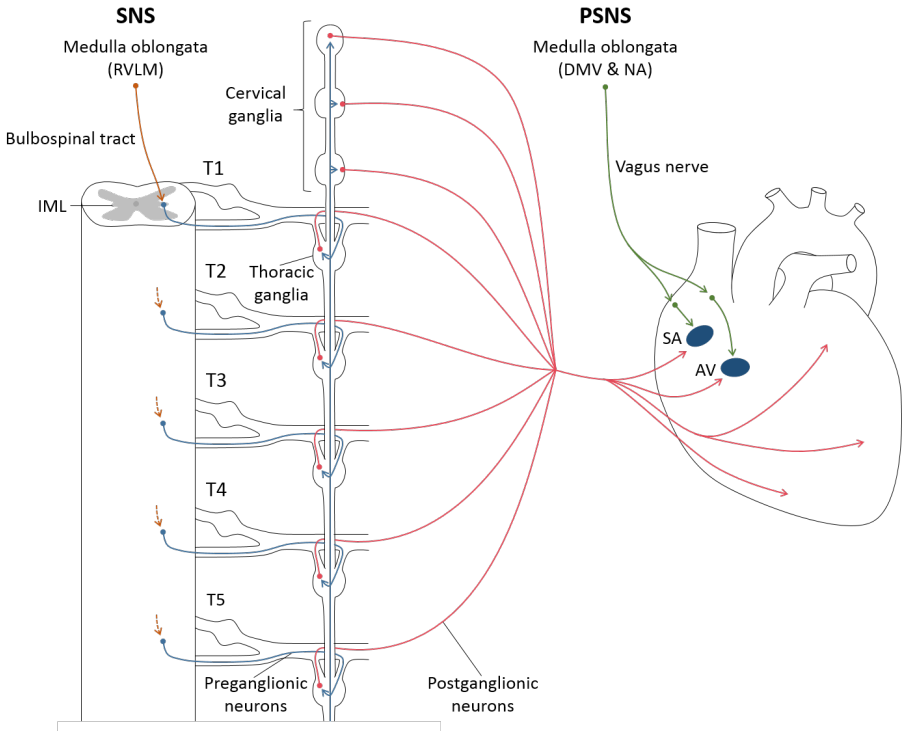

Figure 1.1. Schematic of the autonomic innervation of the heart. AV, atrioventricular node; DMV, dorsal motor nucleus of the vagus; IML, intermediolateral nucleus; NA, nucleus ambiguous; PSNS, parasympathetic nervous system; RVLM, rostral ventrolateral medulla; SA, sinoatrial node; SNS, sympathetic nervous system.[17–20]

1.2.1.3 The cardiac plexus

The cardiac plexus is a network of nerves which serves to innervate the myocardium of the interseptal walls (between the atria, and the ventricles, respectively), the two nodes of the conducting system and some vasculature, with both the PSNS and SNS.[17] Due to its range of activity, it is located at the base of the heart, ventral to the carina of the trachea and posterior to the aortic arch.[17]

1.2.2 Rhythmic contractions

A heartbeat consists of two beats: first, the atria contract in synchrony and subsequently, the ventricles do the same, however with more force.[3] This creates a rhythmical flow of blood through the heart.[1,3] The gross muscular contractions are generated thanks to the microscopic contractions of thousands of cardiomyocytes in the myocardium of these chambers.[3] Unlike skeletal muscle, cardiac muscle requires a nearly constant release fluctuations of calcium ions into the cytoplasm and constant anaerobic metabolism to sustain contractions and relaxations.[3]

1.2.3 The microscopic conducting system

The conducting system of the heart is made up of specialized cardiac muscle cells which have the ability to conduct electrical impulses throughout the tissue.[3] The signals sent from the brain descend through the autonomic nerves transferring the stimuli to nodes, located in the right atrial wall.[3] These nodes are formed by the aggregation of the specialized cardiomyocytes abovementioned.[2,3] The SA node, also known as the cardiac pacemaker is located near the entry of the major venous vessels.[3] The received signals generate numerous depolarization events within the cell, which will result in a HR of about 70 beats per minute (bpm) in healthy and resting human conditions[3] with PSNS dominance (autonomic input) versus 100 bpm without the latter.[29] In rats, resting HR remains at approximately 290-370 or 350-400 bpm depending on the time of the day and strain (Wistar and Wild-type, respectively).[30] The signal then flows through the internodal pathway to reach the second atrial node: the atrioventricular (AV) node, located in the septum near the junction of the right atrium and the right ventricle.[3] From this point on forward, the stimuli descend down the interventricular septa through a bundle of conducting fibers, consisting of only specialized cardiomyocytes, called the bundle of His.[3] Approximately half way down the septum, the bundle branches into right and left bundles to surround both ventricles.[3] The fibers continue

to descend and once they reach the apex of the heart, their direction veers upwards to envelop the ventricles; these new branching fibers are called Purkinje fibers.[2,3] Purkinje fibers are located in the myocardium of all chambers but can be found in greater numbers in the interventricular septa.[1] The directionality of all fibers and rhythmicity of stimuli is important for the ventricles to contract upwards for blood to exit and flow through the semilunar valves.[3] Purkinje fibers, as all other constituents of the conducting system, are made of specialized cardiomyocytes.[1] Intracellularly, these cardiomyocytes are distinct from others because of their disorganized myofibrils, and increased number of mitochondria and glycogen stores, which serve to provide these cells with sufficient energy for their high functional demands and increased ability to resist hypoxia.[1] In addition to these adaptations, to increase their conduction ability, these cardiomyocytes share numerous intercellular channels called gap junctions which allow the propagation of electrical stimuli from cell-to-cell via the flow of ions.[1]

1.2.4 Intercalated discs

Cardiomyocytes are connected end-to-end by intercalated discs, which have dense areas of condensed specialized proteins.[1–3] Intercalated discs have two surfaces: a lateral surface (perpendicular to the directionality of the cell and electrical stimuli), and a transverse surface (parallel to the cell).[1–3] The two surfaces have distinct transmembrane proteins with different functions.[1–3] On the lateral surfaces of the intercalated disc, many gap junctions serve for communication and conduction of electrical stimuli; thanks to these channels, depolarization signals are able to rapidly spread throughout the tissue to generate contraction.[1–3] On the transverse surfaces, both macula adherens (desmosomes; also found on the lateral surfaces) and fascia adherens (FA) are numerous and function to securely anchor cells together.[1–3] Desmosomes and FA are attached to intermediate cytoskeletal and actin filaments,

respectively to reduce mechanical stress during contraction.[1] Cardiomyocytes are closely attached with a space of 15-20 nm between cells.[3]

1.2.5 Generation of contraction - Summary

To generate the contraction of cardiomyocytes and subsequently, the entire cardiac tissue, it is imperative to have a large influx of calcium ions into the sarcoplasm.[2,3] Once the depolarization of a cell is induced, calcium channels on the plasma membrane and on the sarcoplasmic membrane, will open and let a large influx of calcium ions.[2,3] This induces intracellular signal transduction, the activation of multiple different pathways and even further calcium-induced calcium release.[2,3] Calcium ions are crucial to induce conformational changes in proteins (i.e., tropomyosin and troponin) blocking myosin-binding domains on thin filaments.[3] Once myosin heads of the thick filaments are able to attach to the actin filaments, the sarcomeres are then able to shorten in synchrony and therefore contract the entire length of the cell.[3] T-tubules, as previously described, are key to effectively conduct the electrical stimuli and cause depolarization deep into the cell, near all contractile apparatus.[2,3] The specific receptors that are involved in the influx of calcium ions into the sarcolemma are the calcium-release channels and the ryanodine receptors, located on the plasma and sarcoplasmic membranes, respectively.[31] In summary, many proteins and secondary messengers partake in cardiac contraction.[2,3]

1.2.6 The cardiac cycle

Figure 1.2.A. includes pressure-volume (PV) data obtained via placement of a catheter in the LV. One PV loop which represents one cardiac cycle.[32] The bottom-right most corner of the loop represents the end of cardiac diastole, the relaxation and filling phase; at this stage, the heart is filling with blood.[32] The heart then enters cardiac systole, the contraction phase.[32] The first stage of systole involves isovolumetric contraction where the pressure increases with no changes in volume.[32] The increase in

pressure causes the aortic valve to open to allow for blood ejection out of the LV and therefore causes a reduction in volume.[32] Then, diastole commences with a reduction in pressure.[32] Once the pressure is lower than in the atrium, the ventricle will be able to fill with blood and therefore increase in volume until the end of diastole.[32]

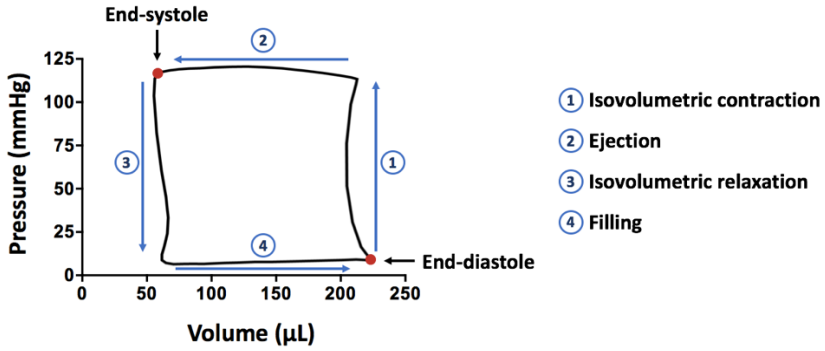

Figure 1.2. Representative pressure-volume loop at resting conditions. The different phases of one cardiac cycle are explained.

1.3 The renin-angiotensin-aldosterone system & the heart

The main role of the renin-angiotensin-aldosterone system (RAAS) is to maintain hemodynamic homeostasis thanks to endocrine and paracrine secretions from many organs of the body.[33] First, RAAS will be activated in response to low blood pressures to release the hormone renin from the kidney.[33] Renin converts angiotensinogen (Ao; primarily secreted by the liver) to angiotensin I (ANGI).[33] Angiotensin converting enzyme (ACE; secreted by the pulmonary and renal epithelium) will then convert ANGI to angiotensin II (ANGII) which will directly act on multiple organs (i.e., heart, kidney, adrenal cortex and brain).[33] ANGII will stimulate the adrenal cortex to secrete aldosterone which will cause ion and fluid retention in the kidneys to ultimately increase blood pressure.[33] At the cardiac level, increased levels of ANGII can induce changes in coronary vascular function, muscle metabolism, inflammation, structural remodelling (i.e., fibrosis and hypertrophy) and increased cardiomyocyte apoptosis.[33] ANGII and atrial

natriuretic peptide (ANP; although primarily produced by atrial cardiomyocytes) can also be secreted by ventricular cardiomyocytes when stretch receptors on the cells are activated (Figure 1.4.).[33] Additionally, stretch activation of the same cell will cause additional Ao to be released from the cardiomyocyte (mRNA levels of Ao in the heart are less than 0.1% than in the liver).[33–37] Stretch and ANP will act on cardiac fibroblasts to secrete more Ao and the precursor of renin.[33] Both processes will ultimately lead to further increases ANGII levels via a positive feedback loop.[33] As any other biological pathway, there must be a negative regulator. In this case, ANGII, itself, will bind to ANGII plasma membrane receptors (i.e., ANGII receptor 1 (AT1)) on cardiac fibroblast to inhibit renin and angiotensin release.[33] Interestingly, NE, released from sympathetic neurons, will indirectly increase ANGII levels in the heart by promoting Ao production and release from cardiomyocytes, and Ao and renin's precursor from fibroblasts.[33]

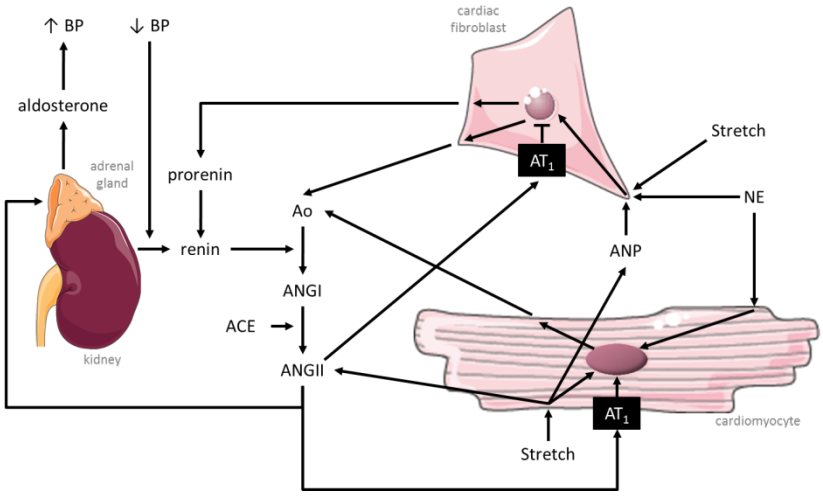

Figure 1.3. Molecular pathways of angiotensin II production in the heart. ACE, angiotensin converting enzyme; ANGI, angiotensin I; ANGII, angiotensin II; ANP, atrial natriuretic peptide; Ao, angiotensinogen; AT_1, ANGII receptor 1; BP, blood pressure; NE, norepinephrine.[33] Images used from © Servier with permission (licensed by CC BY 3.0).

1.4 Cardiac muscle homeostasis

1.4.1 Cardiac plasticity

When the heart is subjected to different types of molecular or physical stimuli, it will adapt in terms of its muscle structure and shape of its chambers.[38] In other words, the heart is able to change in according to its physiological needs.[38] For example, if there are changes in cardiac loading, pressure and volume changes will be detected by cardiac mechanical receptors, which will induce cardiac remodelling through a cascade of intracellular pathways.[38] This remodelling can either be physiological (i.e., exercise and pregnancy) or it can be pathological (i.e., denervation, immobilization, biochemical stresses, etc.).[38]

1.4.2 Regeneration of cardiac muscle

Past studies have shown that the incapability for cardiac myofibers to regenerate was due to the absence of satellite cells (stem cells), otherwise found in skeletal muscle.[1,2] It is additionally thought to be due to the post-mitotic status of cardiomyocytes with low to no regeneration ability.[39] Recent studies investigating heart transplants have found that 0.1% of cardiomyocytes were seen to have nuclei undergoing mitosis suggesting that cardiac cells could in fact have some ability to regenerate despite its weakness.[2] Whether these findings indicate increased cytokinesis or simply karyokinesis remains unclear. Regardless of this evidence, this potential regenerative ability of these cells would be very low.[1]

1.4.3 Hypertrophy & atrophy

Cardiac muscle cells are known to cease multiplication shortly following birth.[39] As the newborn heart is incapable of achieving the demands of an adult heart, in terms of function and mechanics, the organ must increase in size.[39] However, if the cells are no longer multiplying, the cells themselves must compensate for growth. Hypertrophy is the increase in size of muscle fibers,[3] which allows the growth of tissue to respond to new physical demands.[39] Hypertrophy can be eccentric (change in mass, dilation of

the chamber lumens and sarcomeral deposition in series) or concentric (change in mass, no dilation of the lumens and thickening of the muscular walls due to sarcomeral deposition in parallel).[38] Eccentric hypertrophy occurs after volume overload, whereas concentric hypertrophy occurs after pressure overload.[38] During hypertrophy, the cell will exhibit intracellular changes such as increased cytoplasmic volume, increased mitochondrial density, decreased myofibril size and increased sarcomere concentration.[40] Researchers hypothesize that these changes are caused by the increased demand in energy resulting in increased mitochondria fusion and are due to the increased cytoplasmic space required to transport high energy molecules.[40] In addition to an increase in cardiomyocyte size, in pathological situations, other molecular event also occur during hypertrophy which can include fibrosis in the extracellular matrix and increased cell death.[38] It is important to note that pathological hypertrophy often precedes cardiac dysfunction and heart failure; therefore, itmust be taken seriously.[38]

A certain degree of hypertrophic cardiac growth is crucial to the development of the organism to maintain appropriate cardiac function.[39] Hypertrophy can be adaptive and maladaptive. Following endurance and strength exercise, the heart will adapt to the physical demands.[38] However, if hypertrophy is uncontrolled or unnecessarily up-regulated, it can become maladaptive and therefore pathogenic.[39] For example, chronic hypertension will increase cardiac demand causing the tissue to respond by up-regulating hypertrophic pathways.[39] The expansion of cells will impair myofibril organization subsequently inducing cardiomyocyte cell death and decreasing cardiac output, which all together will increase the odds for heart failure.[39] Additionally, cardiac hypertrophy, in addition to fibrotic remodelling, and cell death, has been seen to be triggered by a constant over activation of the SNS.[41,42] Distinguishing physiological versus pathological hypertrophy can be complex as both are caused by cardiac overloading and in certain cases the cause (stimuli) and effect are indiscernible.[43]

Cardiac atrophy is the opposite of hypertrophy where heart mass is decreased in size.[38] It can occur when the patient is immobilized and experiences no-to-low mobility for long periods of time, for example, after high-level SCI and after decreases in cardiac preload (the amount of stretch of the ventricle after diastole; non-invasively estimated with end-diastolic volume (EDV) and pressure (Ped)).[38] During atrophy, cells are exhibiting more protein degradation and less protein synthesis events causing the balance to shift and the heart cells to decrease in size.[38] Molecular pathways involved in atrophy will be discussed in greater detail in the following section.

1.5 Cardiac consequences of SCI

The SC plays a crucial role in transporting sensory, motor and visceral information between the brain and the periphery. Unsurprisingly, due to its importance and omnipresent involvement, an injury to the SC can induce various catastrophic consequences on vital functions. In addition, due to the intricate organization of nerves exiting the SC at various levels to innervate different organs, injury level and severity will greatly determine the magnitude and quantity of secondary consequences on the body. Following SCI, not only is life quality significantly reduced, but life expectancy is said to decrease by 30% compared to able-bodied subjects.[44]

In 2010, the Canadian annual incidence for SCI was 4,259 with a total population of 85,556 in Canada [44] and 2.5 million worldwide.[45] Although SCI only affects 0.25% of the Canadian population,[44] it is an immense burden on health care system by reason of the gravity and multitude of complications following injury.[46] On average, traumatic SCI (i.e., caused by an external physical incident)[44] costs 2.67 billion Canadian dollars every year.[46]

If SCI occurs above the sympathetic innervation of the heart and vessels (T1-T5 and T1-L2, respectively),[47] the cardiovascular system will be devoid of supraspinal control from the cardiovascular

control center in the brainstem.[48] In other words, the sympathetic signals originating in the RVLM and descending through the SC are abruptly terminated due to the injury. This loss of supraspinal sympathetic control is thought to explain the decrease in many cardiac structural indices seen in the clinic since the 1980s. For example, Kessler *et al.* [49] reported decreases in LV EDV, LV SV, CO and estimated LV mass in patients with tetraplegia (i.e., C8-T1 or above) compared to paraplegia (i.e., T1 or below). These cardiovascular physiological changes, in addition to reduced physical activity, dyslipidemia (abnormal lipid levels),[50–53] increased risk for metabolic syndrome (increased obesity,[54] insulin resistance [55] and odds for type 2 diabetes [56]), blood pressure instability [57,58] and increased arterial stiffness [59] lead to premature onset and increased odds for cardiovascular disease (CVD) in this population by 2.67 fold compared to able-bodied subjects.[60] Unsurprisingly, CVD is the leading cause of death in this population.[60]

1.5.1 Systolic and diastolic function following SCI

1.5.1.1 Systolic dysfunction following SCI

Multiple clinical studies investigating cardiac function following SCI have contradictory results. Both Kessler *et al.* and Currie *et al.* reported decreased SV and CO in quadriplegic patients compared to paraplegics, indicating worsened function with higher level of injury.[49,61] West *et al.* demonstrated systolic dysfunction, with decreased LV ejection fraction (EF; % of blood volume ejected by the LV per beat), CO and SV in tetraplegic athletes compared to able bodied subjects.[62] In contrast, Driussi *et al*. reported no change in either SV or EF and increased LV contractility (explained to compensate for decreased venous return and inability to increase HR).[63] On the other hand, de Groot *et al.* indicated no systolic dysfunction following SCI with a decreased trend for CO.[64] Despite these inconsistent findings, a meta-analysis performed by our research team, which examined echocardiographic measures of cardiac structure and function, has indicated that SV is decreased with no change in EF following chronic SCI.[65]

EF, though used widely in the clinic, is not an ideal measure to infer cardiac systolic function as it is load-dependent which means it truly does not infer the intrinsic function of the heart but the function of the entire cardiovascular system. Additionally, as EF is load-dependent, if cardiac volumes are greatly and proportionally reduced, EF will not be changed significantly, rendering EF impractical to infer systolic function in this situation. To truly study intrinsic cardiac function *in vivo,* it is required to remove confounds of altered loading conditions. A method has been developed to uncouple the heart from the rest of the cardiovascular system by occluding the inferior vena cava (IVC) *in vivo*. Doing so will subsequently decrease preload and create a series of PV loops with different volumes. The slope of all connecting end-diastolic pressure and volume points is used as an index of intrinsic LV contractility, the end-systolic pressure-volume relationship (ESPVR; also called end-systolic elastance (Ees)). As occluding a vessel is highly invasive, it is only suited for pre-clinical studies involving animals.[66] With this technique and using rodent models of SCI, our laboratory has demonstrated twice in different strains of rats (Wistar and lean Zucker) that systolic dysfunction, load-dependent and -independent, is decreased following high thoracic SCI, as evidenced by decreases in pressures, the maximal rate of LV systolic pressure increment (dP/dt_{max}) and ESPVR.[62,63]

1.5.1.2 Diastolic dysfunction following SCI

In clinical research, diastolic function is assessed with LV filling velocities, obtained via non-invasive techniques (i.e., echocardiography). Many studies disagreed on how diastolic function changed following SCI as these data were wildly inconsistent. [63,67–71] However, a recent meta-analysis was performed by our research group and it reported a decrease in diastolic function in the human SCI population.[65] In pre-clinical studies, diastolic dysfunction is assessed more accurately with more-invasive techniques such as LV catheterization and IVC occlusions.[62,63] In these studies, diastolic function can be inferred with two load-dependent measures with LV catheterization: tau (LV diastolic time constant) and -

dP/dt_{min} (maximal rate of LV diastolic pressure decrement). Intrinsic cardiac diastolic function can be inferred with the load-independent index for compliance: the end-diastolic pressure-volume relationship (EDPVR; the non-linear fit of all end-diastolic volume and pressure points). A reduction in diastolic function following high-level SCI in pre-clinical settings has not yet been confirmed as load-independent and -dependent data are not in agreement. EDPVR is reported to not change significantly in the sub-acute and chronic settings following severe high-level SCI (complete transection at the 3rd thoracic segment (T3)[72] and severe contusion at the 2nd thoracic segment (T2)[73]), while both tau and $-dP/dt_{min}$ were significantly decreased in the chronic stage following complete T3-SCI but not in the sub-acute phase following severe T2 contusion.[72] Due to this discrepancy, more pre-clinical research on diastolic function post-SCI is required and for this, new contemporary methods to measure intrinsic diastolic function accurately are currently being designed in our laboratory.

1.5.1.3 Mechanisms affecting cardiac function following SCI

The function of the heart following high-level SCI can be negatively affected by multiple mechanisms: loss of supraspinal sympathetic [74] and sympathoadrenal control,[75,76] altered neurohumoral control (i.e., decreased circulating NE and increased ANGII in the chronic phase post-SCI),[72] reduced physical activity [77] and cardiac unloading due to a reduction in blood volume and pressure.

Immediately and several hours following traumatic SCI, there is a sudden loss or depression in spinal reflexes, defined as spinal shock, and in sympathetic tone below the level of injury, defined as neurogenic shock which leads to hypotension and bradyarrhythmias.[78,79] High-level injuries with loss of supraspinal sympathetic control to the heart and the vasculature can have drastic impacts on systemic hemodynamic function due to reduced sympathetic activity below the level of injury.[74,80] Additionally, if the level of injury incapacitates signals to reach the adrenal medulla, circulating catecholamine levels will remain low even during conditions typically requiring the activation of the SNS (i.e., stress and

exercise).[75,76] Due to reduced direct vascular sympathetic activity below the level of injury,[80–82] reduced NE circulation [48,75,76] and reduced motor control to the skeletal muscle pump,[83,84] vessels will no longer constrict effectively, blood pressure will acutely decrease [85] and blood will pool at the extremities and the splanchnic area, affecting venous blood return.[48,85–93] Venous pooling, causing reduced venous pressure and reduced pressure gradient between the venous circuit to the right atrium, and reduced blood volume will ultimately decrease blood delivery back to the heart (which will decrease preload).[92,94] Acutely after injury, decreased vasoconstriction of the arteries,[85] due to the loss of sympathetic control to the vasculature,[80–82] and its subsequent decrease in blood pressure [85] should reduce afterload (the amount of force the ventricle must generate to eject blood). In the chronic phase, vessels will have undergone remodelling due to changes in limb use, blood pressure and increase in arterial shear stress,[85] which will cause stiffening of the vasculature.[85] Furthermore, both acutely and chronically, low blood pressure will increase circulating ANGII,[33] which has been observed to directly cause atrophic [95–97] and fibrotic remodelling [98] in skeletal and cardiac muscle, respectively.

Collectively, altered neurohumoral control and loss of supraspinal sympathetic control following SCI lead to cardiac unloading further impacting cardiac function. Additionally and interestingly, in a study comparing moderate and severe high-thoracic contusions, our research team have shown that with only 10% of neuronal sparing (descending sympathetic neurons) cardiac function is preserved.[99]

Recently, our laboratory has performed two experiments to study cardiac function following SCI: 1) by stimulating adrenergic receptors in the heart with the administration of a β_1 agonist (dobutamine) in SCI rats,[73] and 2) by investigating the effects of intact and absent supraspinal sympathetic control (by varying the level of injury). Both studies show normal cardiac function in rats treated with dobutamine [73] and in rats with intact sympathetic control. These results imply that the loss of supraspinal sympathetic control may be the key determinant of cardiac dysfunction following SCI.

1.5.2 Cardiac and cardiomyocyte structure following SCI

Clinical studies have investigated cardiac structure with echocardiography due to the inability to use more invasive techniques on human subjects. All report decreases in estimated LV mass in quadriplegic patients (with loss of supraspinal sympathetic control) compared to either able bodied subjects or paraplegic counterparts.[49,64,100] In a pre-clinical study in our laboratory, Wistar rats showed decreases in total cardiac mass 4 weeks post severe T2 contusion by approximately 35% ($p<0.01$)[73] Squair *et al.* was the first study to report significant atrophy of cardiomyocytes in length (by approximately 22%; T2 93.9 ±8.54 versus control CON 121 ±5.98 μm, $p<0.01$) and Z-line width (by approximately 26%; T2 7.25 ±0.82 versus 9.82 ±1.80 μm, $p<0.05$) with no change in sarcomere length following high-thoracic sub-acute SCI, confirming the presence of cardiac atrophy.[73]

In addition to loss of cardiac mass, the T2 contusion rats demonstrated reduced body mass [72,73] and reduced lower-limb use following SCI. Weight-loss and reduced physical activity, by themselves, can cause cardiac atrophy.[101] As our current explanation hypothesis for cardiac atrophy following SCI is due to the loss of supraspinal sympathetic control, this could jeopardize our rationale for why there might be atrophic remodelling following SCI. However, outside of the SCI field it has been shown that ablation of sympathetic neurons to the heart, alone, caused cardiac atrophy in a rodent model with no changes in body mass or physical activity.[102]

As cardiomyocytes have been shown to atrophy following high-thoracic SCI in rodents with loss of supraspinal sympathetic control, the study of the cellular and molecular pathways involved in this atrophy was required. In the literature, there were no studies which investigated any cellular remodelling pathways associated with cardiac atrophy post-SCI. Nevertheless, there are many publications investigating skeletal muscle atrophy following denervation or disuse, and one publication investigating cardiac atrophy following pharmacological ablation of sympathetic neurons (with 6-hydroxy-dopamine; 6-

OH-DOPA).[102] These studies assisted our research team to target important genes associated with the two main proteolytic pathways of the cell: the ubiquitin proteasome system (UPS) and autophagy.

In a healthy cell, protein synthesis and protein degradation are constantly active and exist at equal rates to maintain homeostasis.[103] Without protein synthesis, the cell would not be able to perform specific biological and essential housekeeping functions.[103] Likewise, protein degradation, also known as proteolysis, is crucial for the survival of the cell as it acts to recycle proteins which are old, misfolded, defective or no longer necessary to avoid any toxic aggregates.[103] If proteolytic pathways are up-regulated, cells will atrophy and cause subsequent shrinkage of the organ.[104]

Proteolysis is an organized process which can be accomplished by multiple different systems.[103] There are five intracellular major proteolytic pathways which include: the UPS, the lysosomal machinery (i.e. endocytosis and autophagy), the calpain enzymes, mitochondrial proteinases and membrane proteinases.[103] All processes use a variety of enzymes called proteases (>200) which hydrolyze bonds between specific pairs of amino acids to break down the entire peptide.[103] Hydrolysis will lead to protein fragmentation thanks to the addition of water and a specialized enzyme as a catalyst.[103]

The mechanisms of calpains, mitochondrial and membrane proteases will not be discussed in this thesis. Special focus and greater detail will be given to the two main proteolytic pathways: UPS and autophagy lysosomal machinery.

1.5.3 The ubiquitin-proteasome system

1.5.3.1 Overview & mechanism

The UPS utilizes a series of specialized enzymes (i.e., E1, E2 and E3 ligases) to tag proteins with ubiquitin (Ub), a small regulatory molecule, for degradation.[104,105] The tagged proteins will then be recognized by a complex of proteases, forming a proteasome, which will break down the peptide bonds

and annihilate the targets into amino acids for recycling.[104,105] Proper function of UPS is crucial to degrade and recycle defective proteins to avoid aggregation and subsequent cell death, or cell atrophy.[104,105] In muscle, there exists additional specialized enzymes to tag sarcomeric proteins.[104] This is particularly important for cardiac muscle as it is the most energy demanding tissue of the body and requires effective and continuous contraction of myofibrils.[1]

The UPS mechanism is schematically summarized in Figure 1.5. Before tagging proteins with Ub, the Ub molecules themselves must be activated by E1 enzymes through the cleavage of ATP.[104] The E1 enzymes will then transfer the activated Ub to an E2 enzyme.[104] The E2 will bind an E3 ligase; different E2-E3 combinations will tag different proteins for degradation.[104] More than 650 E3 ligases have been identified in the human body;[106] but not all will be transcribed in all tissues.[104] This great variety allows for high selectivity for degradation.[104] The rate-limiting step will occur when the E3 ligase is bound to both the E2 enzyme and the targeted protein to transfer the Ub onto the target.[104] Once the target is polyubiquitinated with several Ub, the protein ZNF216 will recognize and deliver the tagged target to the proteasome for degradation.[104]

Studies investigating UPS have largely focused on ubiquitination and not on deubiquitination.[104] Two deubiquitinating enzymes have been identified in skeletal muscle atrophy following disuse and denervation (USP14, ubiquitin carboxyl-terminal hydrolase 14),[107] and fasting (USP19, ubiquitin carboxyl-terminal hydrolase 19).[108] USP19 protein levels were seen to be negatively correlated with muscle mass, which implies that deubiquitination might recycle Ub from degraded targets for more subsequent tagging.[108]

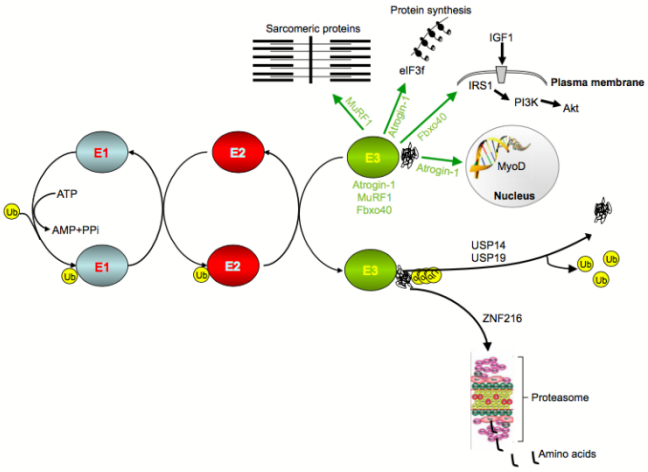

Figure 1.4. Schematic of the ubiquitin proteasome system. Reproduced with © permission from Bonaldo *et al.*[104]

1.5.3.2 Muscle atrophy & UPS

In skeletal muscle atrophy following denervation, the two first identified up-regulated E3 ligases were atrogin-1 (MAFbx; also called muscle atrophy F-box) and muscle ring finger 1 (MuRF1).[104,109] Two important MAFbx targets are myoblast determination protein 1 (MyoD; in skeletal muscle), a muscle-specific transcription factor,[110] and eukaryotic translation initiation factor 3 subunit f (eIF3f), an important translation initiator which binds the small ribosomal unit for translation activation.[111] In addition, MAFbx also targets calcineurin which indirectly induces hypertrophy.[112] MuRF1 is muscle specific and targets sarcomeric proteins for degradation, such as muscle actin, nebulin, titin, myosin heavy/light chains, myosin binding protein C and troponin I.[104,113–117] Two other lesser-investigated E3 ligases involved in atrophy are E3 ubiquitin-protein ligase TRIM32 (TRIM32) and tumor necrosis factor (TNF) receptor associated factor 6 (TRAF6).[104,105] TRIM32 tags for degradation thin filament proteins (i.e., tropomyosin, troponin and actin) and Z-line proteins (i.e., desmin and α-actinin),[118] whereas, TRAF6 up-regulation is required for proper activation of MAFbx and MuRF1 through AMP-activated protein kinase (AMPK) and forkhead box O3 (FoxO3).[119]

MAFbx, MuRF1 and ZNF216 expression is regulated through forkhead box O (FoxO) transcription factors.[104] FoxO transcription factors need to undergo posttranslational modifications (i.e., dephosphorylated, acetylated, etc.) to be able to be translocated into the nucleus and transcribe E3 ligases.[104,120] There are three isoforms: FoxO1, FoxO2 and FoxO3.[104]

In healthy conditions, insulin and insulin-like growth factor 1 (IGF-1) bind to plasma membrane receptors to activate the PI3K-Akt pathways (PI3K, phosphoinositide 3-kinase; Akt, protein kinase B) which leads to hypertrophy.[121] This causes Akt to be phosphorylated to promote protein synthesis through the mammalian target of rapamycin (mTOR) pathways and inhibit protein degradation by phosphorylating FoxO.[121]

In cases of disuse and fasting where levels of insulin and IGF-1 are low or mechanical unloading of the muscle, Akt does not get phosphorylated and will cause the dephosphorylation and therefore translocation of FoxO into the nucleus to transcribe atrophy genes (atrogenes; i.e., E3 ligases).[121,122] In the case of denervation, loss of trophic support dephosphorylates FoxO3 (via β_2 adrenergic signalling), which causes increased up-regulation of MAFbx.[102,120] However, with time FoxO3 is progressively acetylated and is tagged for degradation if catabolic conditions are not maintained.[120] If catabolic conditions continue, FoxO3 will remain activated and will cause UPS and autophagy up-regulation.[120] During high energy stress, elevated AMPK levels, due to increased AMP:ATP ratio, will up-regulate UPS atrogene transcription by phosphorylating FoxO3 at Akt-independent binding sites.[104,123–125] Other inducers of UPS, include circulating increased oxidative stress, ANGII (i.e., via decreased Akt phosphorylation or increased oxidative stress via activation of AT1), transforming growth factor beta (TGF-β), and tumor necrosis factor α (TNFα) and TNF-like weak inducer of apoptosis (TWEAK) which activate nuclear factor kappa B (NF-κB) transcription factors.[95,104,105,126–130] A summary diagram of pathways associated with muscle atrophy can be found in Figure 1.6.

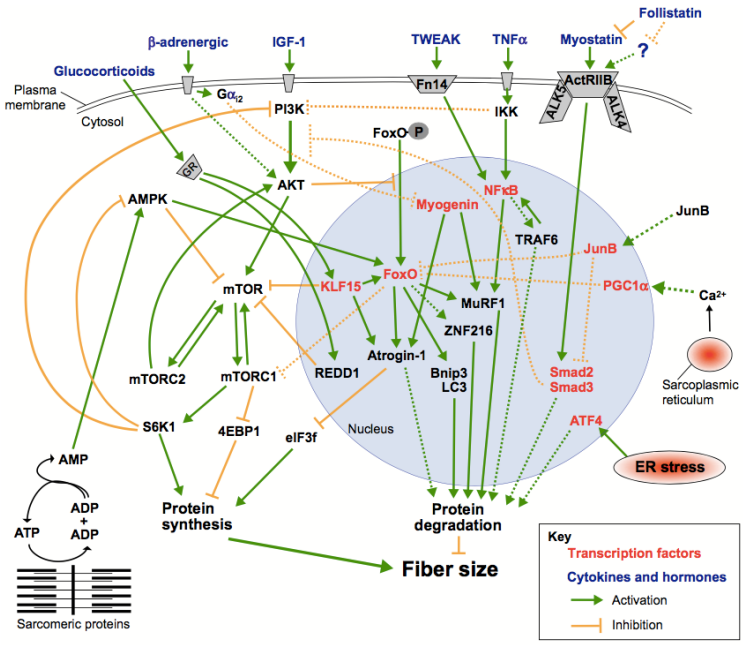

Figure 1.5. Pathways involved in protein degradation and synthesis. Adapted with © permission from Bonaldo *et al.*[104]

1.5.4 Autophagy

1.5.4.1 Overview & mechanism

Autophagy is a process of protein degradation which utilizes the formation of vesicles within the cells around bulks of less-transient proteins and organelles.[104,131,132] There exist different types of autophagy (i.e., macroautophagy, microautophagy, mitophagy, etc.), however, this section will solely focus on macroautophagy as it is the most investigated in situations of muscle atrophy.[104]

For initiation and the formation of a phagophore (once called isolation membrane), the formation of serine/threonine-protein kinase ULK1 (ULK1) complex (composed of: autophagy related protein (ATG) 13 , ULK1, ATG101, FAK family kinase-interacting protein of 200 kDa (FIP200)) is required to activate class III PI3K (beclin 1 (BCN1), phosphatidylinositol 3-kinase (Vps) Vps34, Vps15, ATG14) and subsequently generate phosphatidylinositol 3-phosphate (PI3P).[133,134] For elongation of the phagophore, two more complexes are required.[134] First, ATG5 and ATG12 must be covalently bonded by ATG7 and ATG10.[135–137]

The newly bonded ATG5-ATG12 can then bond to ATG16-like protein (ATG16L) to form the first required complex.[138,139] Second, microtubule-associated protein 1 light chain 3 (LC3) must be lapidated by the ATG5-ATG12-ATG16L complex, then conjugated to phosphatidylethanolamine by ATG7 and ATG3 to form LC3II, the second complex.[140,141] LC3II will complete elongation of the phagophore into an autophagosome (as enclosed vesicle).[142] For mitophagy, the specialized form of autophagy for mitochondria, there exist specialized proteins involved in the recruitment of mitochondria to the phagophore (i.e., PTEN-induced kinase 1 & Parkin complex (PINK1-PRKN), sporozoite surface protein P36p (p52) and BCL2/adenovirus E1B 19 kDa protein-interacting protein 3 (Bnip3) factors which will tag the surface of the organelle with Ub).[104] A simplified diagram of all proteins required for autophagy completion can be found in Figure 1.7.

Lysosomes are intracellular vesicles surrounded with a phospholipid bilayer, which enclose an acidic environment favorable for enzyme activation.[103] Lysosomes will fuse with endosomes containing extracellular contents (produced via endocytosis) or with autophagosomes to form an auto-lysosome.[21,103] The proteases located in the lysosomes will take action and digest the contents of the fused vesicle.[103] Permeases, located in the vesicle membrane, will transport molecules back into the cytosol for recycling.[143]

Autophagy is up-regulated in periods of crisis when cells require rapid recycling of amino acids as nutrients [103]. Some inducers of autophagy include cellular stress,[144] aging,[143] fasting/starvation [103,133] and denervation (Figure 1.6.).[104] The activation of the PI3K-Akt-mTOR pathway and the elevated levels of insulin can inhibit autophagy (Figure 1.6.).[133] High AMP:ATP ratio will cause increased in AMPK, which will inhibit these autophagy inhibitors (Figure 1.6.).[133] In addition, previously discussed FoxO transcription factors are also able to translocate to the nucleus and transcribe crucial autophagy-related proteins (Figure 1.6.).[104,105]

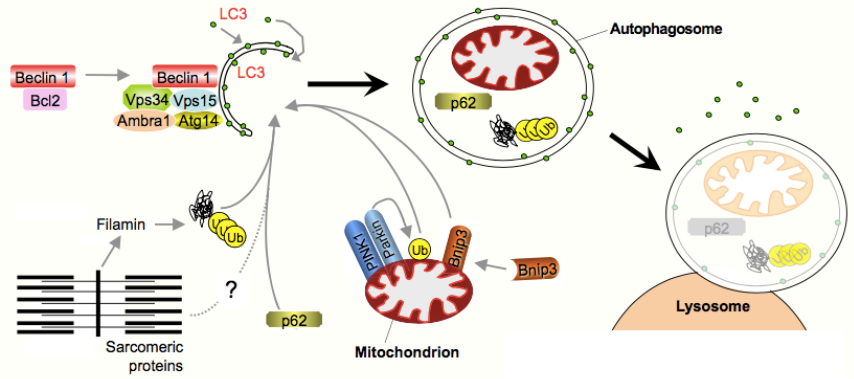

Figure 1.6. A schematic of macroautophagy activation for purpose to degrade proteins in bulk. Proteins targeted for degradation (i.e., filamin) by autophagy are tagged with ubiquitin (Ub) and transported to the site of phagophore elongation via p52. Adapted with © permission from Bonaldo *et al.*[104]

1.5.4.2 Muscle atrophy & autophagy

The up-regulation of autophagy related proteins (mostly BCN1) indicating increased protein degradation has been found in studies investigating both skeletal muscle atrophy following denervation and fasting,[104] and cardiac atrophy following denervation and mechanical unloading.[102,145] Cardiomyocyte remodelling caused by autophagy following cardiac stress was seen to be regulated by increased ANGII [146] via AT1.[96]

1.5.5 The ubiquitin-proteasome system and autophagy following SCI

Our research team conducted a study to investigate the expression of both UPS and autophagy in cardiac tissue following high-thoracic chronic SCI.[72] Male lean Zucker rats were either subjected to T3 complete transections or uninjured (CON; controls).[72] At the end of the study (12 weeks), cardiac tissue was collected for histology and gene expression analyses.[72] Unsurprisingly, cardiac mass estimated via magnetic resonance imaging (MRI) decreased by approximately 29% in T3-SCI rats compared to uninjured rats.[72] In terms of cell atrophy, the study reports similar findings to Squair *et al.* [73], with decreased cardiomyocyte length (by approximately 17%; T3 79.8 ±10.7 vs. 96.0 ±5.52 μm, $p<0.05$) and Z-line width (by approximately 19%; T3 7.25 ±0.39 vs. 8.92 ±0.23 μm, $p<0.001$) following high-thoracic chronic SCI.[72]

This cell atrophy was associated with the up-regulation of both UPS and autophagy in the T3 rats compared to uninjured rats.[72] Western blots showed significant up-regulation for MuRF1 and BCN1 proteins in T3 rats compared to CON.[72] mRNA expression analyses showed significant up-regulation of UPS (MuRF1 and MAFbx), autophagy, (ATG12 and BCN1), TGFβ receptors (TGFβR1 and R2) and ANGII receptors (AT1 and ANGII receptor 2 (AT2)) following SCI compared to the controls.[72] Additionally, T3 rats had 50% more circulating ANGII and 81% less circulating NE compared to CON.[72] Although, mechanical loading and stretch at the level of the cardiomyocytes were not quantified in this study, T3 rats experienced cardiac unloading compared to CON.[72] All results indicate cardiac atrophy to be associated with the up-regulation of proteolytic pathways chronically following high-thoracic SCI in rodents which may be partly induced by changes in neurohumonal pathways (increased ANGII), changes in neuromechanical loading (cardiac unloading) and the loss of descending sympathetic control to the heart (decreased trophic input).[72]

To decipher a time-sensitive treatment to decrease the magnitude of cardiac atrophy in the SCI population, we must first investigate when these molecular changes are occurring and then characterize in greater detail the signalling pathways and molecules involved in cardiomyocyte atrophy after SCI.

1.5.6 Temporal regulation of remodelling pathways in atrophy

Once again, although there are no published studies in the literature investigating the temporal effects of SCI on cardiac atrophy at the molecular level, some pre-clinical studies have investigated the temporal effects of denervation in both cardiac (ablation of sympathetic neurons) and skeletal muscle.[102,147–149] The ablation of sympathetic neurons with a chemical agent causes complete loss of sympathetic control to the heart, while a high-thoracic SCI eliminates the majority of supraspinal sympathetic input to the heart the sub-lesional sympathetic circuitry remain intact which may be

important for reflexive cardiac control. Although both ablation of sympathetic neurons and SCI, are drastically different procedures, the former gives us insight on the molecular events occurring in the heart when completely devoid of any SNS input and provides direction for SCI research. Furthermore, the vast majority of denervation research investigates skeletal muscle. While skeletal muscle has distinct morphological features and regenerating capacity,[1,2] its research is relevant as all myocyte types share common cellular properties.

Both Li *et al*. (skeletal muscle denervation) and Zaglia *et al*. (cardiac muscle denervation) report the up-regulation of UPS (i.e., MuRF1) at their first tested time point, one day following denervation [102,147] with a peak at day 3 post-denervation.[147] Autophagy activity was increased following day 30 post-denervation, indicating it is further activated later than UPS.[102] UPS proteins remained significantly up-regulated compared to the control at the last time point in the study of Li *et al*. (14 days post-denervation).[147] However, contrary to the results from Li *et al*. and our preliminary experimental results, Zaglia *et al*. reported normalized UPS and autophagy mRNA levels, and normalized UPS protein levels at eight days following denervation in cardiac muscle.[102,147] Additionally, Zaglia *et al.* reported a decrease in Akt-pathways (protein synthesis) at day one following denervation which remained low until study termination, one month post-treatment.[102]

As gross cardiac atrophy should be subsequent to the molecular up-regulation of protein degradation and down-regulation of protein synthesis pathways, it seems logical that cardiomyocyte atrophy would occur at a later time. In the literature, the time following denervation to cause significant atrophy is less conclusive. Significance for gross tissue atrophy was seen one,[102] three [149] and five days [150] following denervation. These inconsistencies could be due to the type of muscle (cardiac vs. skeletal), the muscle itself (gastrocnemius vs. tibialis anterior), method for denervation (pharmacological ablation of neurons vs. physical denervation) or the sample size in the analysis.

1.6 Closing remarks

Following chronic high-thoracic SCI in clinically relevant models, our research team has reported the occurrence of systolic contractile dysfunction and cardiomyocyte atrophy following severe contusion SCI and complete transection at high-thoracic levels.[72,73] Further studies in our laboratory demonstrated the up-regulation of major proteolytic pathways, UPS and the autophagy lysosomal machinery, in the heart following chronic SCI,[72] the activation of which has been shown to be critical in induction of skeletal and cardiac muscle atrophy.[72,102,151–153] Despite numerous clinical and pre-clinical studies confirming the physiological aspects of our findings (i.e., reduced LV volume and cardiac dysfunction),[19,49,73,154] our understanding of the cellular and molecular events underlying cardiac atrophy post-SCI remains limited. Moreover, there have been no studies that have investigated the temporal progression of cardiac remodelling from acute-to-chronic SCI, which impedes our ability to develop a time-sensitive treatment for this population. The study is the first to define the temporal changes in cardiac function and structure, as well as the molecular pathways underlying these responses, across the acute to chronic continuum post-SCI.

Chapter 2. Aims and hypotheses

The primary aim for this thesis project was to investigate the temporal effects of acute high-thoracic SCI on LV cardiac function (i.e., ESPVR), proteolysis (i.e., gene expression of key UPS and autophagy targets) and cardiomyocyte atrophy (i.e., cardiomyocyte length and width). This overarching aim was tested as three different questions.

1) Does cardiac dysfunction begin to occur in the acute phase following high-thoracic SCI? If yes, when does it begin to occur?
2) Is there a change in the regulation of the two-main intracellular proteolytic pathways (UPS and autophagy) in the acute phase following high-thoracic SCI? If yes, when does it begin to occur?
3) Is LV cardiomyocyte atrophy significant in the acute phase following high-thoracic SCI? If yes, when does atrophy begin to occur?

Hypothesis 1. Systolic dysfunction will occur immediately following high-thoracic SCI due to immediate loss of cardiac descending supraspinal sympathetic control, while diastolic dysfunction will not occur in the acute phase of SCI due to there being no sufficient time for structural remodeling.

Hypothesis 2. There will be an up-regulation of proteolytic pathways occurring during the acute phase following high-level SCI. As UPS activity can be altered by sympathetic input [102], humoral levels[72] and mechanical loading,[105,122] and as there is an immediate loss of cardiovascular descending sympathetic control and loss of lower-limb muscle control following T3-SCI, UPS regulation will increase immediately post-SCI and will then decrease back to basal levels while remaining at a higher level than pre-injury. Contrarily to UPS, there is no clear picture of the timeline of autophagy regulation following neural trauma and it is therefore difficult to hypothesize an exact timing. Autophagy will be up-regulated within the acute timeline post-SCI in cardiac tissue due to the immediate changes in blood pressure and subsequent increase in circulating ANGII, which is known to activate the pathway.[72,98,126,155]

Hypothesis 3. As atrophy should be subsequent to the shift in protein homeostasis, LV cardiomyocyte atrophy will occur after the upregulation of proteolytic pathways and therefore will be discernible multiple days following high-thoracic SCI.

Chapter 3. Materials and methods

3.1 Overview

A schematic overview of the methods can be found in Figure 3.1. Male Wistar rats (n=49) were assigned to two groups which differed in the type of surgery: a dorsal durotomy with no SCI (SHAM) or a complete transection at the 3rd thoracic segment (T3-SCI). To study the temporal effects of acute SCI, T3-SCI animals were terminated at different time points along the acute timeline: 12 hours (n=9), 1 day (n=8), 3 days (n=10), 5 days (n=7) and 7 days post-SCI (n=9). SHAM rats were euthanized at the last time point, 7 days post-operatively (n=6). At pre-intervention and at different time points along the acute timeline (1 day, 2 days, 4 days and 6 days post-surgery), volumetric and functional cardiac indices were obtained *in vivo* via echocardiography in the 7-day T3-SCI and SHAM groups. At termination, for all groups except the 12-hour group, functional load-dependent and -independent cardiac indices were obtained via LV PV catheterization. Following all euthanasia, cardiac tissue was harvested for all groups to assess cardiomyocyte morphology via immunofluorescence and to quantify gene expression of key targets of the two main proteolytic pathways. Furthermore, femurs were collected and measured to standardize cardiomyocyte dimensions.

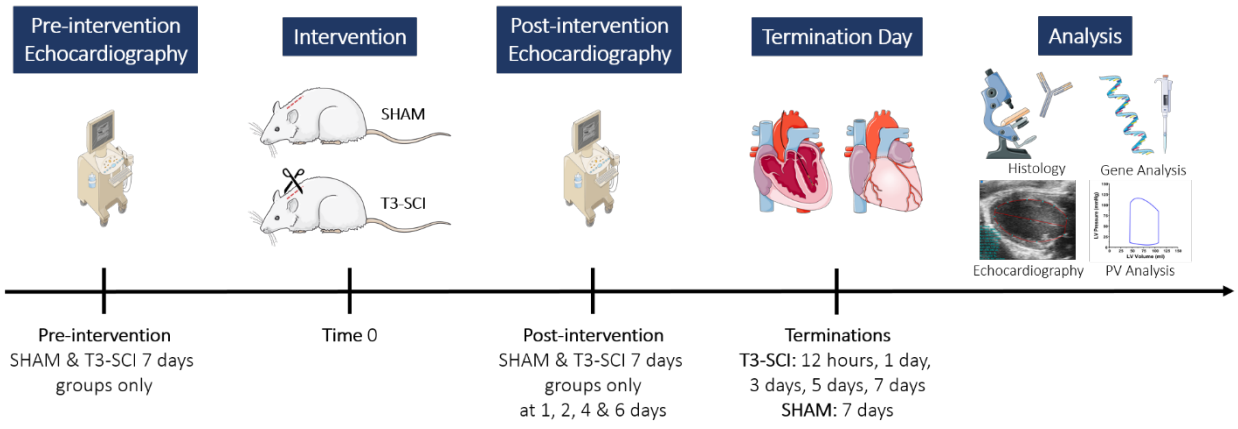

Figure 3.1. Overview of methods. PV, pressure-volume; SHAM, dorsal durotomy with no SCI; T3-SCI, SCI at 3rd thoracic segment. Images used from © Servier with permission (licensed by CC BY 3.0).

3.2 Ethics and disclaimer

Ethics approval was granted by UBC. All staff in contact with the animals were certified and trained by the UBC Animal Care Committee. All protocols involving the use of animals and biological tissue were conducted in strict accordance with the Canadian Council for Animal Care. All techniques and equipment employed in this study have been used frequently in our laboratory in the past; thus, familiarity with data collection and analysis was not of any concern. Additionally, to ensure the collection of reliable data, each procedure (i.e., surgery, tissue excision, tissue sectioning, confocal imaging, etc.) was performed by the same individual throughout the study. Finally, all data were blinded for analysis.

3.3 Animals

Due to the high number of replicates required, rats were the most adequate animal model for such study. We decided to use male Wistar rats as they have commonly been studied in the field of high-thoracic SCI for over 15 years and animal care for this type and level of SCI, sex and strain has been developed in great detail at our facility.[156] The Wistar strain has been repeatedly used in studies investigating the effects of SCI on the cardiovascular system.[73,99,154,157] Furthermore, males were chosen over females for consistency with previous pre-clinical cardiovascular-SCI research and because males constitute over 74% of the Canadian human population with traumatic SCI.[44] A total of 49 rats were ordered from Charles River Laboratories (Wilmington, MA, USA) to be between the age of 10-11 weeks old and approximately 300 to 325 g. It was crucial for rats to not vary in age (>1 week of age) to minimize differences in heart size changes due to maturation. Rats were received at the animal care facility (ICORD Vivarium) at least 7 days before the beginning of the study to allow for acclimatisation to their new environment, diet, handling, restraint and staff.

3.4 Groups and termination time-points

There were six groups of rats which differed in surgery type (T3-SCI versus SHAM) and termination time-points. 43 rats underwent a complete transection SCI at the T3 level and six rats underwent a dorsal durotomy with no damage to the SC (SHAM). SHAM rats served as controls to reduce the effects of surgery as confound variables (i.e. injections, drugs, anesthesia, anxiety, frequent handling and restraint, post-operative pain, etc.).

We were interested in the acute phase of SCI, which is generally defined to be up to one week post-SCI in rats.[158–160] The time of the T3-SCI was considered to be time=0 and five endpoints were investigated along the acute timeline. The following times were chosen for a temporal homogenous spread: 12 hours, 1 day, 3 days, 5 days and 7 days post-SCI.

While reviewing chronic studies from our research group with similar procedures and outcomes, a post-hoc G*Power (v. 3.1.9.3) analysis indicated that for 80% power a sample size of two-to-four animals per group would be sufficient to detect a between-group comparison for the key functional outcome, ESPVR, and a sample size of four-to-six animals per group for the key structural outcomes, cardiomyocyte length and width. Due to high mortality following this SCI model (0-10%),[156] a sample size of eight rats was chosen to account for such possibility. For our controls, we deemed sufficient to retain a sample size of six SHAM rats to be terminated on day 7 post-surgery (the last endpoint).

Group 1: Complete T3 SCI and terminated at 12 hours post-SCI (T3-SCI 12 hours)

Group 2: Complete T3 SCI and terminated at 1 day post-SCI (T3-SCI 1 day)

Group 3: Complete T3 SCI and terminated at 3 days post-SCI (T3-SCI 3 days)

Group 4: Complete T3 SCI and terminated at 5 days post-SCI (T3-SCI 5 days)

Group 5: Complete T3 SCI and terminated at 7 days post-SCI (T3-SCI 7 days)

Group 6: Dorsal durotomy with no SCI and terminated at 7 days post-durotomy (SHAM)

Table 3.1. List of investigated dependent variables, organized per method

Method and outcome	Variable	Notes
Echocardiography (PSLAX)		
Volumes	EDV (μL)	Index of preload
	ESV (μL)	
Systolic function	SV (μL)	
	CO (mL/min)	
	EF (%)	
	FS (%)	
Catheterization		
Arterial hemodynamics	SBP (mmHg)	
	DBP (mmHg)	
	MAP (mmHg)	Index of afterload
	HR (bpm)	
LV systolic function	ESPVR (mmHg/μL)	Index of contractility
	SW (mmHg*mL)	
	Pmax (mmHg)	
	Pdev (mmHg)	
	dP/dt_{max} (mmHg/s)	
	TPR (mmHg/mL)†	Index of afterload
	Ea (mmHg/μL)	Index of afterload
	Ea/ESPVR	Index of ventricular-arterial coupling
	PRSW (mmHg)	
LV diastolic function	$-dP/dt_{min}$ (mmHg/s)	
	Ped (mmHg)	
	Tau (ms)	
Histology		
Cardiomyocyte dimensions	Length (μm)	Measured with connexin-43
	Width (μm)	Measured with α-actinin
	CSA (μm^2)	Measured with WGA
	Volume (μm^3)	Measured with CSA and length
Gene analysis		
RNA extraction, cDNA synthesis and qPCR	Fold change each target	Targets in Table 3.2.

CO, cardiac output; CSA, cross-sectional area; DBP, diastolic blood pressure; dP/dt_{max}, maximal rate of systolic pressure increment; $-dP/dt_{min}$, maximal rate of diastolic pressure decrement; Ea, arterial elastance; Ea/ESPVR, ventricular vascular coupling ratio; EDV, end-diastolic volume; EF, ejection fraction; ESPVR, end-systolic pressure-volume relationship; ESV, end-systolic volume; FS, fractional shortening; HR, heart rate; LV, left-ventricle; MAP, mean arterial pressure; Pdev, developed pressure; Ped, end-diastolic pressure; Pmax, maximum pressure; PRSW, preload recruitable stroke work ; PSLAX, parasternal long-axis view; SBP, systolic blood pressure; SV, stroke volume; SW, stroke work; Tau, diastolic time constant; TPR, total peripheral resistance; WGA, wheat-germ agglutinin. †, TPR calculated with CO obtained via echocardiography and MAP obtained via catheterization (TPR=MAP/CO).

3.5 Issues with internal validity

Independently, age, weight-loss, reduced physical activity and stress can cause cardiac atrophy.[101] Therefore, it was critical to control for such confounds. All rats were ordered to be the same age and were fed an enriched diet pre- and post-surgery to avoid excessive weight loss following the intervention. Due to the loss of motor control in their hind limbs, rats required additional help to move around their cages to find food, water and shelter. Therefore, to help with mobility and to promote physical activity, cages were equipped with plastic grids underneath the bedding for rats to grasp and facilitate locomotion. Proper acclimatization to their new environment is crucial to reduce confounds, to ensure data reliability, to alleviate anxiety and post-intervention complications.[156] Therefore, animals arrived at the facility and were started on their new diet a week prior to the first intervention. Additionally, animal care personnel visited the rats daily with gradual increases in handling time and frequency to ensure human contact became stress-free before surgery day.[156]

3.6 Pre-surgery animal care

3.6.1 Housing

The rats were located in rooms with controlled temperature and 12-hour light-dark cycles. All rats were housed in 250 cm^2 cages containing a maximum of 4 cagemates. No animals were housed individually as they require social enrichment. For the comfort of the rats, cages included bedding and transparent red polycarbonate huts. Cages were changed regularly to ensure bedding remained dry to avoid any possible infections.

3.6.2 Nutrition and hydration

All groups were fed an enriched diet before the start of the study (i.e. normal rat chow in addition to cereal, fruit, spinach, nutritive transport gel, etc.). As previously mentioned, an enriched diet is critical

to avoid any cardiac atrophy due to total weight loss following SCI for the T3 animals. In addition, it is required to acclimatize the rats to the diet before surgery to avoid any reluctance to ingest new foods during post-operative care. Water and food were provided ad libitum.

3.6.3 Antibiotics

Enrofloxacin was administered to the rats subcutaneously once a day, three days pre-operatively (Baytril, 10 mg/kg).

3.7 Pre-surgery data collection: echocardiography (for T3-SCI 7 days and SHAM groups)

The clinical literature indicates preference for MRI imaging over all types of echocardiography for more precise and accurate measurements of cardiac structure.[161,162] However, due to smaller hearts and higher HR in rodents, MRI has not yet been claimed the gold standard for pre-clinical rodent cardiac imaging.[163] With echocardiography, high frame rates can be achieved for greater temporal resolution,[163] which is advantageous for our model. We used a transthoracic echocardiography system (Vevo 3100 imaging system, FUJIFILM VisualSonics) with a rodent transducer (MX250; 13-24 MHz liner array transducer) (used in [73,99,154]). As we were interested in the difference between pre- and post-operative measures along the acute timeline, this method was deemed adequate and non-invasive for our purposes. A parasternal long-axis (PSLAX) view with B-mode imaging was obtained and used to assess systolic function and volumes. The latter were obtained by tracing the epicardial border of the LV. All analyses were performed after data collection with commercially available software (Vevo Lab). For all echocardiographic variables, see Table 3.1.

Due to the non-invasive nature of echocardiography, the animal was anaesthetized with isoflurane alone (first with 5% induction with 2 L min^{-1} O_2 in an induction box then 1-2% induction with a nose cone). For this procedure, the rat was shaved ventrally (thoracic area) and lightly attached to the

ultrasound platform with surgical tape. The lubricated probe was placed on the rat's thorax to image the heart to obtain echocardiography images. During this procedure, the ventilation and heart rate of the animal was monitored at all times. Once the procedure was completed, the rat was placed individually in a clean and comfortable cage to be monitored closely until anaesthesia fully wore off.

Echocardiography images for these groups (T3-SCI 7 days and SHAM) were taken at pre-intervention, 12 hours, 1 day, 2 days, 4 days, and 6 days post-surgery under isoflurane.

3.8 T3-SCI and SHAM surgeries

All staff present in the surgical room were certified for their specific tasks. All equipment and solutions were aseptic and sterile, respectively.

3.8.1 Anesthesia and preparation

After weighting the animal, the rat was anesthetized with inhalant isoflurane in a clean induction chamber lined with paper towel (5% induction with 2 L min^{-1} O_2). Once the animal had lost the righting reflex, the animal was taken out of the induction chamber to be placed on its ventral side and fitted with a nose cone (1-2% induction with 2 L min^{-1} O_2, depending on depth of anesthesia of the animal).

To avoid drying of the eyelids and the cornea, ocular lubricant was generously placed on the entire eye of the rodent. To prepare the site for dorsal durotomy, the site of incision was shaved and disinfected three times with alternating chlorhexidine (Hibitane) and 70% alcohol. Pre-surgical care (i.e., shaving and disinfecting) was performed as instructed by the UBC Animal Care Committee to reduce any risks of contaminating the surgical wound. To avoid dehydration during surgery, warmed Lactated Ringer's solution was injected subcutaneously before surgery (10 mL/kg).

Combination of analgesics and antibiotics was injected subcutaneously: buprenorphine (Temgesic 0.02 mg/kg) and enrofloxacin (Baytril 10 mg/kg). Once all pre-surgical care was completed and the

palpebral and toe pinch reflexes were lost, surgery was commenced. At any point, if the animal showed any signs of a lack of oxygenation or had an irregular respiration rate, all procedures were paused immediately to attend to the animal's needs.

At all times during pre-operation preparation, durotomy, SCI and immediately post-operative care, the animal remained on a heat source (i.e., water-circulating blanket) or in an incubator to keep body temperature at 37°C degrees.

3.8.2 Dorsal durotomy (for both SHAM and T3-SCI animals)

The animal was placed in a prone position and a 5 mL syringe was positioned underneath its neck to elevate the thoracic vertebrae. The surgeon palpated the vertebral column to locate the T2 vertebra thanks to its uniquely long neural spine. An incision at the dorsal midline from C8-T2 was done with a scalpel. Next, with blunt scissors, the trapezius was carefully dissected. Once again, the neural spine of T2 was located and this allowed to attain and cut the dura between the T2 and T3 vertebrae with micro-scissors. For SHAM animals, the intervention stopped at this stage.

3.8.3 Spinal cord injury (only for T3-SCI animals)

After the opening of the dura was achieved, the surgeon cut the SC with micro-scissors and suctioned a segment of approximately 0.5 cm at the T3 level. With a dissecting microscope, the surgeon ensured a complete injury with no remaining tissue connecting the two blunted ends of the SC. Gelfoam, a hemostatic, was placed between the rostral and caudal ends to stop potential bleeding, fill the now empty space and ensure no touching of the newly blunted ends. All surgical tools were autoclaved for each first use of the day and sterilized with a glass bead sterilizer between individual surgeries.

Although, a complete transection is not the most common type of injury in the clinic as most injuries can be defined as partial or combinations of lacerations, contusions and compressions,[164] severe

contusions and complete transections at high-thoracic levels have shown to have nearly identical effects on the cardiovascular system in a rodent model.[73,99] A complete injury was chosen as this type of injury, where the possibility of differential sparing at the site of injury is minimal, is preferred in experimental scenarios due to increased consistency between subjects compared to a contusion, and our research team has reported preserved cardiac function with 10% of sparing.[99] Additionally, the majority (55%) of SCI patients suffer from cervical injuries.[165] Therefore, in regard to the level of injury, it would be most clinically valid to utilize a model with a higher-level injury than T3. However, a higher-level injury could damage the nerves innervating the rat forelimb muscles (C2-T1 [166]), which could paralyze the forelimbs and incapacitate the rats to groom and move around the cage to find food and water. In addition, as the level and severity of the injury is increased, the risk for secondary complications, including cardiovascular dysfunction, is increased.[74,167] To avoid tetraplegia and jeopardizing the rats' well-being, a T3 injury has been commonly administered in the field of SCI as a compromise.[156] Due to the expansion of the secondary injury in the SC, a T3 injury will damage most of T2 and part of T1, essentially causing the loss of sympathetic control to the heart without rendering the rats tetraplegic as most SPN originate at the T2 level in rats.[168] Although, animal care for T3 rats remains challenging, a group of researchers from our facility have implemented an animal care protocol for this model which helped to ensure the best possible management for the rats and to minimize the burden of high-thoracic SCI compared to lower level injuries.[156]

3.8.4 Suturing

The trapezius muscle was sutured with continuous absorbable monocryl (4-0). Whereas the skin was sutured with interrupted non-absorbable prolene (4-0).

3.9 Post-surgery animal care

3.9.1 Immediately post-operation

All animals, which underwent surgery (durotomy + T3-SCI or durotomy alone), were placed in a thermo-regulated incubator (37°C degrees), immediately following suturing. The incubator was lined with simple laboratory mats to avoid heat loss and eye irritation from bedding particles. Staff closely monitored the rats every 5-10 minutes until all anesthesia effects had worn off. Water gel and treats were given close to the animals as mobility was impaired by analgesics and previous anesthesia. Once rats were recovered from the anaesthesia, they were placed in their initial cages and monitored every hour up to 8 hours post-operation.

3.9.2 Continued antibiotics & pain management

Following the surgeries, the same analgesics and antibiotics (buprenorphine every 12 hours and enrofloxacin every 24 hours) were administered subcutaneously for a duration of 3 days post-operatively and if needed.

3.9.3 Housing, nutrition and hydration

The same housing arrangements as described above in *pre-surgery animal care* were respected (Section 3.6.1.). One difference post-operatively was the choice of bedding. Oats were used up to three days post-intervention as under analgesics rats tended to chew on the regular bedding. To avoid constipation and intestinal blockages, we decided to place the rats on a comestible bedding with abundant leaves of spinach. In addition, to encourage movement of paraplegic rats, rubber grids were placed under the bedding to provide grip surfaces. Water and the enriched diet were continued to be provided ad libitum. Food was made to be easily accessible and placed at distinct areas to promote

physical activity from the paraplegic animals. Once again to avoid dehydration, additional warmed lactated Ringer's solution was injected subcutaneously as needed.

3.9.4 Bladder care

During the first week following high-thoracic SCI, T3-SCI animals had their bladders expressed manually by staff as micturition (i.e., detrusor muscle, urethral sphincters and bladder neck, which are innervated from the sympathetic T10-L2 and parasympathetic S2-S4 nerves) was temporarily impaired.[156,169] Gentle and careful bladder care is crucial to avoid rupture of the bladder.[156] The reflexive micturition commonly returns within one week to 10 days.[156] However, due to the endpoints of this study, bladder care was performed for all T3-SCI animals until euthanasia. Additionally, sperm blockages were removed and bladders were emptied at least four times a day, every 6-8 hours.

3.9.5 Health assessments

The rats were closely monitored four times daily. Upon the first morning visit of each day, rats were weighted and assessed for weight loss, physical appearance, behaviour, clinical signs, wounds and any other concern. To aid distinction of pain levels in rodents, staff utilized the Facial Rat Grimace scale.[170] Even though experts have been skeptical of this scale,[171] it was followed, per the suggestions of the UBC Animal Care Committee, in addition to other behavioural indices (i.e., grooming, arching, flinching, abdominal press, writhing, staggering and twitching). All data per rat were manually recorded onto monitoring sheets and added up to obtain a total score. If the score equaled or exceeded 20 points, the rat was to be euthanized. Fortunately, this never occurred in the present study.

3.10 Termination day data collection: *in vivo* outcomes

3.10.1 Anesthesia

The animal was anaesthetised under urethane (1200-1500 mg/kg) instead of inhalant isoflurane because urethane provides a more stable anesthetic for long-term surgical procedures, such as LV catheterization.[66] Urethane was administered via intraperitoneal injection in small increments every 15 minutes until the animal was at surgical plane (loss of righting, palpebral and toe-pinch reflexes).

3.10.2 Catheterization

For LV catheterization, rats were verified to be in surgical plane under urethane anaesthesia and placed in a supine position. The following are widely-used procedural steps for the insertion of the admittance PV catheter (Transonic, 1.9F rat PV catheter) into the LV and these can be found in greater and pictorial detail in Nature Protocols.[66]

First, the rat's neck was elevated with a 5mL syringe. The surgeon made an incision from the lower jaw to the sternum through cutaneous, subcutaneous tissue and superficial muscles. All tissue (i.e. salivary glands, sternohyoid and sternomastoideus muscles) obstructing the right carotid and trachea was carefully displaced to the side. At this stage, the rat underwent a tracheotomy to be intubated for the potential need of supportive respiratory care. Once the carotid was isolated from surrounding tissue and from the vagal nerve, a total of three sutures were required. Two sutures were looped and tightly held around the most anterior and posterior ends of the artery. The last suture was loose and placed towards the middle of both previous sutures, which would later serve to secure the catheter to the carotid once placement was ideal within the animal. Thanks to the sutures in place, the carotid was able to be lightly stretched allowing the surgeon to incise its anterior end. The catheter, pre-soaked in warm saline, was advanced posteriorly through the micro-incision in the carotid. Once the catheter was inside the carotid

artery, the posterior suture was released and the catheter was quickly advanced approximately 2-3 cm into the artery, after which the middle suture was lightly fastened to keep the catheter in place and to prevent any bleeding. The animal was left to rest for 10 minutes after which basal arterial data were collected once fully stable (i.e., systolic, diastolic and arterial blood pressures, and heart rate). After the collection of arterial data, the catheter was inserted via pressure guidance and guided by echocardiography, if required. The ideal position of the admittance PV catheter in the LV was checked and confirmed by echocardiography. Following another 10 minutes of rest and stable vitals, basal PV LV data were recorded for 10 minutes. All data were collected via Labchart 8.1 (AD Instruments, USA) with the PVAN add-on, which is capable of generating and displaying the corresponding PV loops in real-time.

From these PV loops, collected at baseline, many cardiac load-dependent indices are measured and used to infer systolic and diastolic function (listed in Table 3.1.). Such cardiac indices include volumes and pressures: end-systolic volume (ESV), EDV, SV, end-systolic pressure (Pes), end-diastolic pressure (Ped), LV developed pressure (Pdev) and minimum and maximum pressures and volumes (Figure 3.2.A.). The area of the loop can be measured to infer stroke work (SW), the amount of work done by the ventricle (Figure 3.2.A.). Arterial elastance (Ea) is the ratio of LV Pes to SV and a measure of afterload (Figure 3.2.A.). The remaining indices such as tau, dP/dt_{max} and $-dP/dt_{min}$ are measured via Labchart.

Next, to obtain load-independent measures, inferior vena cava (IVC) occlusions were performed by isolating the blood vessel via a ventral laparotomy (closed-chest approach). Occluding the IVC with a cotton-tip applicator allowed for reduced venous return to the heart. This generated multiple PV loops with changing preload. Load-independent measures are important to infer the intrinsic function of the heart and not of the entire cardiovascular system (listed in Table 3.1.). From an occlusion, we measured two functional variables: preload recruitable stroke work (PRSW; relationship between SW and EDV) and

ESPVR. ESPVR is an index of contractility and is the linear slope connecting all end-systolic PV points (Figure 3.2.B.).

In this thesis, systolic function from catheterization data was inferred with the following indices: maximum pressure (Pmax), Pdev, SW, dP/dt_{max}, Ea, ESPVR and PRSW. How well the heart and vasculature are working together was measured via the ventricular-arterial coupling ratio, which is calculated by dividing Ea by ESPVR (Ees). Concerning diastolic function, it was inferred with dP/dt_{min}, Ped and tau. Cardiac volumes, CO, EF and FS were inferred from echocardiography data due to higher accuracy.

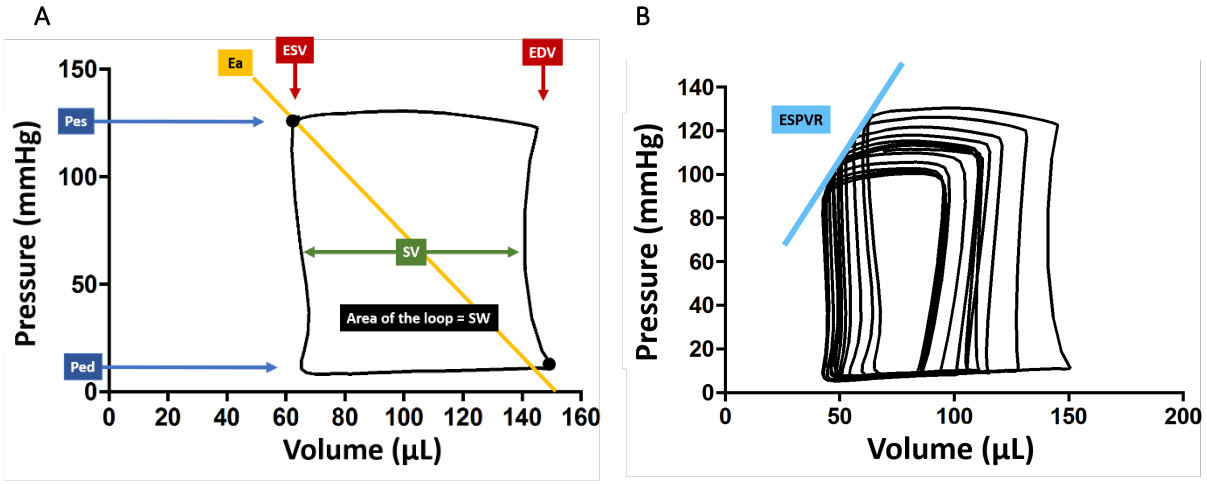

Figure 3.2. Representation of pressure-volume data obtained via left-ventricle catheterization and inferior vena cava occlusions. In *panel A*, one pressure-volume loop is shown with its labeled cardiac indices obtained from the baseline recording. In *panel B*, a series of loops was generated via IVC occlusions to measure ESPVR. Ea, arterial elastance; ESV, end-diastolic volume; ESPVR, end-systolic pressure-volume relationship; ESV, end-systolic volume; Ped, end-diastolic pressure; Pes, end-systolic pressure; SV, stroke volume; SW, stroke work.

3.11 Euthanasia

3.11.1 Surgical endpoints

At the end of the *in vivo* outcome procedures, as the rat remained under deep urethane anesthesia, a last reflex check was performed before euthanasia. Euthanasia was completed after the

righting, palpebral, toe-pinch reflexes were all confirmed to be lost. To euthanize the anesthetized animal, a bilateral pneumothorax cut (from the posterior end of the thoracic cavity) and an excision of the heart were performed.

3.11.2 Non-surgical endpoints

If at any time an animal was suffering of physical injuries, such as severe self-mutilation, unhealable wounds or was unable to eat or drink, the animal was planned to be euthanized. As mentioned previously, all abnormal behaviours, physical injuries and weight loss were recorded as part of the regular daily monitoring and if the score equaled or exceeded 20 points, euthanasia was to be performed. Fortunately, no abnormal behaviours were noted and no rats were euthanized prior to the experimental endpoint.

3.12 Collection of tissues

3.12.1 Cardiac tissue post-mortem

After completion of the bilateral pneumothorax procedure, the lower posterior half of the heart was excised for molecular investigation. The apical portion of the heart was sectioned for gene analysis (mRNA extraction, cDNA synthesis and qPCR). For tissue destined for mRNA quantification, the tissue was placed immediately in RNA later solution in 4°C degrees overnight before the suctioning of the solution and storage at -80°C degrees. Once the apex was excised, transcardial perfusion was achieved first with phosphate-buffered saline (PBS) then with 4% paraformaldehyde for fixation. After successful fixation, a cross-sectional cut at mid-ventricular level was collected for histology and sent to Wax-it Histology Services at UBC for paraffin embedding.

3.12.2 Femur post-mortem

The femur was collected following completion of fixation. The femur was then later measured in length (cm) for the standardization of structural cardiac indices.

3.13 Genetic analysis

3.13.1 RNA expression – mRNA extraction, cDNA synthesis and PCR

To measure gene expression, the dorsal lateral quadrant of each apex (previously stored in -80°C degrees) was thawed and manually dissected with sterile surgical blades. First, RNA extraction was performed following via the Invitrogen TRIzol™ Reagent procedure (Thermo Fischer Scientific 15596026). The only modification to this protocol was an increased incubation time of 12 hours in isopropanol at -20°C. Before proceeding to cDNA synthesis, RNA concentration, purity and integrity was controlled via a spectrophotometer at optical densities of 260 and 280 nm (NanoDrop™ 2000; Thermo Fisher Scientific). An A260/A280 ratio of approximately 1.8-2 was deemed pure and acceptable for continuing on. Part of the controlled RNA underwent reverse transcription into cDNA via the SuperScript™ VILO™ MasterMix protocol (Thermo Fisher Scientific 11755-50). To amplify and quantify the cDNA, samples were loaded (in duplicates, which were later averaged) in the Applied Biosystems™ ViiA 7 Real-Time PCR System (Applied Biosystems), using the PowerUp™ SYBR® Green PCR Master-Mix kit (Applied Biosystems A25780). The fold changes of each target were calculated with the ΔΔCt method compared to SHAM and compared to the housekeeping gene β-actin.

3.13.2 UPS and autophagy targets investigated

To investigate proteolytic activity, the gene expression of key targets of UPS and autophagy pathways were investigated. The chosen targets and their primer sequences are reported below in Table 3.2.

Table 3.2. Targets investigated

Pathway	Target	Primer Sequence (forward and reverse)
UPS	*MAFbx*	5'-ACTTCTCAGAGCGGCAGATCC-3'
		5'-CTCTGGGTTGTTGGCCGT-3'
	MuRF1	5'-GCAGGAATGCTCCAGTCGG-3'
		5'-GTGAGCCCCGAACACCTT-3'
Autophagy	*ATG7*	5'-AGACCTTGAGCGTGCGTATG-3'
		5'-AACTGCTACTCCATCTGTGGG-3'
	ATG12	5'-CCCAGAAACAGCCATCCCA-3'
		5'-TCACATAAATAAACAACTGCTCCGA-3'
	BECN1	5'-CGTCGGGGCCTAAAGAATG-3'
		5'-GCTCTCTCCTGGTTTCGCC-3'
Housekeeping	*β-actin*	5'-GGGAAATCGTGCGTGACT-3'
		5'-GCGGCAGTGGCCATCTC-3'

ATG7, autophagy related 7; ATG12, autophagy related 12; BECN1, beclin 1; MAFbx, muscle atrophy F-box; MuRF1, muscle RING-finger protein 1.

3.14 Histology

Once a cross-sectional disc of the heart at mid-ventricular level, destined to histology, was excised from the organism, the tissue was fixed, dehydrated, embedded in paraffin (as explained in Section 3.12.1.) and sectioned at 7 μm before proceeding to staining.[3] In this study, we used immunofluorescence to visualize target proteins and study LV cardiomyocyte morphology.

3.14.1 Staining for cardiomyocyte morphology

To study cardiomyocyte morphology, we used immunofluorescence histology on a cross-section of the heart. After sectioning our tissue at a depth of 7 μm per slice with a microtome, the deparaffinising process (with different concentrations of xylene and ethanol) was followed by rehydration, antigen-retrieval with tri-sodium citrate buffer, washes with PBS with Triton (PBS-T 1%) for permeabilization of

the plasma membrane and 2-hour blocking of the tissue (1% bovine serum albumin (BSA) and 10% normal donkey serum (NDS); for the prevention of non-specific binding of antibodies). The primary (on for overnight) and secondary Abs (on for 2 hours) solutions (diluted in 1% BSA) were then sequentially added to the slides. Before mounting the slides, multiple PBS-T washes were performed to wash off any excess secondary Abs (3 x 5 min). Finally, DNA was stained with Hoechst's for nuclear staining (3 x 5 min with PBS), which was followed by multiple required washes (3 x 5 min with PBS) and three dips in distilled water.

We used a quadruple stain technique to visualize: 1) the cell membranes with wheat germ agglutinin (WGA 1:2000, Thermo Fisher Scientific 1853992), 2) the Z-lines with α-actinin (rabbit primary 1:400, Abcam EP2529Y; secondary 1:1000 donkey anti-rabbit AF546, Jackson ImmunoResearch 711-586-152), 3) the gap junctions located at the intercalated discs with connexin-43 (goat primary 1:1000, Cedarlane NBP1-51938; secondary 1:1000 donkey anti-goat AF647, Jackson ImmunoResearch 705-606-147), and 4) the nuclei with Hoechst stain (Hoechst 33342 reagent 1:10000, Thermo Fischer Scientific 1874027). The entire protocol is a three-day process and results in a quadruple immunofluorescence stain which serves to visualize, under a confocal microscope (Zeiss Axio Observer, equipped with a Yokogawa Spinning Disk), single cardiomyocytes longitudinally or in a cross-sectional manner in the myocardium, both depicted in Figure 3.3.

WGA is a lectin, which binds carbohydrates located on the plasma membrane of all mammalian cells.[172] Under the confocal microscope, the cells appear to be delineated by green, which facilitates width, length and cross-sectional area (CSA) measurements. To measure cardiomyocyte width, we stained for α-actinin, a protein located at the Z-lines of the sarcomeres.[13,14] It functions to keep the thick filaments in place within the hexagonal structure of a sarcomeral unit.[13,14] The neighboring α-actinin proteins in one cell form a linear structure across the cardiomyocyte, allowing us to measure width. It is

important to ensure the red line being measured is straight and not bent. If bent, it could possibly be two overlapping cardiomyocytes and lead to an incorrect measurement. To measure cardiomyocyte length, connexin-43 is stained and visualized. Six connexin-43 proteins form a connexon and two connexons in adjacent cell membranes form a gap junction at the cardiac intercalated discs (end-plates).[2] As discussed earlier, gap junctions serve to relay signals from cell-to-cell; in cardiac tissue more specifically, they communicate electrical signals for the purpose of actuating cardiac contraction.[2]

3.14.2 Imaging

One heart section per rat was imaged. A minimum of 10 images per section were taken at 20x magnification with a confocal microscope. Both longitudinally (located in the myocardium) and cross-sectionally oriented (located in the sub-epicardium) myocytes were imaged to measure length and width, and CSA, respectively. All imaging was performed in the free wall of the LV.

3.14.3 Analysis

All measurements of length, width and CSA were performed in ImageJ by a blinded individual (Fiji, bundled with 64-bit Java 1.8.0 112, version 1.52e). All cardiomyocytes with measurable indices and confirmed identity (presence of α-actinin in the cytoplasm) were quantified. For CSA analysis, to ensure consistent measurement along the cell, it must have had a red-stained cytoplasm and a centrally located nucleus. We have used a method to automate CSA measurements with ImageJ which involved an image conversion to grayscale (8-bit) then the application of a B&W threshold and dark-background. This allowed us to automate the measurement in one-click. For accuracy and verification, the selection of the cells was done manually.

When processing the heart, we could not control for which stage in the cardiac cycle the cardiomyocytes were fixed (i.e., contracted or relaxed) and how the cardiomyocytes were sectioned (i.e.,

at or away from the midline of the cell) which could affect length and width measurements, respectively. Therefore, to prevent the underestimation of cardiomyocyte dimensions, we had a high sample size per group and analyzed a high number of cells per rat. In total, a minimum of 130 lengths, 210 widths and 100 CSA measurements were measured per rat. All cardiomyocyte dimensions, were averaged per rat and then per group. Cardiomyocyte volume (assumed to be of cylindrical shape) was calculated by multiplying CSA and length.

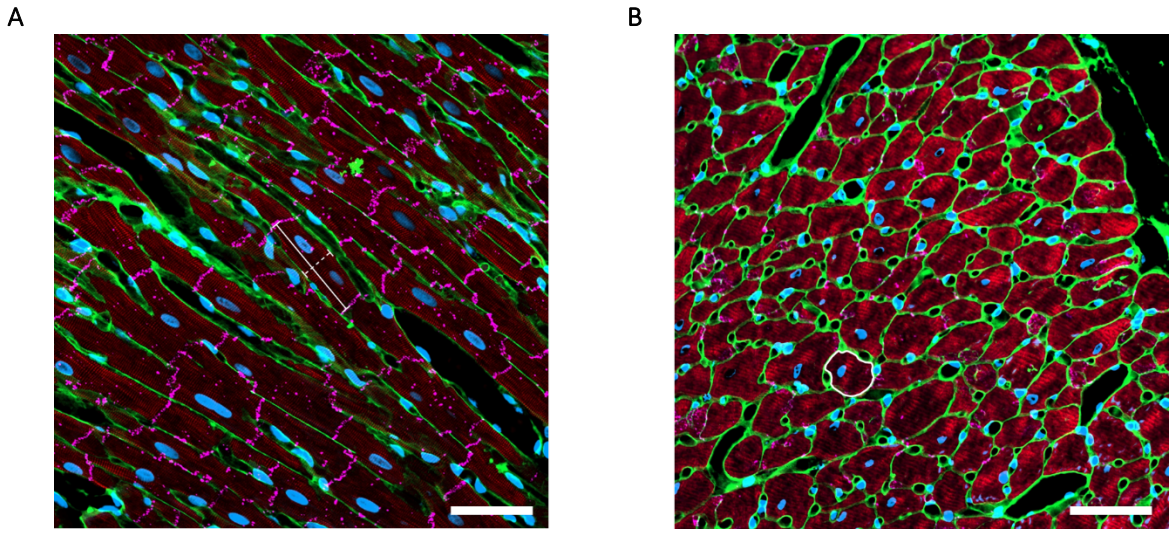

Figure 3.3. Quadruple immunofluorescent stain to visualize and measure cardiomyocyte dimensions. Wheat germ agglutinin, green; α-actinin, red; connexin-43, pink; Hoechst nuclei staining, blue. These images were taken with a confocal microscope at a magnification of x20 with a scale bar of 50μm. *Panel A*, longitudinal view of the myocardial free-wall of the LV. The solid and dotted lines represent a cardiomyocyte length and width, respectively. *Panel B*, cross-sectional view of the sub-epicardial/epicardial free-wall of the LV, with a circled representative CSA measurement.

3.15 Statistics

All descriptive and statistical inferential tests were performed with GraphPad Prism (version 6.0e) with set α=0.05 ($p<0.05$). Before inputting inferential statistics, we performed outlier (Q=5%) and normality tests. Kurtosis and skewness were used to determine if the data sets were normal or not;

values between ± 1.96 were deemed normal. Variables which showed normality were analyzed with parametric tests and the ones that violated normality were analyzed with non-parametric tests.

For demographic data (i.e., body mass at pre-intervention and at termination, and femur length), ANOVAs were performed with Tukey's post-hoc test (all group comparisons) to investigate between-group differences as body mass loss can affect cardiac atrophy and femur length was used for standardization. For all longitudinal analyses (i.e., echocardiography pre- and post-intervention) for the SHAM and 7 days T3-SCI groups, we performed two-way repeated measures ANOVA (time x group) with Dunnett's post-hoc comparisons (within-group) and Sidak's post-hoc comparisons (between-group). For histological and molecular analyses, all replicates per rat were averaged. All PV measures, cardiomyocyte dimensions and mean target fold changes were statistically analyzed with one-way ANOVAs for between-subject analyses (group). If data were normal, a Dunnett's post-hoc comparison (all groups compared to SHAM) was performed. If data were non-normal, a Kruskal-Wallis tests with Dunn's post-hoc comparisons was performed (all groups compared to SHAM).

3.16 Exclusion of data and standardization

Out of the 49 rats, a total of 45 rats reached termination day and four died prematurely during or closely after SCI surgery. This totals the mortality rate of complete T3-SCI in this study to be 8.2%, which is in the range previously reported in similar experiments (0-10%).[156] One rat was excluded from all analyses due to poor health before and at termination. This particular rat showed clinical signs of a bladder infection and possible sepsis (i.e., lethargy, pale skin, and an extensive blood clot found in its bladder) which can confound results. Partial and complete data were obtained and utilized from 44 rats. Special exclusion criteria for certain analyses can be found in the following paragraphs and all sample sizes per type of analysis in their relevant result sections.

PV data were not collected for the 12 hours T3-SCI group. This was due to some rats having arrhythmic hearts immediately following the high-level SCI,[78] which made it practically impossible to catheterize the heart without damaging the apparatus. Furthermore, there are other potential ethical implications of conducting multiple surgeries in such a close time frame to each other. No additional rats were excluded for PV analysis.

For histology, cardiac tissue was collected precisely at planned termination times immediately after completion of the *in vivo* experiments. We were able to collect and fix 45 hearts for histology. Out of these 45 samples, five rats were excluded for the following reasons. One rat was excluded from all analyses from this study, as above-mentioned, and four other rats were excluded due to poor perfusion quality, causing late fixation of the tissue post-mortem. As fresh tissue must be fixed immediately after death, we decided to not trust the tissue as lack of blood supply to the organ will cause a decline in tissue quality. All cardiomyocyte dimensional data were standardized to femur length, which is an approach used in our laboratory previously.[72,99] Body mass highly fluctuates following SCI due to administration of opioids and surgery, therefore femur length was deemed more stable and accurate as a method of standardization. Our method of standardization followed the instructions in Hagdorn *et al*., which suggested dividing one-dimensional measurements by femur length (cm), area (two-dimensional) measurements by squared femur length (cm^2) and volumetric (three-dimensional) measurements by cubed femur length (cm^3).[173] No outliers for cardiomyocyte dimensions were detected.

Chapter 4. Results

4.1 Demographics

4.1.1 Demographics at termination

Demographics obtained at termination are provided in Table 4.1. Body mass was similar between all groups at pre-intervention (p=0.175). At termination, body mass differed between groups due to differential termination time points along the acute setting post-SCI (p=0.006). As body mass fluctuated significantly acutely post-SCI, all dimensional indices were standardized to femur length as it did not differ in any of the groups (p=0.638).[173]

Table 4.1. Group demographics at termination

	SHAM	12 hours	1 day	3 days	5 days	7 days	p
Body mass at pre-intervention (g)	328.6 (3.0)	348.9 (11.4)	361.8 (16.8)	325.3 (5.5)	359.5 (14.3)	354.6 (9.6)	0.175
Body mass at termination (g)	334.2 (3.1)	370.5 (15.8)	392.2 (19.7)	320.4 (4.9)	333.3 (14.9)	315.3 (11.9)*	0.006
Femur length (cm)	3.54 (0.02)	3.54 (0.05)	3.63 (0.05)	3.53 (0.04)	3.57 (0.05)	3.58 (0.04)	0.638

Values are means (standard error of the mean; SE). The last column indicates the p value for one-way ANOVAs. Post-hoc, *p<0.05 versus 1 day. For body mass at both pre-intervention and at termination, sample sizes are as follows: n=6 for SHAM, n=9 for 12 hours T3-SCI, n=7 for 1 day T3-SCI, n=6 for 3 days T3-SCI, n=7 for 5 days T3-SCI and n=8 for 7 days T3-SCI. The same sample sizes apply for femur length data, except for the 3 days T3-SCI group which was n=7.

4.1.2 Body mass along the acute timeline in the 7 days T3-SCI and SHAM groups

All means, SEs and p values for body mass obtained along the acute timeline in SHAM and 7 days T3-SCI rats are reported and illustrated in Table 4.2. and Figure 4.1.A. There was an interaction effect between time and group for body mass (p<0.001), as well as a main effect for time (p<0.001). Post-hoc tests revealed that body mass was significantly higher in T3-SCI rats compared to SHAM rats at 2 days post-surgery (p=0.039) but did not differ at pre-injury or 6 days post-injury between the two groups.

4.2 In-vivo echocardiography data – Temporal cardiac volumetric and functional indices following the 7 days T3-SCI and SHAM groups

4.2.1 Heart rate

Changes in HR from pre- to post-surgery are reported and illustrated in Table 4.2 and Figure 4.1.B., respectively. There was an interaction effect between time and group for HR ($p<0.001$), as well as a main effect for group ($p=0.002$). Post-hoc analyses revealed that HR was significantly lower in the T3-SCI rats compared to the SHAM rats at 1, 2 and 4 days post-surgery (all $p<0.001$), and HR was not different from SHAM at day 6 post-SCI ($p=0.163$).

4.2.2 Volumetric cardiac indices and systolic function

EDV, ESV, SV, CO, EF and FS from pre- to post-surgery are reported and illustrated in Table 4.2. and Figure 4.1., respectively. There was a significant interaction effect between time and group for EDV and SV (both $p<0.001$), whereby EDV and SV were initially higher in T3-SCI vs. SHAM pre-surgery but subsequently became lower than SHAM by day 6 post-SCI (both $p<0.05$). There was an interaction effect between time and group for ESV ($p=0.006$). Post-hoc tests revealed a lower ESV in the SHAM group at pre-surgery versus the T3-SCI group ($p=0.056$), while ESV did not differ between the groups at any other time-point post-surgery (all $p>0.658$). In the T3-SCI group, ESV was reduced acutely post-SCI at all time-points versus their pre-injury values (all $p<0.001$). There was an interaction effect between time and group for CO ($p=0.001$), and post-hoc tests revealed significantly reduced CO at 4 and 6 days in the T3-SCI group compared to SHAM (both $p<0.05$). There were no other changes of note in any other indices of cardiac function on echocardiography.

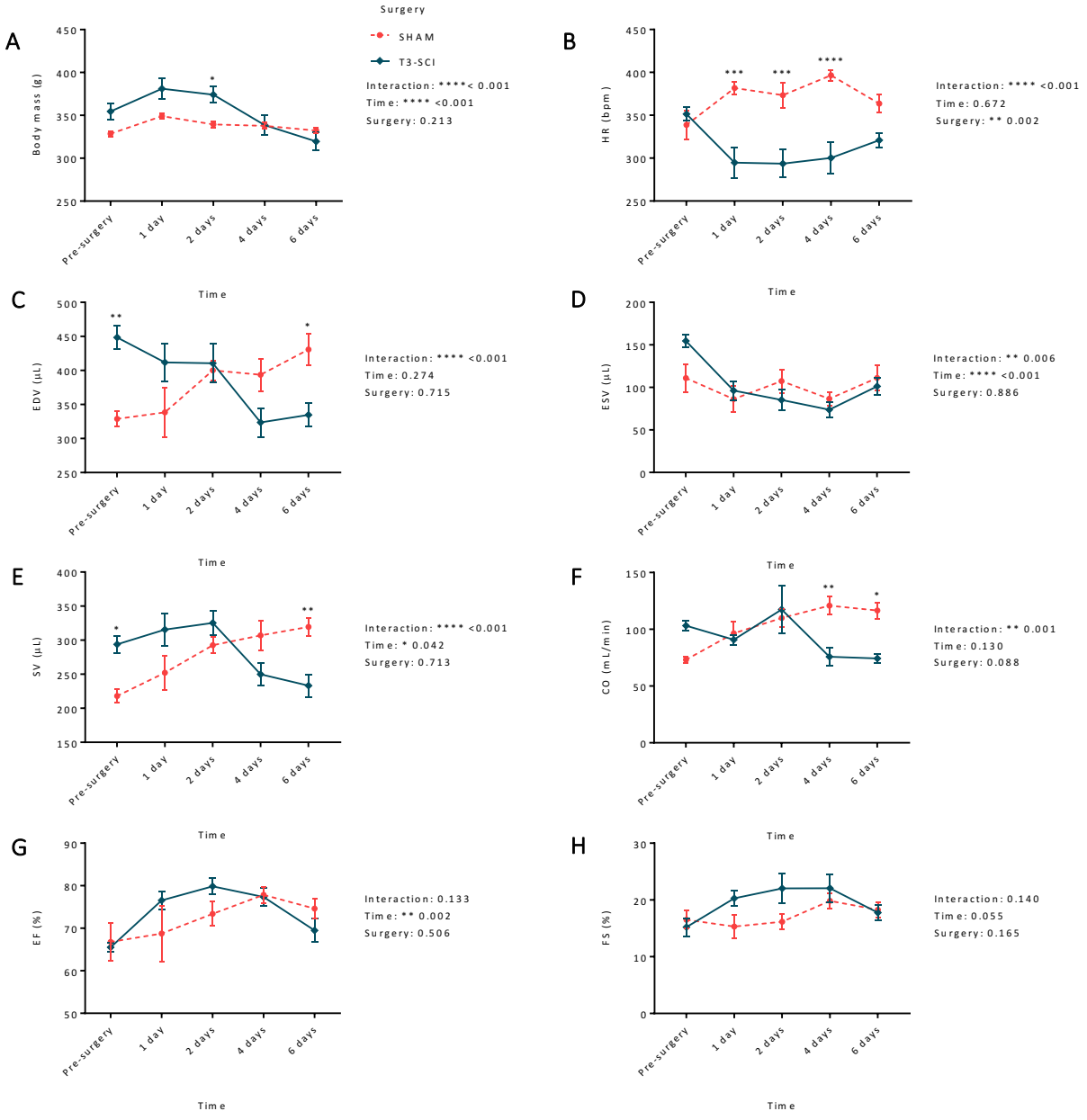

Figure 4.1. Body mass and echocardiographic indices measured along the acute timeline of rats that have undergone SHAM and T3-SCI surgeries. *A)* Body mass; *B)* HR, heart rate; *C)* EDV, end-diastolic volume; *D)* ESV, end-systolic volume; *E)* SV, stroke volume; *F)* CO, cardiac output; *G)* EF, ejection fraction; *H)* FS, fractional shortening. Group means are plotted as symbols, while standard errors of the mean are represented with error bars (mean ± SE). The p values for the repeated measures two-way ANOVAs are included by each variable. For simplicity we have shown only the significant post-hoc comparisons with symbols on the figures, *p<0.05, **p<0.01, ***p<0.001 and ****p<0.0001. All sample sizes, means and SEs are provided in Table 4.2.

Table 4.2. Parasternal long-axis volumetric and functional indices following SHAM and T3-SCI along the acute timeline

	SHAM					T3-SCI					p		
	Pre-surgery	1 day	2 days	4 days	6 days	Pre-surgery	1 day	2 days	4 days	6 days	Time	Surgery	Interaction
Body mass (g)	329 (3)	349 (3)**	339 (3)**	338 (4)*	332 (3)	355 (10)	381 (12)**	374 (10)**†	339 (11)**	320 (10)**	<0.001	0.213	<0.001
HR (bpm)	339 (17)	382 (7)*	373 (15)	397 (6)*	364 (11)	351 (8)	295 (18)**††	294 (16)**††	300 (19)*††	321 (9)	0.672	0.002	<0.001
Volumes													
EDV (µL)	329 (11)	338 (37)	400 (15)	394 (24)	431 (24)*	449 (18)††	412 (27)	411 (28)	324 (21)**	335 (17)**†	0.274	0.715	<0.001
ESV (µL)	111 (16)	86 (15)	107 (14)	87 (8)	111 (15)	155 (7)	96 (11)**	85 (12)**	74 (9)**	101 (10)**	<0.001	0.886	0.006
Systolic function													
SV (µL)	218 (10)	252 (25)	293 (12)*	307 (22)*	320 (13)**	294 (13)†	315 (23)	325 (18)	250 (17)	233 (17)*†	0.042	0.713	<0.001
CO (mL/min)	73.2 (2.7)	96.5 (10.1)	109.9 (8.2)	120.9 (8.1)*	116.5 (7.0)*	103.2 (4.5)	90.8 (4.4)	117.4 (20.7)	75.8 (8.0)†	74.3 (4.2)†	0.130	0.088	0.001
EF (%)	66.8 (4.4)	68.7 (6.6)	73.4 (2.8)	77.9 (1.9)*	74.6 (2.4)	65.5 (1.0)	76.6 (2.2)*	79.8 (1.9)**	77.4 (2.2)*	69.5 (2.8)	0.002	0.506	0.133
FS (%)	16.5 (1.6)	15.3 (2.0)	16.2 (1.4)	19.8 (1.4)	18.3 (1.4)	15.2 (1.6)	20.3 (1.4)	22.0 (2.5)*	22.1 (2.4)*	17.8 (1.4)	0.055	0.165	0.140

Values are means (SE) with n=6 for SHAM and n=8 for T3-SCI. CO, cardiac output; EDV, end-diastolic volume; EF, ejection fraction; ESV, end-systolic volume; FS, fractional shortening; SV, stroke volume. The last column indicates the p values for two-way repeated measures ANOVAs. Within-group post-hoc tests versus pre-injury, *p<0.05 and **p<0.001. Between-group post-hoc tests, †p<0.05 and ††p<0.001.

4.3 In-vivo catheterization data – Cardiovascular functional and pressure-volume indices

4.3.1 Basal arterial hemodynamics

Graphical representations of all hemodynamic variables can be found in Figure 4.2. Means, SEs and p values are reported in Table 4.3. Systolic blood pressure (SBP) was significantly decreased acutely following T3-SCI ($p=0.001$) compared to SHAM. Post-hoc analyses revealed significant reductions at 3 days ($p=0.049$), 5 days ($p<0.001$) 7 days ($p=0.014$), and a trend for reduced SBP at 1 day post-SCI compared to SHAM ($p=0.068$). DBP was significantly reduced post-SCI versus SHAM ($p=0.026$). However, post-hoc testing versus SHAM revealed that the only group which showed a significant decrease in DBP was the 5 days T3-SCI group ($p=0.044$), while all other time-points, including the last time-point (7 days), showed no significant differences in DBP (all $p>0.612$). Mean arterial pressure (MAP) was significantly decreased acutely following T3-SCI ($p=0.002$) with post-hoc tests versus SHAM revealing significant lower MAPs in the 5 and 7 days T3-SCI groups (both $p<0.05$).

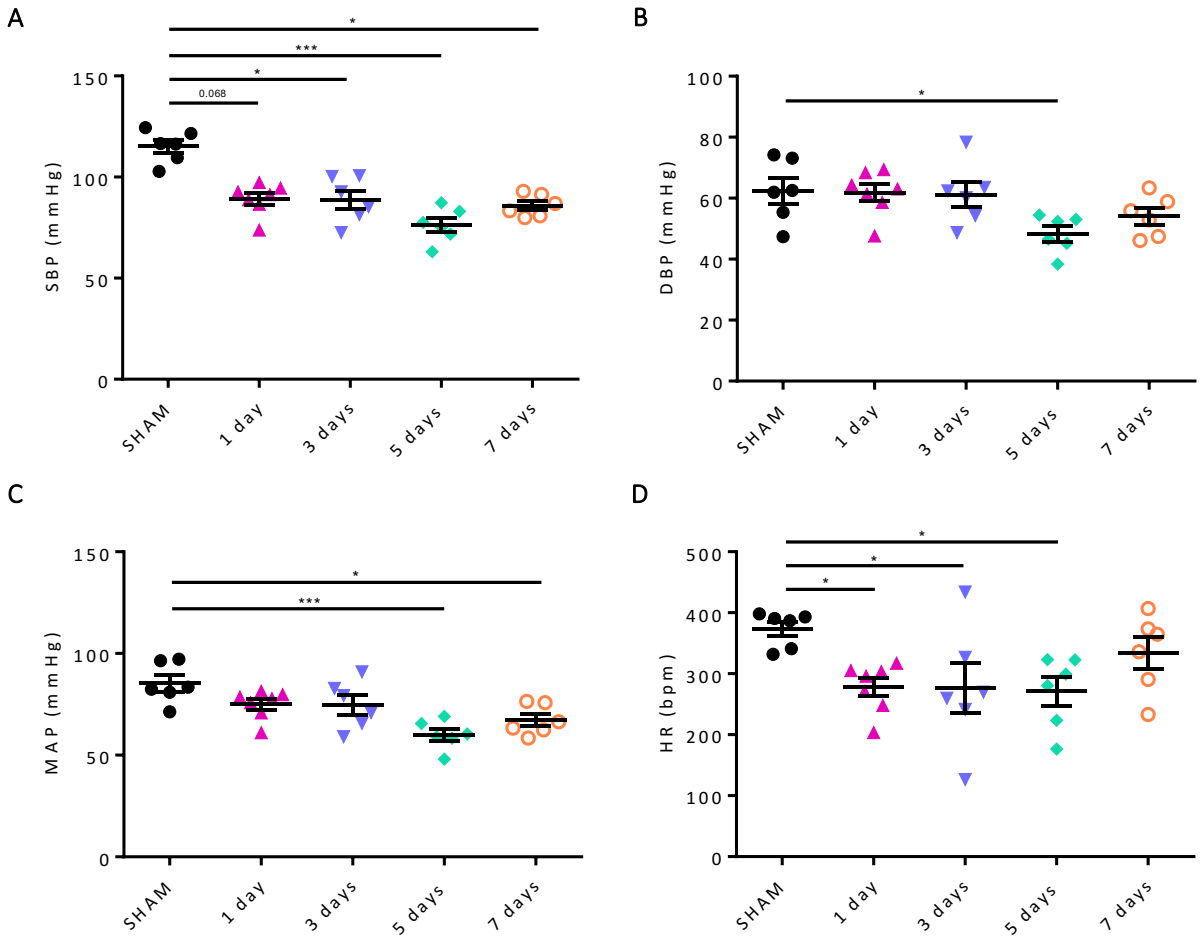

Figure 4.2. Basal hemodynamics following SHAM surgery and at different time-points following T3-SCI. SHAM rats were terminated at 7 days post-surgery. *A)* SBP, systolic blood pressure; *B)* DBP, diastolic blood pressure; *C)* MAP, mean arterial pressure; *D)* HR, heart rate. Individual rat means are plotted as symbols, while group means and standard errors are represented with error bars (mean ± SE). One-way ANOVAs post-hoc tests versus SHAM, *p<0.05 and ***p<0.001. All sample sizes, means and standard errors are provided in Table 4.3.

Table 4.3. Hemodynamic responses to SHAM surgery and T3-SCI at different termination time points

	SHAM	1 day	3 days	5 days	7 days	p
SBP (mmHg)	115.2 (3.2)	89.3 (2.9)	88.8 (4.5)*	76.3 (3.5)***	85.9 (2.2)*	0.001
DBP (mmHg)	62.4 (4.2)	61.8 (2.8)	61.2 (4.1)	48.3 (2.5)*	54.1 (2.7)	0.026
MAP (mmHg)	85.3 (4.0)	75.1 (2.7)	74.8 (4.8)	60.1 (2.9)***	67.2 (3.0)*	0.002
HR (bpm)	374 (12)	278 (15)*	276 (41)*	271 (24)*	334 (26)	0.030

Values are means (SE). DBP, diastolic blood pressure; HR, heart rate; MAP, mean arterial pressure; SBP, systolic blood pressure. The last column indicates the p value for one-way ANOVAs. Post-hoc tests versus SHAM, *p<0.05 and ***p<0.001. Sample sizes are as follows: n=6 for SHAM, n=7 for 1 day T3-SCI, n=6 for 3 days T3-SCI, n=6 for 5 days T3-SCI and n=6 for 7 days T3-SCI.

4.3.2 Basal cardiac pressure-volume responses

All load-dependent and -independent means, SEs and p values are reported in Table 4.4. Averaged PV loops per group and representative IVC occlusions are illustrated in Figure 4.3.

4.3.2.1 Left-ventricular pressure-volume derived load-independent function

ESPVR, used to infer systolic function, was significantly decreased acutely post-SCI (p=0.005) (Figure 4.4.A.). Post-hoc analyses revealed that at all T3-SCI time-points, except 3 days, ESPVR was significantly lower versus SHAM (all p<0.05). Nonetheless, the 3 days T3-SCI group tended to have a lower ESPVR versus SHAM (p=0.051). Contrarily to ESPVR, PRSW was not seen to differ in any of the groups (p=0.531).

4.3.2.2 Left-ventricular pressure-volume derived load-dependent function

All load-dependent variables which infer systolic function were significantly different following T3-SCI. Pmax (p=0.005), Pdev (p<0.001) and dP/dt_{max} (p=0.006) were significantly reduced at all T3-SCI time-points versus SHAM (Figure 4.4.C. and D.). Unstandardized (Figure 4.4.B.) and standardized (to femur length) SW were significantly lower in the 3, 5 and 7 days T3-SCI groups versus SHAM (SW p=0.004; standardized SW p=0.013). Although Ea was not significantly different in any of the groups (p=0.145), it tended to be lower in the 1 day T3-SCI group versus SHAM (post-hoc: p=0.059) (Figure 4.4.E.). Furthermore, Ea/ESPVR, the ventricular vascular coupling ratio, was significantly increased in the 1, 5 and 7 days T3-SCI groups versus SHAM (p=0.011) (Figure 4.4.F.).

All T3-SCI time-points, except 3 days (post-hoc: p=0.063), showed significant or strongly suggested reduced $-dP/dt_{min}$ values versus SHAM (p=0.006) (Figure 4.5.A). On the contrary, other load-

dependent variables which infer diastolic function showed no significant changes in the T3-SCI groups versus SHAM (Ped p=0.766; tau p=0.224) (Figure 4.5.B).

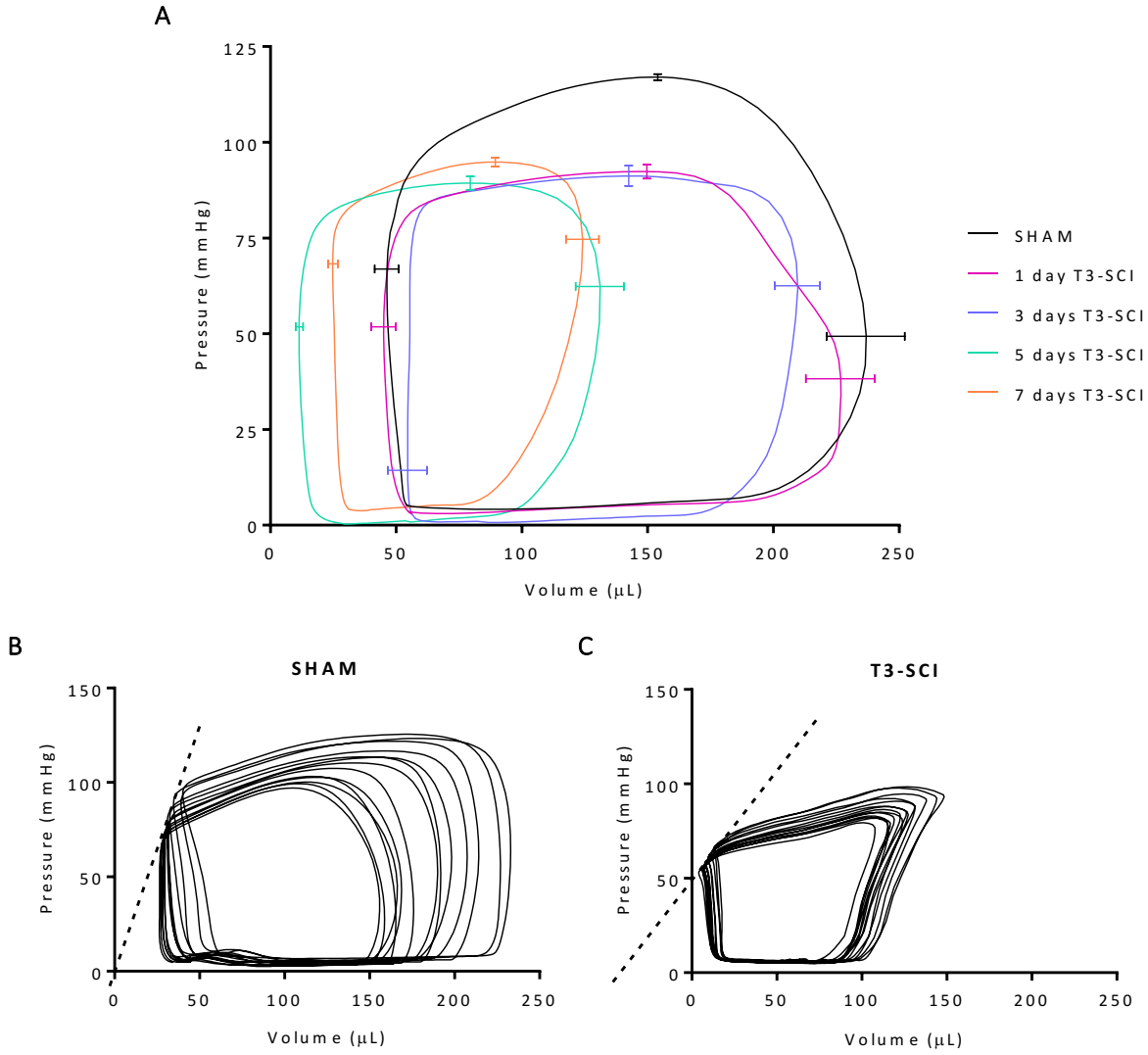

Figure 4.3. Averaged baseline pressure-volume loops and representative inferior vena cava occlusions obtained via LV catheterization. *A)* Averaged baseline PV loops of all experimental groups. Error bars represent SEM. *B)* Representative IVC occlusion following SHAM surgery. *C)* Representative IVC occlusion following T3-SCI in the acute phase following injury. The dotted lines represent representative ESPVR values. ESPVR, end-systolic pressure-volume relationship; IVC, inferior vena cava; LV, left-ventricle; PV, pressure-volume; SCI, spinal cord injury.

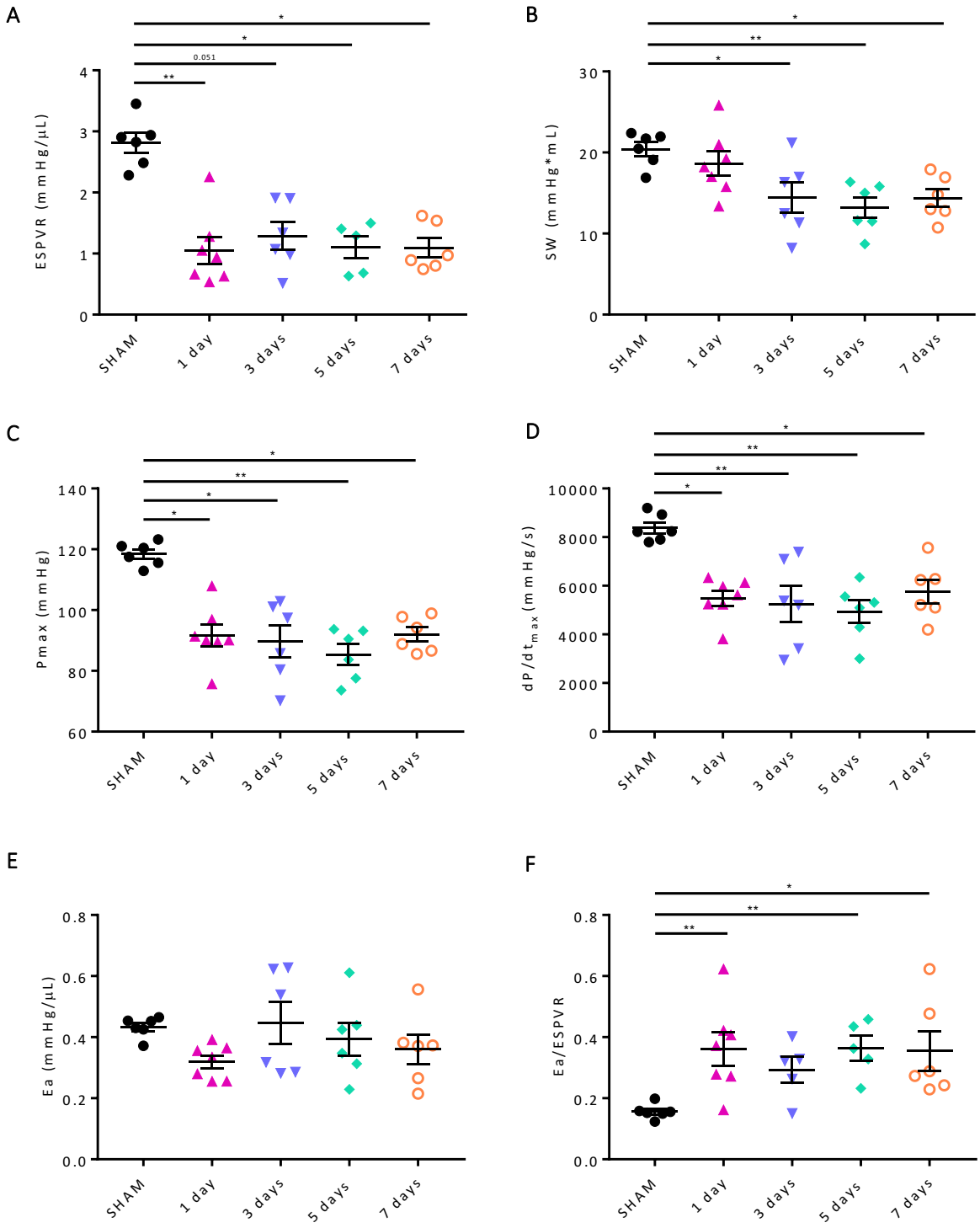

Figure 4.4. Systolic function following SHAM surgery and at different times points following T3-SCI. *A)* ESPVR, end-systolic pressure-volume relationship; *B)* SW, stroke work; *C)* Pmax, maximum pressure; *D)*

dP/dt_{max}, maximal rate of systolic pressure increment; *E)* Ea, arterial elastance; *F)* Ea/ESPVR, ventricular vascular coupling ratio. Individual rat means are plotted as symbols, while group means and standard errors are represented with error bars (mean ± SE). One-way ANOVAs post-hoc tests versus SHAM, *p<0.05 and **p<0.01. All sample sizes, means and standard errors are provided in Table 4.4.

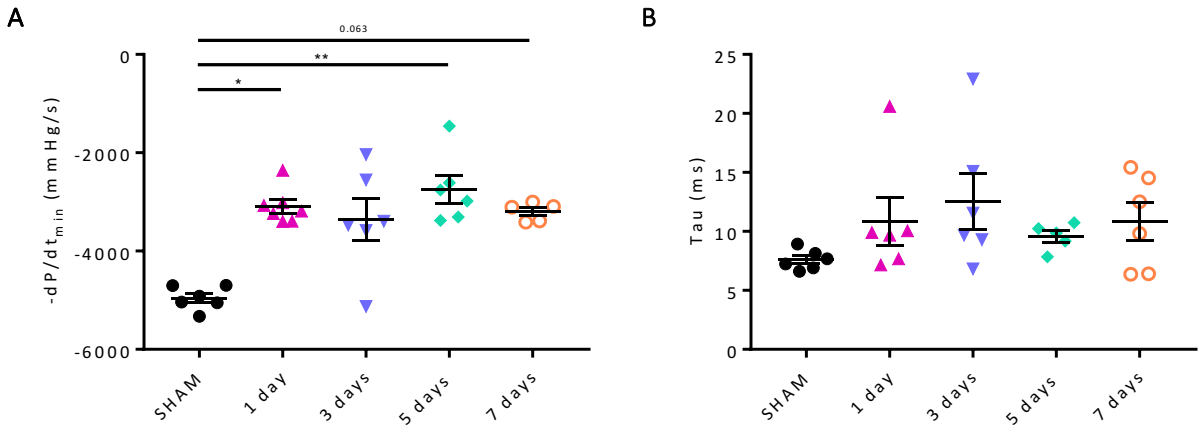

Figure 4.5. Diastolic function following SHAM surgery and at different times points following T3-SCI. *A)* $-dP/dt_{min}$, maximal rate of diastolic pressure decrement; *B)* Tau, diastolic time constant. Individual rat means are plotted as symbols, while group means and standard errors are represented with error bars (mean ± SE). One-way ANOVAs post-hoc tests versus SHAM, *p<0.05 and **p<0.01. All sample sizes, means and standard errors are provided in Table 4.4.

Table 4.4. Cardiac functional responses following SHAM surgery and T3-SCI at different termination time points

	SHAM	1 day	3 days	5 days	7 days	p
Systolic function						
ESPVR (mmHg/µL)	2.82 (0.17)	1.05 (0.22)**	1.29 (0.22)	1.10 (0.18)*	1.10 (0.16)*	0.005
SW† (mmHg*mL)	20.42 (0.86)	18.62 (1.51)	14.42 (1.89)*	13.17 (1.23)**	14.37 (1.11)*	0.004
Standardized SW† (mmHg*mL/cm^3)	4.58 (0.16)	3.90 (0.29)	3.34 (0.46)	2.92 (0.37)**	3.12 (0.32)*	0.013
Pmax† (mmHg)	118 (2)	92 (4)*	90 (5)*	85 (3)**	92 (2)*	0.005
Pdev† (mmHg)	119 (2)	91 (2)****	91 (6)****	88 (3)****	91 (1)****	<0.001
dP/dt_{max} † (mmHg/s)	8383 (230)	5475 (320)*	5241 (745)**	4935 (472)**	5765 (481)*	0.006
TPR (mmHg/mL)	1.32 (0.21)	1.69 (0.20)	1.72 (0.34)	1.82 (0.26)	1.38 (0.14)	0.464
Ea† (mmHg/µL)	0.43 (0.01)	0.32 (0.02)	0.45 (0.07)	0.39 (0.05)	0.36 (0.05)	0.145
Ea/ESPVR	0.16 (0.01)	0.36 (0.06)**	0.29 (0.04)	0.36 (0.04)**	0.36 (0.06)*	0.011
PRSW† (mmHg)	122 (7)	121 (16)	121 (9)	106 (10)	141 (17)	0.531
Diastolic function						
$-dP/dt_{min}$ (mmHg/s)	-4957 (98)	-3094 (135)*	-3361 (432)	-2750 (286)**	-3201 (83)	0.006
Ped† (mmHg)	4.49 (1.46)	5.03 (3.73)	2.12 (1.45)	1.47 (1.00)	3.19 (2.63)	0.766
Tau (ms)	7.58 (0.35)	10.84 (2.01)	12.56 (2.36)	9.57 (0.50)	10.85 (1.61)	0.224

Values are means (SE). Standardized SW was divided by femur length^3 (cm^3).[173] dP/dt_{max}, maximal rate of systolic pressure increment; $-dP/dt_{min}$, maximal rate of diastolic pressure decrement; Ea, arterial elastance; Ea/ESPVR, ventricular vascular coupling ratio; ESPVR, end-systolic pressure-volume relationship; Pdev, developed pressure; Ped, end-diastolic pressure; Pmax, maximum pressure; PRSW, preload recruitable stroke work; SW, stroke work; Tau, diastolic time constant; TPR, total peripheral resistance. The last column indicates the p value for one-way ANOVAs. Post-hoc tests versus SHAM, *p<0.05, **p<0.01 and ****p<0.0001. †, sample sizes are as follows: n=6 for SHAM, n=7 for 1 day T3-SCI, n=6 for 3 days T3-SCI, n=6 for 5 days T3-SCI and n=6 for 7 days T3-SCI.For ESPVR and PRSW: n=6 for SHAM, n=7 for 1 day T3-SCI, n=6 for 3 days T3-SCI, n=5 for 5 days T3-SCI and n=6 for 7 days T3-SCI. For $-dP/dt_{min}$: n=6 for SHAM, n=7 for 1 day T3-SCI, n=6 for 3 days T3-SCI, n=6 for 5 days T3-SCI and n=5 for 7 days T3-SCI. For tau: n=6 for SHAM, n=6 for 1 day T3-SCI, n=6 for 3 days T3-SCI, n=5 for 5 days T3-SCI and n=6 for 7 days T3-SCI.

4.4 Molecular data – Gene analysis for protein degradation pathways

All sample sizes, mean fold changes and SEs per group for all UPS and autophagy targets are reported in Table 4.6. The following results describe an increase in UPS and no changes in autophagy gene expression in LV tissue acutely post-SCI.

Table 4.5. Quantitative real-time PCR targets, primers and fold changes following SHAM surgery and T3-SCI at different termination time points

	SHAM	12 hours	1day	3 days	5 days	7 days	p
UPS							
MAFbx	1.06 (0.15)	3.57 (0.48)***	2.33 (0.51)	2.26 (0.19)*	1.94 (0.22)	1.73 (0.21)	0.005
MuRF1	1.02 (0.10)	1.38 (0.10)	1.38 (0.23)	1.49 (0.17)	1.66 (0.28)	1.03 (0.33)	0.288
Autophagy							
ATG7	1.03 (0.12)	1.64 (0.16)	1.36 (0.23)	1.30 (0.08)	1.32 (0.21)	1.59 (0.32)	0.355
ATG12	1.01 (0.09)	1.20 (0.13)	1.11 (0.16)	1.07 (0.11)	1.14 (0.20)	1.43 (0.25)	0.716
BECN1	1.01 (0.06)	1.07 (0.15)	1.21 (0.24)	1.05 (0.10)	1.04 (0.14)	1.14 (0.11)	0.964

Values are mean fold changes (SE) with n=6 for all groups. *ATG7*, autophagy related 7; *ATG12*, autophagy related 12; *BECN1*, beclin 1; *MAFbx*, muscle atrophy F-box; *MuRF1*, muscle RING-finger protein 1. The last column indicates the p value for one-way ANOVAs. Post-hoc tests versus SHAM, *p<0.05 and ***p<0.001.

4.4.1 UPS

The fold changes of UPS marker, *MAFbx*, were significantly increased following T3-SCI by approximately 3.37-fold versus SHAM (p=0.005) (Figure 4.8.A.). Post-hoc analyses revealed that *MAFbx* levels were significantly increased compared to SHAM at 12 hours and 3 days post-SCI (both p<0.05) (Figure 4.8.A.). *MAFbx* peaked at 12 hours and tended to gradually decrease back-down with time (Figure 4.8.A.). The fold changes of UPS marker, *MurF1*, were not significantly changed in any of the T3-SCI groups versus SHAM (p=0.288) (Figure 4.8.B.). However, *MurF1* tended to be up-regulated in all but one animal acutely post-SCI with a gradual increase starting at the first time-point, 12 hours, and a peak at 5 days post-SCI versus SHAM (Figure 4.8.B.). *MuRF1* appeared to decrease back towards SHAM levels by 7 days post-SCI (Figure 4.8.B.).

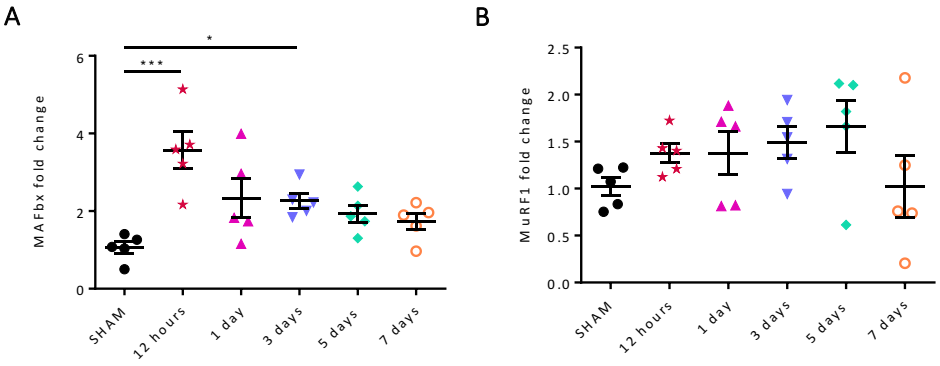

Figure 4.6. RNA fold changes of UPS targets following SHAM surgery and T3-SCI at different time points along the acute spectrum (n=6). *A) MAFbx*, muscle atrophy F-box; *B) MuRF1*, muscle RING-finger protein 1. Individual rat mean fold changes are plotted as symbols, while group means and standard errors are represented with error bars (mean ± SE). All means, standard errors and p values are provided in Table 4.6. MAFbx, one-way ANOVA, Kruskal-Wallis test (p=0.005) and Dunn's post-hoc, *p<0.05 and ***p<0.001.

4.4.2 Autophagy

The fold changes of autophagy markers, *ATG7*, *ATG12* and *BECN1*, were not significantly changed in LV cardiac tissue at any time-point following T3-SCI versus SHAM (all p>0.355) (Figure 4.9.).

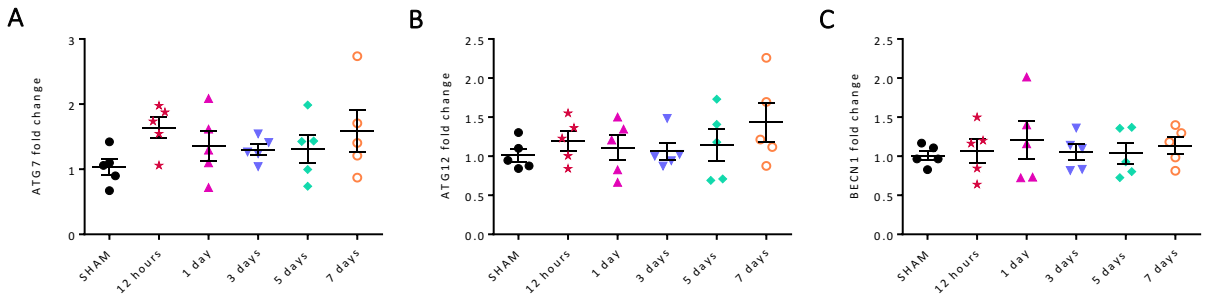

Figure 4.7. RNA fold changes of autophagy targets following SHAM surgery and T3-SCI at different time points along the acute spectrum (n=6). *A) ATG7*, autophagy related 7; *B) ATG12*, autophagy related 12; *C) BECN1*, beclin 1. Individual rat mean fold changes are plotted as symbols, while group means and standard errors are represented with error bars (mean ± SE). All means, standard errors and p values are provided in Table 4.6.

4.5 Histological data – Cardiomyocyte dimensions

All final sample sizes and histological measurements for all groups are reported in Table 4.5. All longitudinally oriented cardiomyocyte data (i.e., length and width) pertained to the myocardial layer of the LV free-wall, while cross-sectionally oriented data (i.e., CSA) pertained to the sub-epicardial and epicardial layers of the LV free-wall. No significant atrophy was found in any of the SCI groups versus the SHAM group. However, trends will be discussed in the following sections.

Table 4.6. LV myocardial cardiomyocyte dimensions following SHAM surgery and T3-SCI at different termination time points

	SHAM	12 hours	1 day	3 days	5 days	7 days	p
Standardized							
Length (μm/cm)	25.64 (0.80)	24.86 (0.76)	24.82 (0.56)	23.95 (0.77)	23.93 (0.70)	23.49 (0.63)	0.328
Width (μm/cm)	4.42 (0.29)	4.28 (0.18)	3.91 (0.24)	4.07 (0.15)	4.29 (0.18)	4.05 (0.15)	0.609
Length to width ratio	5.91 (0.39)	5.91 (0.34)	6.46 (0.33)	5.93 (0.33)	5.62 (0.29)	5.61 (0.24)	0.503
CSA ($\mu m^2/cm^2$)	35.2 (4.8)	29.1 (2.4)	25.2 (1.2)	32.2 (3.5)	31.0 (3.7)	27.0 (2.2)	0.207
Volume ($\mu m^3/cm^3$)	927 (122)	684 (69)	623 (28)	762 (77)	748 (98)	622 (49)	0.146
Unstandardized							
Length (μm/cm)	90.79 (2.48)	87.72 (1.76)	89.95 (2.15)	84.88 (3.17)	86.26 (1.70)	84.10 (2.07)	0.264
Width (μm/cm)	15.66 (1.00)	15.15 (0.67)	14.22 (0.96)	14.41 (0.58)	15.49 (0.71)	14.49 (0.49)	0.763
CSA ($\mu m^2/cm^2$)	439 (57)	375 (32)	330 (13)	395 (43)	400 (37)	344 (26)	0.368
Volume ($\mu m^3/cm^3$)	40716 (5024)	31453 (2725)	30585 (417)	32683 (3305)	34446 (3108)	28264 (1818)	0.189

Standardized values were corrected to femur length.[173] Values are means (SE). CSA, cross-sectional area. The last column indicates the p value for one-way ANOVAs. Variables obtained via the longitudinal view (standardized and unstandardized length and width) had sample sizes of: n=6 for SHAM, n=9 for 12 hours, n=7 for 1 day, n=5 for 3 days, n=5 for 5 days and n=8 for 7 days. Variables obtained via the cross-sectional view (CSA and standardized volume) had sample sizes of: n=5 for SHAM, n=5 for 12 hours, n=7 for 1 day, n=4 for 3 days, n=5 for 5 days and n=7 for 7 days. Unstandardized volume had sample sizes of: n=5 for SHAM, n=5 for 12 hours, n=6 for 1 day T3-SCI, n=4 for 3 days T3-SCI, n=5 for 5 days T3-SCI and n=7 for 7 days T3-SCI.

4.5.1 Cardiomyocyte length and width

There was no significant cardiomyocyte atrophy in either length or width, standardized to femur length, following T3-SCI at any time-point along the acute spectrum versus SHAM (both p>0.328) (Figure 4.6.C.). Post-hoc analyses revealed that standardized length tended to gradually decrease along the acute spectrum with the lowest value at 7 days post-SCI versus SHAM (p=0.145). Unstandardized length showed similar trends to its standardized counterpart (p=0.264; post-hoc SHAM versus 7 days: p=0.135). Standardized width, length-width ratio and unstandardized width did not show any significant cardiomyocyte atrophy or trends (all p>0.503). A cardiomyocyte with representative length and width is illustrated in Figure 4.6.A.

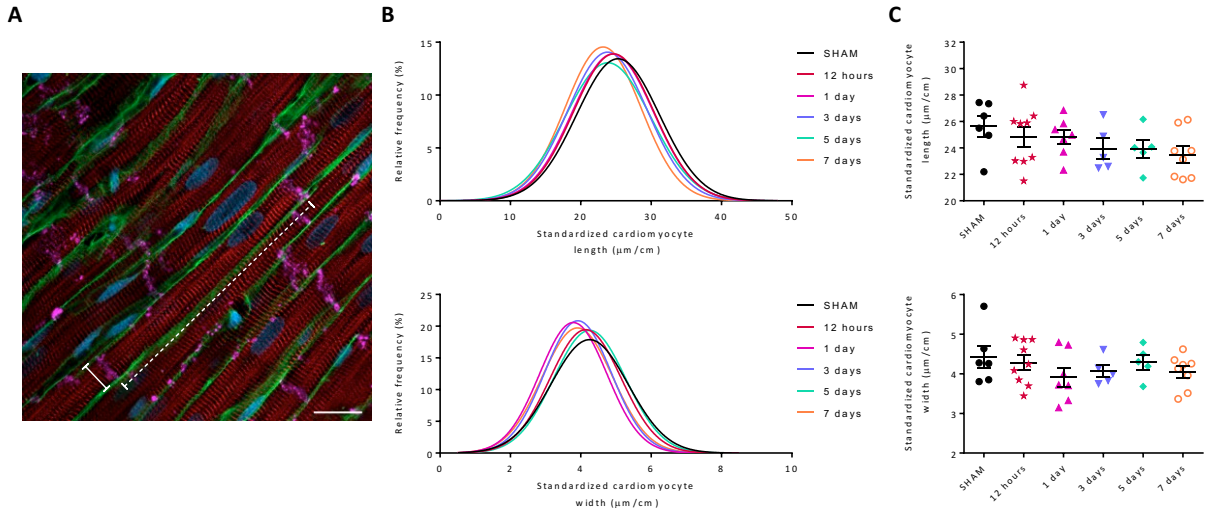

Figure 4.8. LV myocardial cardiomyocyte length and width following SHAM surgery and T3-SCI at different termination time points. Longitudinally oriented cardiomyocytes are imaged in the LV myocardial free-wall and all cardiomyocyte dimensions (µm) are standardized to femur length (cm). In *panel A*, an immunofluorescent image shows a representative cardiomyocyte with a scale bar measuring 20 µm (x63). Stained targets include: connexin-43 in far-red (pink; intercalated discs), α-actinin in red (Z-lines), wheat germ agglutinin in green (plasma membrane) and DNA in blue (nuclei). The dotted and solid lines indicate the length and width of a cardiomyocyte, respectively. In *panel B*, frequency distributions show skewness, kurtosis and the range of measurements obtained for standardized length and width (Gaussian fit). In *panel C*, individual rat means are plotted as symbols, while group means and standard errors are

represented with error bars (mean ± SE). All sample sizes, means, standard errors and p values are provided in Table 4.5.

4.5.2 Cardiomyocyte cross-sectional area and volume

Standardized (to femur length) and unstandardized cardiomyocyte CSA were not significantly decreased following T3-SCI at any time-point in the acute setting versus SHAM (both $p>0.207$) (Figure 4.7.C.). Post-hoc testing indicated that standardized cardiomyocyte CSA at 1 day post-SCI tended to be lower versus SHAM ($p=0.074$). An immunofluorescent image with representative CSA is illustrated in Figure 4.7.A. Similarly to CSA, standardized (to femur length) and unstandardized cardiomyocyte volume were not seen to significantly decrease following T3-SCI at any time-point along the acute spectrum versus SHAM (both $p>0.146$) (Figure 4.7.C.). Furthermore, post-hoc tests revealed that standardized cardiomyocyte volume at 1 day and 7 days post-SCI tended to be lower versus SHAM ($p=0.086$ and $p=0.075$, respectively).

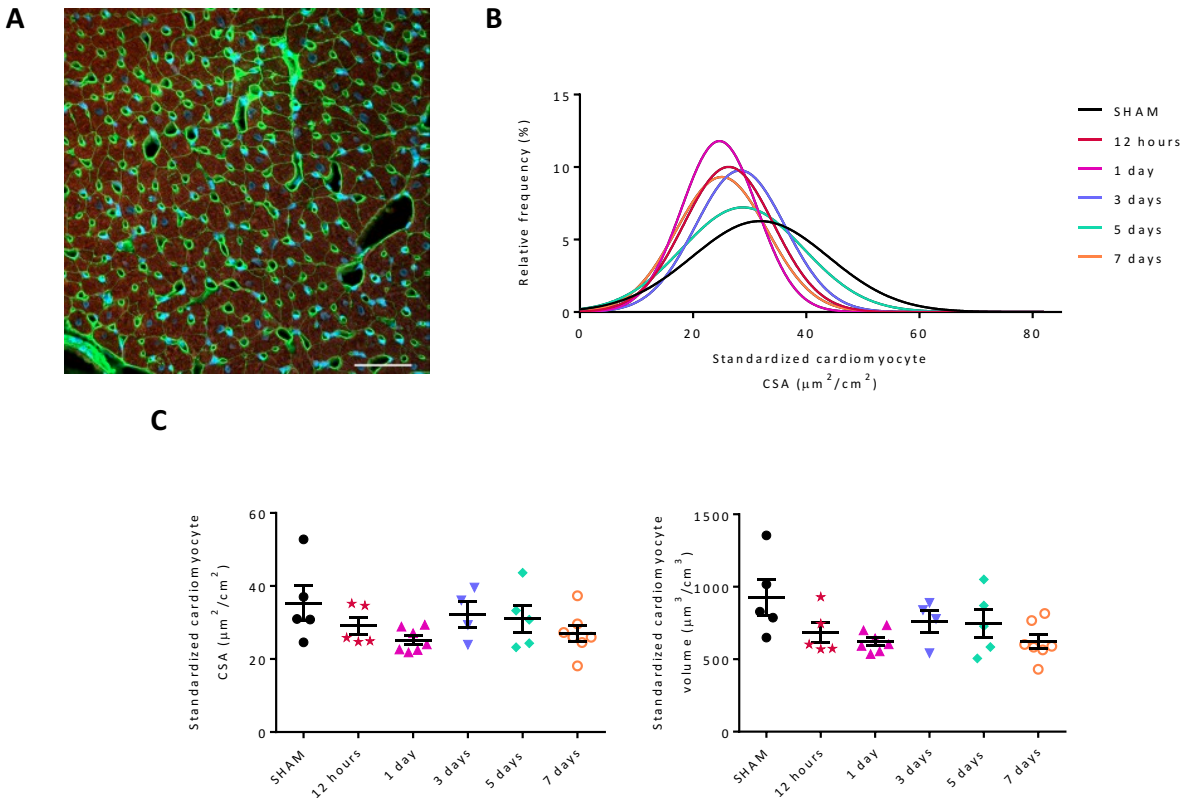

Figure 4.9. LV myocardial cardiomyocyte cross-sectional area and volume following SHAM surgery and T3-SCI at different termination time points. Cross-sectionally oriented cardiomyocytes are imaged in the LV epicardial LV free-wall. Cross-sectional area (μm^2) and volume (μm^3) are standardized to femur length^2 (cm^2) and femur length^3 (cm^3), respectively. *Panel A* shows an immunofluorescent image of representative cardiomyocytes from all groups with a scale bars measuring 50 µm (x20). Stained targets include: α-actinin in red (Z-lines to identify cardiomyocyte cytoplasm), wheat germ agglutinin in green (plasma membrane) and DNA in blue (nuclei). In *panel B*, frequency distributions show skewness, kurtosis and the range of measurements obtained for standardized cross-sectional area (Gaussian fit). In *panel C*, individual rat means are plotted as symbols, while group means and standard errors are represented with error bars (mean ± SE). All sample sizes, means, standard errors and p values are provided in Table 4.5.

Chapter 5. Discussion

In this study, we aimed to investigate the temporal effects of acute high-level SCI on cardiac function, proteolysis and structure in an experimental model with LV catheterization, echocardiography, histology and gene expression analysis. This is the first study to demonstrate that a reduction in cardiac function precedes structural remodelling following acute experimental high-thoracic SCI. We report reduced load-dependent and -independent systolic function and ventricular-arterial uncoupling but no change in diastolic function acutely post-SCI, which could be explained respectively by the immediate loss of cardiac descending sympathetic control along with cardiac unloading, and no sufficient time for structural remodelling. Furthermore, it appears that cardiomyocyte dimensions are yet to be affected in the acute setting but this effect, which we know occurs in the chronic setting, is likely driven by the upregulation of UPS gene expression that we observed acutely post-SCI.

5.1 Hemodynamics, cardiac volumes and function

5.1.1 Hemodynamics were negatively affected acutely following high-thoracic SCI

We found reduced SBP and MAP acutely post-SCI and these findings mirror what has been previously described in sub-acute and chronic studies from our laboratory with similar injury models.[72,73,154,157] Furthermore, our MAP results are in agreement with a clinical meta-analysis, performed by our research group.[65] The observed decreased in blood pressure in this thesis and the literature is likely explained by the lack of vasomotor tone in the vasculature due to the loss of supraspinal sympathetic input to the majority of the cardiovascular system following high-level SCI.[48,85,93]

We observed an acute decrease in HR following high-thoracic SCI which returned to basal levels at the end of the acute phase, 6-7 days post-SCI. The decrease in HR in the early acute phase post-SCI could be explained by the lack of sympathetic input to the heart, which incapacitates its chronotropic

functions.[78] An increase in HR in the later phase of acute SCI could be a compensatory mechanism by the PSNS (decreased input) to attempt to counteract the reduction in SV observed at the end of the acute phase. That HR values were comparable to controls at the end of the acute phase is in agreement with chronic pre-clinical data from our laboratory[72] and clinical data.[65]

5.1.2 Cardiac volumes were reduced acutely following high-thoracic SCI

We report a significantly lower EDV and SV in the T3-SCI group compared to SHAM at 6-days post-surgery. Our findings are in agreement with both pre-clinical and clinical literature following sub-acute and chronic SCI, which also indicate lower EDV and SV following high-level SCI.[65,72,73,157] The reduction in EDV post-SCI is most likely explained by the reduction in preload post-injury due to venous pooling in the splanchnic region and lower limbs, which is subsequent to the loss of sympathetic control to lower-limb skeletal vasculature and impairment of the skeletal muscle pump (innervated by L2-S1) as well as a reduction in blood volume.[48,83,93,94,174,85–92] This influence of preload on LV volume function was demonstrated in a previous study which elicited an increase in preload via chronic passive hind-limb exercise and showed improved EDV and SV in SCI rats following severe T2 contusions.[154] Interestingly, we found that EDV was actually significantly lower in the SHAM at group pre-surgery compared to the T3-SCI group and then increased with time. The former occurrence is perhaps due to lower but non-significant body mass in the SHAM group at the pre-surgery as these animals were slightly younger by 4-5 days. The latter could be explained by maturation with time as these animals were adults but remained juvenile.

There were no differences in ESV between the T3-SCI and SHAM groups along the acute timeline, however, there was an interaction effect for ESV, whereby ESV was different at pre-surgery in the two groups. Although there were no differences post-surgery in the SHAM and SCI groups, the SCI rats had significantly reduced ESV post-SCI at all time-points compared to their pre-surgery values. The reduction in ESV post-SCI observed in this thesis is in agreement with pre-clinical and clinical research performed by

our group, which also indicate a significant reduction in ESV in the chronic stages post-SCI.[65,72] While the chronic reduction in ESV could partly be explained by the well-known cardiac atrophy post-SCI, this hypothesis is not suitable to explain our acute findings as there was no significant atrophy in this study. Additionally, the acute reduction in ESV cannot be accounted for by an increase in contractility as ESPVR was reduced at all time-points post-SCI. Instead, the reduction in ESV is most likely to be explained by the reduction in afterload, observed as a non-significant reduction in Ea, which is subsequent to the loss of sympathetic control to the vasculature (innervated by T1-L2),[48] incapacitating vasoconstriction and causing a reduction in arterial blood pressure, observed as reduced SBP and MAP. Similarly to EDV, ESV was increased, along with SBP and MAP, in SCI rats which underwent passive hind-limb exercise.[154] It is important to note that the reduction in cardiac volumes in the T3-SCI group is most likely not due to weight loss as there was no significant main effect of surgery on body mass.

5.1.3 Systolic function and ventricular-vascular coupling were impaired at the first acute time-point post-SCI and persisted throughout the acute setting

The reduced systolic LV function observed in the T3-SCI group compared to SHAM, demonstrated as acute reductions in SV, SW, CO, Pmax, Pdev, dP/dt_{max} and ESPVR, is in accordance with pre-clinical sub-acute (5 weeks following severe T2 contusion in Sprague-Dawley rats)[73] and chronic studies (12 weeks following T3 complete SCI in lean Zucker rats),[72] performed by our research team. Furthermore, SV and CO are also significantly reduced in clinical studies following chronic high-level SCI.[65]

The acute reductions in SV, SW and CO could be explained by the unloading of the heart and subsequent reduction in cardiac volumes post-SCI, as suggested by past pre-clinical research which reported improved CO and SV when increasing preload via passive hind-limb exercise following severe T2 contusions.[154,157] Due to the high-level injury, there is a loss of descending sympathetic control to the lower-limb vasculature and impairment to the skeletal muscle pump.[48,83,85–93,174] The decreased

sympathetic input to the skeletal muscles of the lower-limbs leads to venous pooling in the lower-limbs and splanchnic area and therefore reduced preload,[48,83,85–93,174] which was demonstrated as reduced EDV post-SCI in this thesis. The decreased sympathetic input to the vasculature leads to the inability to vasoconstrict,[48] subsequent reduction in blood pressure and therefore reduced afterload, which was implied by reduced MAP and the non-significant but notable reduction in Ea acutely post-SCI in the present study.

Pressure generation and contractility were reduced immediately following high-level severe SCI, as suggested by reductions in pressures (Pmax and Pdev), dP/dt_{max} and ESPVR starting at the first investigated PV time-point, one day post-SCI. Pressure reductions are most likely explained by the direct loss of descending sympathetic control to the vasculature and heart due to the injury itself, incapacitating its ionotropic functions, and cardiac unloading. This potential explanation is supported by past studies from our research group which have shown that sympathetic stimulation of the heart via dobutamine (a β_1 agonist with some β_2 and α_1 agonistic abilities) improved LV pressure generation capacities in rats with severe high-level contusions,[73] while increasing preload via passive hind-limb exercise attenuated reductions in the rate of contraction +dP/dt and the rate of relaxation -dP/dt post-SCI.[154,157] Au contraire, no improvements in ESPVR post-SCI were observed in rats which underwent passive hind-limb exercise,[157] indicating that decreased contractility post-SCI must predominantly be due to the loss of cardiac sympathetic input. Importantly, reduced ESPVR in T3-SCI groups highly implies that the intrinsic systolic function of the heart is impaired acutely post-SCI. To decipher the effects of descending sympathetic control on intrinsic systolic function, ESPVR should be assessed following different levels of complete SCI, above and below the innervation of the cardiovascular system. An unpublished study from our research group investigated complete T3 (reduced cardiovascular sympathetic control) versus L2 (intact cardiovascular sympathetic control) transections in Wistar rats. The results showed lower systolic

function (i.e., ESPVR, dP/dt_{max} and pressures) in the T3 rats versus L2 rats 8 weeks post-SCI. Furthermore, we reported reduced systolic function (i.e., ESPVR, dP/dt_{max} and pressures) following complete T3 transection (12 weeks post-SCI)[72] and severe T2 contusion (5 weeks post-SCI)[73], while Lujan *et al.* reported no reduction in dP/dt_{max} following complete T5 transection 21 days post-SCI (intact cardiac sympathetic control).[175] In addition, Currie *et al.* reported lower LV function in tetraplegic athletes with cervical injuries compared to their paraplegic counterparts with mid-thoracic to lumbar injuries.[61] Altogether, our findings and the literature suggest that descending sympathetic control to the cardiovascular system is crucial for both load-dependent and -independent LV function.

Pre-clinical research has reported increased Ea/ESPVR ratios, indicating ventricular-arterial uncoupling sub-acutely and chronically following high-level SCI.[72,73] In the present study, the increase in Ea/ESPVR, driven by the significant decrease in contractility, implies ventricular-arterial uncoupling occurs acutely post-SCI and is largely due to cardiac dysfunction. Such ventricular-arterial uncoupling has been associated with reduced LV mechanical efficiency, reduced exercise capacity and LV remodelling, increasing the risk for heart failure.[176,177]

In pre-clinical and clinical research, EF is not altered after chronic SCI despite clear changes in both EDV and ESV.[65,72] This is in agreement with our acute findings: no changes in EF and FS at the end of the acute phase post-SCI compared to SHAM. EF and FS, more specifically EF, are often used in research for inferring systolic function as they can be non-invasively measured. However, these are not adequate measures when volumes are highly reduced (i.e. in the SCI field) as these changes will be concealed by the ratios. The latter might explain why we report altered volumes but no changes in EF and FS six days and chronically post-SCI.

Altogether, we report for the first time a reduction in systolic function and the occurrence of cardiovascular uncoupling acutely post-SCI, and further demonstrate these occurrences following high-

thoracic SCI in an additional strain of rats (Wistar), which are most likely due to the combined action of decreased cardiac sympathetic control and cardiac unloading. How such events post-SCI could be disadvantageous are discussed in Section 6.2.2.

5.1.4 There was no strong evidence of diastolic dysfunction acutely post-SCI

-dP/dt$_{min}$ was the only diastolic functional index which significantly changed acutely post-SCI versus SHAM. An increased -dP/dt$_{min}$ post-SCI indicated an impaired rate of pressure decrement. This impairment is likely to be explained by the decrease in pressure gradient between the LV and the arterial system, and the decrease in preload post-SCI. -dP/dt$_{min}$ is known to be affected by MAP and EDV,[178] which were both decreased in this study post-SCI and follow the latter hypothesis. The increase in -dP/dt$_{min}$ is in accordance with chronic SCI pre-clinical studies from our laboratory, which have showed significantly [72] and non-significantly [73,154] impaired -dP/dt$_{min}$ post-SCI.

As all other diastolic indices (Ped and tau) showed no changes following T3-SCI compared to SHAM, we cannot confidently assert an occurrence of diastolic dysfunction acutely following high-thoracic SCI in our experimental model. The lack of distinct changes in diastolic function acutely post-SCI could be explained by the insufficient time for cardiac unloading to cause structural remodelling, which has been detected chronically post-SCI (i.e. concentric remodelling and suggested collagen deposition).[63,154,179] A reduction in diastolic function at a more chronic time is expected as such is observed in pathologies associated with development of cardiac fibrosis and LV remodelling (i.e., aortic stenosis, myocardial infarction and hypertension).[180–182]

As mentioned in *diastolic dysfunction following SCI* (Section 1.5.1.2.), pre-clinical and clinical SCI studies have not reached a consensus on the occurrence of intrinsic cardiac diastolic function chronically post-SCI as data collection techniques and injuries are not consistent.[63,67–71] Here, our results further perpetuate the question of diastolic function post-SCI.

5.2 Protein degradation

5.2.1 UPS gene expression was up-regulated in the early stages of acute SCI

The RNA fold change of UPS target, *MAFbx*, was significantly increased in the acute phase following high-thoracic SCI in LV tissue. *MAFbx* peaked at the first experimental T3-SCI time-point by 3.37-fold (12 hours post-SCI) and tended to gradually decrease back to SHAM levels. These results closely mirror what was found by Zaglia *et al.* when investigating cardiac atrophy and protein regulation following denervation via chemical ablation of sympathetic neurons.[102] They have reported a two-fold increase in *MAFbx* gene expression via RT-qPCR at their first time-point, 1 day post-denervation.[102] Although our *MAFbx* fold change was not significantly higher in the 1 day T3-SCI group compared to SHAM, the mean fold change at 1 day showed a two-fold increase comparable to Zaglia *et al.* values.[102] Contrarily to Zaglia *et al.*, we did not observe *MAFbx* gene expression levels to return to SHAM levels at approximately a week post-intervention.[102] At the last time-point of this thesis, 7 days post-SCI, *MAFbx* tended to be increased versus SHAM at a non-significant value of 1.73 ±0.21. This value is similar to the value our research team has previously reported in the chronic phase post-SCI using the same injury model in a different strain of rats (Zucker lean), where we reported a significant increase of *MAFbx* gene expression at a significant value of 1.80 ±0.79 compared to SHAM at 12 weeks post-SCI.[72] These results suggest that, following high-thoracic SCI, *MAFbx* gene expression is immediately increased, peaks at 12 hours, then gradually decreases within the acute phase but sustains an elevated expression into the chronic phase. Elevated transcription of *MAFbx* could imply an increase in its E3 ligase activity and therefore an increase in degradation of its target proteins, such as eIF3f,[111] which could explain the atrophy seen in in the chronic setting post-SCI.

The RNA fold change of UPS target, *MuRF1*, was not significantly affected by high-thoracic SCI in the acute phase. However, *MuRF1* tended to increase immediately post-SCI with a peak at 5 days post-SCI

and seemed to decrease back to SHAM levels at the end of the acute phase. Li *et al*. and Zaglia *et al*. reported a significant increase in the regulation of *MuRF1* at one day following denervation in skeletal and cardiac muscle, respectively,[102,147] with a peak at day 3 in skeletal muscle.[147] *MuRF1* remained significantly up-regulated compared to the control at 14 days post-denervation in the study of Li *et al*., while in the study performed by Zaglia *et al.* levels had returned to control levels by day 8.[102,147] Although, the reason why our results for this target have not reached significance is likely due to low expression in one animal in the 5 days T3-SCI group, in general, our *MuRF1* results are in accordance with the literature. The slight discrepancy in *MuRF1* timing between studies could be explained by different injury type (physical and chemical denervation versus SCI), different type of muscle (skeletal versus cardiac muscle), and different rodent species and strains (Sprague-Dawley rats and mice versus Wistar rats). An increase in *MuRF1* gene expression could indicate an increase in its E3 ligase activity and therefore an increase in the degradation of sarcomeric proteins,[104,113–116] which could explain, along with the *MAFbx* results, the trending decrease in cardiomyocyte length seen in this thesis (Section 5.3.1). In our laboratory, we previously reported an increase in *MuRF1* RNA and protein levels 12-weeks following a complete T3 transection.[72] More investigation is required in the sub-acute and chronic phases post-SCI between the first and 12th week to map the temporal changes of MuRF1 activity.

Although there were no significant changes in the fold change of *MuRF1*, our results indicate that UPS, one of the main proteolytic pathways, was up-regulated immediately following high-thoracic SCI and may be sustained at higher levels into the chronic phase. Our results suggest an increase in protein degradation activity in LV tissue acutely following high-thoracic SCI in a complete T3 transection rodent model. However, to confidently conclude the latter, protein levels of MAFbx and MuRF1 and their own targets would require quantification as RNA fold changes do not specifically correlate with changes in protein levels.

In skeletal muscle wasting research, decreased mechanical loading [105,122] and elevated ANGII levels [95,128–130] are associated with increased UPS activity in the myocytes. As acute SCI leads to cardiac unloading and reduced MAP, followed by increased circulating ANGII levels, neuromechanical and neurohumoral changes could potentially explain the observed UPS up-regulation in cardiac tissue post-SCI. Nonetheless, prior studies investigating cardiac muscle atrophy strongly suggest that sympathetic input is the main factor regulating cardiomyocyte morphology.[183] Firstly, it has been shown that following chemical ablation of sympathetic neurons, up-regulation of UPS activity and cardiac atrophy occurred quickly post-denervation via decreased β_2 adrenergic receptors activation and subsequent FoxO activity.[102] Secondly, more recent studies from the same research team reported major changes in cardiomyocyte dimensions when the heart was denervated physically and chemically, and reported a correlation between cardiomyocyte cross-sectional area, protein degradation and the density of cardiac innervation.[183] The literature and our data further strengthen the hypothesis that the acute up-regulation of UPS observed post-SCI is due to the loss of sympathetic control to the heart. This decrease in trophic input would activate a signalling cascade to dephosphorylate FoxO3, which would allow it to translocate to the nucleus and start transcribing UPS-related genes. This increase in UPS activity would likely cause increased protein degradation, cardiomyocyte atrophy, and further decreases in volumetric indices and cardiac contractile function with time.

5.2.2 No changes in the autophagy gene expression were detected acutely post-SCI

The RNA fold changes of all investigated autophagy markers, *ATG7*, *ATG12* and *BECN1*, were not significantly affected by acute high-thoracic SCI. This suggests that none of these genes underwent increased transcription. Our results are in accordance with Zaglia *et al.*, which reported no changes of RNA levels for all of their chosen autophagy markers (i.e., *P62*, *Bnip3*, *BECN1* and *LC3*) at 8 days following denervation of mice cardiac tissue.[102]

The autophagy results from this thesis refute my hypothesis which stated an expected increase in gene expression of key targets of the pathway as ANGII, an up-regulator of autophagy, is predicted to increase acutely post-SCI due to reduction in blood pressure post-SCI. For future directions, temporal ANGII levels must be quantified to determine if there is an association with increased autophagy post-SCI. Furthermore, protein levels of these markers and their targets should be quantified to observe if their translation is increased and if protein degradation via autophagy is increased, respectively.

Our research team has previously published results involving the increase of *ATG12* and *BECN1* RNA fold changes in cardiac tissue in the chronic stage following the same injury model in a different strain of rat (Zucker lean rats terminated at 12 weeks post-SCI).[72] With those results, we knew that autophagy was affected in the chronic phase post-SCI. From this thesis, our results indicate that autophagy, one of the main proteolytic pathways, is perhaps not yet up-regulated in the acute phase following T3-SCI in our experimental model. Interestingly, Zaglia *et al.* reported an increase in autophagy activity subsequent to UPS up-regulation 30 days post-denervation (LC3II in cardiac muscle).[102] Therefore, it is plausible that autophagy is up-regulated later than UPS in cardiac muscle atrophy following such neural interventions.[102,121]

5.3 Cardiac structure

5.3.1 Histological data suggested the commencement of cardiomyocyte atrophy acutely post-SCI

None of the cardiomyocyte dimensions (standardized to femur length and unstandardized), length, width, CSA or volume, were significantly different in the T3-SCI groups at any time-point versus the SHAM group. Nonetheless, standardized length tended to gradually decrease along the acute setting with the lowest value in the 7 days T3-SCI group versus SHAM. These results suggest that cardiomyocyte atrophy might be initiated acutely without reaching significance. We hypothesize that cardiomyocyte atrophy will be significant early in the sub-acute phase following high-level SCI as length and width have

been reported to be significantly decreased at 5-weeks post-contusion and, in the chronic phase, 12-weeks post-transection,[72,73] and CSA has been observed to decrease 8-weeks post-transection in an unpublished study from our laboratory. The initiation of cardiomyocyte atrophy could be explained by the increase in UPS explained in Section 5.2.1. A potential reason why cardiomyocyte length would decrease prior to width could be the degradation of actin and myosin filaments by E3 ligase, MuRF1, causing either a decrease in the number of sarcomeres or shortening of the sarcomeres.[113,116,117] A previous study from our group, which also reported cardiomyocyte atrophy, did not report significant differences in sarcomere number or length in SCI animals compared to controls.[73] However, sarcomeric number or length were not quantified in this thesis as IF was not deemed accurate for this type of measurement. Such quantification should be investigated next with higher-resolution techniques, such as electron microscopy to measure length of thick filaments (A-bands) and estimate the number of sarcomeres in parallel per cell.

Cardiac atrophy can be caused by a reduction in body mass. However, in this thesis, the decreasing trend in cardiomyocyte length post-SCI was most likely not due to weight loss in our paralyzed animals, as there were no differences in body mass between the SHAM and T3-SCI groups when we collected the samples at termination. Furthermore, our dimensions were standardized to femur length, which also did not differ between groups.

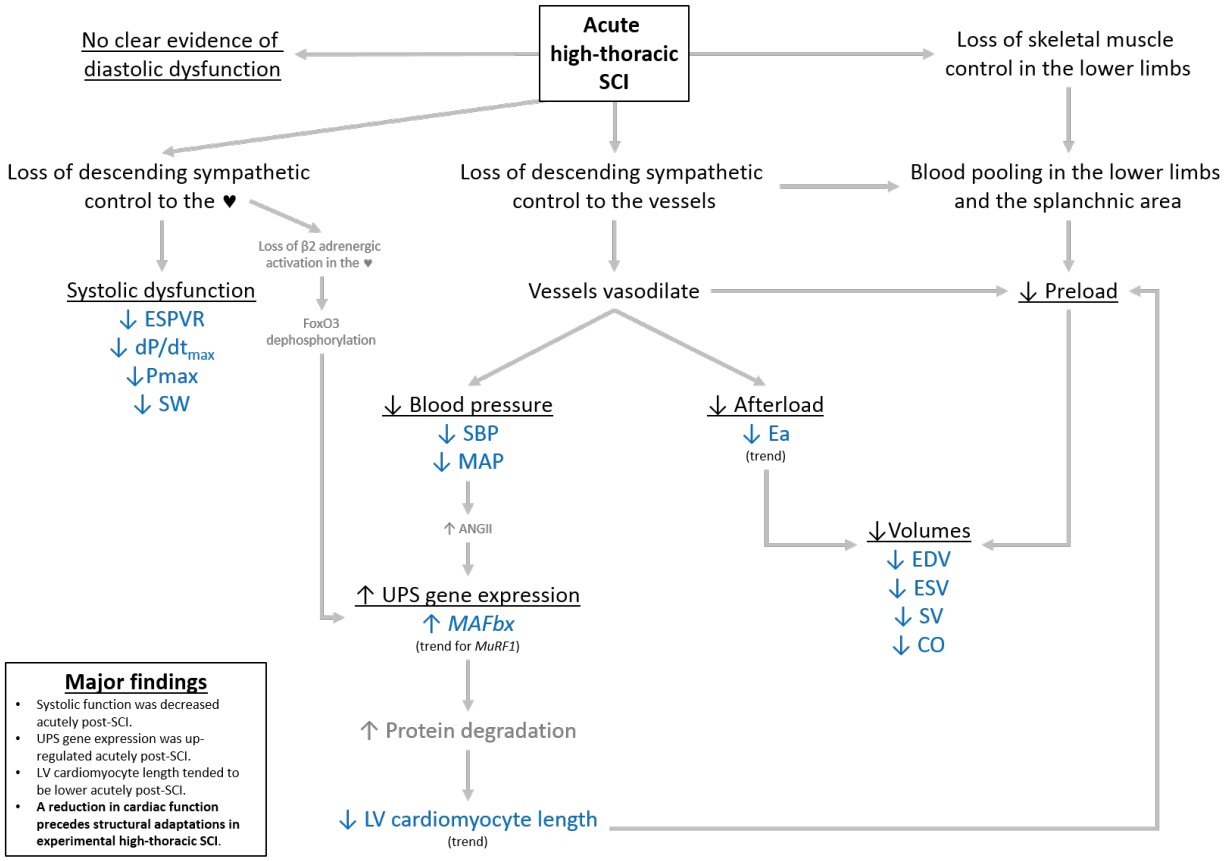

Figure 5.1. Overview of findings. Underlined events are new findings acutely post-SCI. In blue are variables measured in this thesis. In grey are hypothesized events which require more investigation. ANGII, angiotensin II; CO, cardiac output; dP/dt_{max}, maximal rate of systolic pressure increment ; EDV, end-diastolic volume; EF, ejection fraction; ESPVR, end-systolic pressure-volume relationship (index of contractility); ESV, end-systolic volume; FS, fractional shortening; LV, left-ventricle; *MAFbx*, muscle atrophy F-box; MAP, mean arterial blood pressure; *MuRF1*, muscle RING-finger protein 1; Pmax, maximum pressure; SCI, spinal cord injury; SBP, systolic blood pressure; SV, stroke volume; SW, stroke work; UPS, ubiquitin proteasome system.

Chapter 6. Conclusion

The literature and previous findings from our laboratory agreed on the occurrence of systolic dysfunction and cardiomyocyte atrophy with an associated increase in proteolytic activity in the chronic phase following severe high-level SCI. However, previous to this study, there was no research investigating the temporal progression of cardiac dysfunction, cardiac remodelling and the underlying molecular events acutely following high-thoracic SCI. Therefore, there existed a knowledge gap regarding when these events began to occur and in which order they took place. To investigate the temporal effects of acute high-thoracic SCI on LV cardiac function, proteolysis and cardiomyocyte morphology, I conducted a pre-clinical experiment using a T3 complete transection rodent model along with state of the art *in vivo*, histological, and molecular techniques to demonstrate a reduction in cardiac function precedes structural remodelling post-SCI.

6.1 Major findings

Our main functional findings were: 1) systolic function was reduced and ventricular-arterial uncoupling occurred acutely post-SCI; 2) there was no clear evidence of changes in diastolic function acutely post-SCI. We, therefore, report that cardiac dysfunction and vascular-arterial uncoupling took place early in the acute phase, persisted throughout the acute phase and was, therefore, likely due to the immediate loss of descending sympathetic control to the heart. Our molecular findings are: 1) UPS gene expression was increased in LV tissue at the earliest investigated time-point post-SCI; 2) there was no evidence of changes in autophagy regulation in LV tissue acutely post-SCI. We, therefore, report the upregulation of proteolytic pathway activity in cardiac tissue occurred early in the acute setting. Our structural findings were: 1) there was no significant atrophy in any cardiomyocyte dimensions acutely post-SCI; 2) cardiomyocyte length tended to be lower at the end of the acute setting following SCI. We,

therefore, report that cardiomyocyte atrophy was initiated but did not reach significance acutely following high-thoracic SCI. Thus, together the major finding of this thesis was that the reduction in cardiac function preceded cardiac structural remodelling following experimental high-thoracic SCI.

6.2 Relevance

6.2.1 Implications

All the information collected throughout this thesis contributes to the fields of SCI and cardiovascular health, by demonstrating that the acute phase is a crucial and decisive time for the adaptive changes in the heart's function and structure following high-level SCI and should be more thoroughly investigated in future research for potential time-sensitive treatments.

6.2.2 Why should we care about cardiac dysfunction and cardiac atrophy post-SCI?

Firstly, the general population tends to neglect some of the enumerable secondary consequences following SCI and most often do not consider the effects of SCI on the heart. The level and severity of the injury itself and the quantity of secondary complications all have a role in recovery speed, individual well-being and life expectancy. Therefore, all side effects of SCI, direct or indirect, acute or chronic, should be studied as all bodily systems interplay together. Secondly, the acute and chronic changes in heart function and structure observed in this thesis and in the literature could be of adaptive nature instead of maladaptive, contrary to what some might think. As SCI leads to many physiological and postural changes, the heart might simply be adjusting to its new conditions. However, this does not negate the fact that these changes could be deleterious to the individual in certain conditions. For example, a smaller heart, at first, does not seem inconvenient when considering blood volume or lower-limb muscle perfusion as both are decreased following SCI and lead to lesser cardiac demands at resting conditions. However, a smaller heart, vascular-arterial uncoupling and decreased cardiac function can lead to decreased performance

capacity and can be disadvantageous under strenuous conditions such as exercise and other stresses (i.e., autonomic dysreflexia, orthostatic stress, stress, etc.). Finally, in addition to decreased physical activity, dyslipidemia,[50–53] blood pressure instability,[57,58] arterial stiffness [59] and hormonal changes,[55] cardiac dysfunction and cardiac atrophy lead to premature onset and increased risk for CVD observed in individuals with SCI, which is the leading cause of death in this population.[60]

6.3 Strengths, limitations and considerations

6.3.1 Strengths

In this thesis, working with rodents allowed us to perform invasive techniques which would have been impossible to perform on human subjects for ethical reasons (i.e., catheterizations, tissue collection, etc.). In addition, we were capable of collecting robust and accurate cardiac functional and volumetric data thanks to contemporary techniques and equipment such as the use of an admittance catheter, which measures both resistive and conductive capacity, and echocardiography.

6.3.2 Limitations

Due to logistics, we unfortunately were not able to perform an excision of the entire organ in a timely manner without affecting tissue quality for *ex-vivo* experiments. To determine net gross cardiac atrophy, total cardiac mass should be obtained via a clean excision of the heart and subsequent weighing of the tissue after careful removal of all of the associated major vessels.

6.3.3 Considerations

Pre-surgery EDV measures were found to significantly different in our SHAM and T3-SCI groups. This unexpected finding could be explained by a non-significant but slight weight difference between the two groups due to age. Although the rats were ordered to be adults at the time of the study, the rats

remained juvenile enough to undergo growth. The T3-SCI rats were 4-5 days older at the time of surgery compared to the SHAM rats and this was solely due to logistics. Standardization of the measurements with femur length or body mass did not alter the significance of the results. If this study were to be repeated, we would ensure day-to-day age matching between groups and order more mature rats with no potential for further growth. Although this discrepancy between pre-surgery EDV is an important consideration, the deleterious effects of severe and high-level SCI on EDV were clear and indisputable.

6.4 Future directions

6.4.1 Further molecular analyses following acute SCI

To confirm the increase in protein degradation in the acute phase post-SCI, the quantification of protein levels of our UPS targets and their own targets is required via western blots. Furthermore, enzyme-linked immunosorbent assays (ELISA) could be performed to detect circulating NE and ANGII levels in the serum throughout the acute timeline post-SCI. These experiments, informed by what we know in the chronic setting already, would aid to understand the connection between the occurrence of SCI and the regulation of proteolysis in the cardiac tissue post-SCI. Other interesting molecular analyses, which have not yet been investigated following SCI in cardiac tissue, include the density of sympathetic neurons and pathways such as apoptosis and angiogenesis.

6.4.2 Sub-acute time-points following SCI

Additional sub-acute time-points should be investigated to pinpoint the time for cardiomyocyte atrophy and detect the changes in the regulation of autophagy. Next, cardiac atrophy could be measured via measurement of total cardiac mass along the acute and sub-acute timelines.

REFERENCES

1. Ovalle WK, Nahirney PC. *Netter's Essential Histology*. 2nd ed. Elsevier Canada; 2013.
2. Ross MH, Pawlina W. *Histology – a Text and Atlas with Correlated Cell and Molecular Biology*. 6th ed. Baltimore, MD: Lippincott Williams and Wilkins, a Wolters Kluwer business; 2011.
3. Gartner LP, Hiatt JL. *Color Textbook of Histology*. 3rd ed. Philadelphia, PA: Saunders Elsevier; 2007.
4. MacKenna DA, Omens JH, McCulloch AD, Covell J. Contribution of collagen matrix to passive left ventricular mechanics in isolated rat hearts. *Am J Physiol*. 1994;266:H1007-H1018.
5. Weber KT, Sun Y, Tyagi SC, Cleutjens JPM. Review – Collagen network of the myocardium – Function, structural remodeling and regulatory mechanisms. *J Mol Cell Cardiol*. 1994;26:279-292.
6. Hsieh PCH, Davis ME, Lisowski LK, Lee RT. Endothelial-Cardiomyocyte Interactions in Cardiac Development and Repair. *Annu Rev Physiol*. 2006;68:51-66.
7. Gerdes AM, Kellerman SE, Malec KB, Schocken D. Transverse shape characteristics of cardiac myocytes from rats and humans. *Cardioscience*. 1994;5:31-34.
8. Sorenson AL, Tepper D, Sonnenblick EH, Robinson TF, Capasso JM. Size and shape of enzymatically isolated ventricular myocytes from rats and cardiomyopathic hamsters. *Cardiovasc Res*. 1985;19:793-799.
9. Blumberg F, Hort C, Hort W. Distribution of myofibrils and mitochondria in ventricular myocytes – A quantitative light and electron microscopic study in dog and chicken hearts. *Z Kardiol*. 1995;84:154-162.
10. Roos KP. Mechanics and force production. In: *The Myocardium, Second Edition*. San Diego, CA: Academic Press; 1997:235-323.
11. Frank JS. Ultrastructure of the sarcolemma of isolated cardiomyocytes. In: Piper HM, Isenberg G,

eds. *Isolated Adult Cardiomycyotes*. Boca Raton, FL: CRC Press; 1989:125-143.

12. Sommer JR, Johnson EA. Ultrastructure of cardiac muscles. In: Berne RM, Sperelakis N, Geiger SR, eds. *Handbook of Physiology, Section 2: The Cardiovascular System, Volume 1: The Heart*. Bethesda, MD: American Physiological Society; 1979:113-186.
13. Goldstein MA, Michael LH, Schroeter JP, Sass RL. Two structural states of Z- bands in cardiac muscle. *Am J Physiol*. 1989;256:H552-H559.
14. Isobe Y, Warner FD, Lemanski LF. Three-dimensional immunogold localization of alpha-actinin within the cytoskeleton networks of cultured cardiac muscle and nonmuscle cells. *Proc Natl Acad Sci United States*. 1988;85:6759-6762.
15. Eisenberg BR. Skeletal muscle. In: Peachey L, Adrian RH, Geiger SR, eds. *Handbook of Physiology*. Bethesda, MD: American Physiological Society; 1983:73-112.
16. Page E. Quantitative ultrastructural analysis in cardiac membrane physiology. *Am J Physiol*. 1978;235:C147-C158.
17. Battipaglia I, Lanza GA. Autonomic innervation of the heart Role of molecular imaging. In: Slart RH, Elsinga PH, Tio RA, eds. *Autonomic Innervation of the Heart: Role of Molecular Imaging*. Springer-Verlag Berlin Heidelberg 2015; 2015. doi:10.1007/978-3-662-45074-1_1
18. Guyton AC, Hall JE. *Textbook of Medical Physiology*. Philadelphia, PA: Elsevier Saunders; 2006.
19. Partida E, Mironets E, Hou S, Tom VJ. Cardiovascular dysfunction following spinal cord injury. *Neural Regen Res*. 2016;11(2):189-194. doi:10.4103/1673-5374.177707
20. Jänig W. Regulation of organ systems by the lower brain stem. In: *The Integrative Action of the Autonomic Nervous System*. Cambridge University Press; 2009:375-458. doi:10.1017/CBO9780511541667.015
21. Klionsky DJ, Abdelmohsen K, Abe A, et al. Guidelines for the use and interpretation of assays for

monitoring autophagy (3rd edition). *Autophagy*. 2016;12(1):1-222. doi:10.1080/15548627.2015.1100356

22. Gibbins IL, Jobling P, Morris JL. Functional organization of peripheral vasomotor pathways. *Acta Physiol Scand*. 2003;177(3):237-245.

23. Espinosa-Medina I, Saha O, Boismoreau F, et al. The sacral autonomic outflow is sympathetic. *Science (80-)*. 2016;354(6314):893-898.

24. Goyal RK. Implications, Muscarinic receptor subtypes. Physiology and clinical implications. *N Engl J Med*. 1989;321:1022-1029.

25. Burt AM. *Textbook of Neuroanatomy*. Philadelphia, PA: WB Saunders Company; 1993.

26. Ahlquist RP. A study of the adrenotropic receptors. *Am J Physiol*. 1948;153:586-600.

27. Bylund DB, Eikenber DC, Hieble JP, et al. International Union of Pharmacology nomenclature of adrenoceptors. *Pharmacol Rev*. 1994;46(2):121-136.

28. McCraty R, Zayas MA. Cardiac coherence, self-regulation, autonomic stability and psychosocial well-being. *Front Psychol*. 2014;5(SEP):1-13. doi:10.3389/fpsyg.2014.01090

29. Gordan R, Gwathmey JK, Xie L-H. Autonomic and endocrine control of cardiovascular function. *World J Cardiol*. 2015;7(4):204. doi:10.4330/wjc.v7.i4.204

30. Carnevali L, Sgoifo A. Vagal modulation of resting heart rate in rats : the role of stress , psychosocial factors , and physical exercise. *Front Physiol*. 2014;5:1-12. doi:10.3389/fphys.2014.00118

31. Frank JS, Garfinkel A. Immunolocalization and structural configuration of membrane and cytoskeletal proteins involved in excitation-contraction coupling of cardiac muscle. In: Langer GA, ed. *The Myocardium, Second Edition*. San Diego, CA: Academic Press; 1997:1-32.

32. Burkhoff D. Assessment of systolic and diastolic ventricular properties via pressure-volume

analysis: a guide for clinical, translational, and basic researchers. *AJP Hear Circ Physiol*. 2005;289(2):H501-H512. doi:10.1152/ajpheart.00138.2005

33. Dostal D, Baker K. The cardiac rennin-angiotensin system conceptual, or a regulator of cardiac function? *Circ Res*. 1999;97:1037-1041.

34. De Mello W, Danser A. Angiotensin II and the Heart On the Intracrine Renin-Angiotensin System. *Hypertension*. 2000;35(6):1183-1188. doi:10.1161/01.hyp.35.6.1183

35. Van Kats JP, Danser AHJ, Van Meegen JR, Sassen LMA, Verdouw PD, Schalekamp MADH. Angiotensin production by the heart: A quantitative study in pigs with the use of radiolabeled angiotensin infusions. *Circulation*. 1998;98(1):73-81. doi:10.1161/01.CIR.98.1.73

36. Iwai N, Shimoike H, Kinoshita M. Cardiac Renin-Angiotensin System in the Hypertrophied Heart. *Circulation*. 1995;92:2690-2696. doi:10.1161/01.CIR.92.9.2690

37. Lindpaintner K, Lu W, Niedermajer N, et al. Selective Activation of Cardiac Angiotensinogen Gene Expression in Post-infarction Ventricular Remodeling in the Rat. *J Mol Cell Cardiol*. 1993;25(2):133-143. doi:10.1006/jmcc.1993.1017

38. Hill JA, Olson EN. Cardiac Plasticity. *N Engl J Med*. 2008;358(13):1370-1380. doi:10.1056/NEJMra072139

39. Zhu H. Myocardial cellular development and morphogenesis. In: Langer GA, ed. *The Myocardium, Second Edition*. San Diego, CA: Academic Press; 1997:33-80.

40. Vulpis V, Seccia TM, Nico B, Ricci S, Roncali L, Pirrelli A. Left ventricular hypertrophy in spontaneously hypertensive rat: Effects of ACE-inhibition on myocardiocyte ultrastructure. *Pharmacol Res*. 1995;31:375-381.

41. Adameova A, Abdellatif Y, Dhalla NS. Role of the excessive amounts of circulating cate- cholamines and glucocorticoids in stress-induced heart disease. *Can J Physiol Pharmacol*. 2009;87:493–514.

42. Martins da Silvaa MI, Vidigal Ferreirab MJ, Morão Moreira AP. Iodine-123-metaiodobenzylguanidine scintigraphy in risk stratification of sudden death in heart failure. *Rev Port Cardiol*. 2013;32:509–516.

43. Kavazis AN. Pathological vs. physiological cardiac hypertrophy. *J Physiol*. 2015;593(17):3767. doi:10.1113/JP271161

44. Farry A, Baxter D. The incidence and prevalence of spinal cord injury in Canada: overview and estimates based on current evidence. 2010.

45. Lee BB, Cripps RA, Fitzharris M, Wing PC. The global map for traumatic spinal cord injury epidemiology: Update 2011, global incidence rate. *Spinal Cord*. 2014;52(2):110-116. doi:10.1038/sc.2012.158

46. Krueger H, Noonan VK, Trenaman LM, Joshi P, Rivers CS. The economic burden of traumatic spinal cord injury in Canada. *Chronic Dis Inj Can*. 2013;33(3):113-122.

47. Krassioukov A, Biering-Sørensen F, Donovan W, et al. International standards to document remaining autonomic function after spinal cord injury. *J Spinal Cord Med*. 2012;35(4):201-210. doi:10.1179/1079026812Z.00000000053

48. Teasell RW, Arnold JMO, Krassioukov A, Delaney GA. Cardiovascular consequences of loss of supraspinal control of the sympathetic nervous system after spinal cord injury. *Arch Phys Med Rehabil*. 2000;81(4):506-516. doi:10.1053/mr.2000.3848

49. Kessler KM, Pina I, Green B, et al. Findings in quadriplegic and paraplegic patients and in normal subjects. *Am J Cardiol*. 1986;58:525-530.

50. Nash MS, Jacobs PL, Mendez AJ, Goldberg RB. Circuit resistance training improves the atherogenic lipid profiles of persons with chronic paraplegia. *J Spinal Cord Med*. 2001;24(1):2-9. doi:10.1080/10790268.2001.11753548

51. Myers J, Lee M, Kiratli J. Cardiovascular Disease in Spinal Cord Injury. *Am J Phys Med Rehabil*. 2007;86(2):142-152. doi:10.1097/PHM.0b013e31802f0247

52. Liang H, Mojtahedi MC, Chen D, Braunschweig CL. Elevated C-Reactive Protein Associated With Decreased High-Density Lipoprotein Cholesterol in Men With Spinal Cord Injury. *Arch Phys Med Rehabil*. 2008;89(1):36-41. doi:10.1016/j.apmr.2007.08.121

53. Heldenberg D, Rubinstein A, Levtov O, Werbin B, Tamir I. Serum lipids and lipoprotein concentrations in young quadriplegic patients. *Atherosclerosis*. 1981;39(2):163-167. doi:10.1016/0021-9150(81)90065-4

54. Buchholz AC, Bugaresti JM. A review of body mass index and waist circumference as markers of obesity and coronary heart disease risk in persons with chronic spinal cord injury. *Spinal Cord*. 2005;43(9):513-518. doi:10.1038/sj.sc.3101744

55. Lee M, Myers J, Hayes A, et al. C-Reactive Protein, Metabolic Syndrome, and Insulin Resistance in Individuals With Spinal Cord Injury. *J Spinal Cord Med*. 2005;28(1):20-25. doi:10.1080/10790268.2005.11753794

56. Cragg JJ, Noonan VK, Dvorak M, Krassioukov A, Mancini GBJ, Borisoff JF. Spinal cord injury and type 2 diabetes Results from a population health survey. *Neurology*. 2013;81(21):1864-1868. doi:10.1212/01.wnl.0000436074.98534.6e

57. Krassioukov A, Warburton DE, Teasell R, Eng JJ. A Systematic Review of the Management of Autonomic Dysreflexia After Spinal Cord Injury. *Arch Phys Med Rehabil*. 2009;90(4):682-695. doi:10.1016/j.apmr.2008.10.017

58. Krassioukov A, Eng JJ, Warburton DE, Teasell R. A Systematic Review of the Management of Orthostatic Hypotension After Spinal Cord Injury. *Arch Phys Med Rehabil*. 2009;90(5):876-885. doi:10.1016/j.apmr.2009.01.009

59. Lee AHX, Phillips AA, Krassioukov A V. Increased Central Arterial Stiffness after Spinal Cord Injury: Contributing Factors, Implications, and Possible Interventions. *J Neurotrauma*. 2017;34(6):1129-1140. doi:10.1089/neu.2016.4694

60. Cragg JJ, Noonan VK, Krassioukov A V, Borisoff JF. Cardiovascular disease and spinal cord injury: results from a national population health survey. *Neurology*. 2013;81(8):723-728. doi:10.1212/WNL.0b013e3182a1aa68

61. Currie KD, West CR, Krassioukov A V. Differences in left ventricular global function and mechanics in paralympic athletes with cervical and thoracic spinal cord injuries. *Front Physiol*. 2016;7:1-8.

62. West CR, Mills P, Krassioukov A V. Influence of the neurological level of spinal cord injury on cardiovascular outcomes in humans: a meta-analysis. *Spinal Cord*. 2012;50:484-492.

63. Driussi C, Ius A, Bizzarini E, et al. Structural and functional left ventricular impairment in subjects with chronic spinal cord injury and no overt cardiovascular disease. *J Spinal Cord Med*. 2014;37(1):85-92. doi:10.1179/2045772313Y.0000000161

64. de Groot PC, van Dijk A, Dijk E, Hopman MT. Preserved Cardiac Function After Chronic Spinal Cord Injury. *Arch Phys Med Rehabil*. 2006;87(9):1195-1200. doi:10.1016/j.apmr.2006.05.023

65. Williams AM, Gee CM, Voss C, West CR. Cardiac consequences of spinal cord injury: Systematic review and meta-analysis. *Heart*. 2019;105(3):217-225. doi:10.1136/heartjnl-2018-313585

66. Pacher P, Nagayama T, Mukhopadhyay P, Bátkai S, Kass DA. Measurement of cardiac function using pressure-volume conductance catheter technique in mice and rats. *Nat Protoc*. 2008;3(9):1422-1434. doi:10.1038/nprot.2008.138

67. Maggioni MA, Ferratini M, Pezzano A, et al. Heart adaptations to long-term aerobic training in paraplegic subjects: an echocardiographic study. *Spinal Cord*. 2012;50(7):538=542.

68. Sharif H, Wainman L, O'Leary D, Ditor D. The effect of blood volume and volume loading on left

ventricular diastolic function in individuals with spinal cord injury. *Spinal Cord*. 2017;55(8):753-758.

69. De Rossi G, Matos-Souza JR, Costa E, et al. Physical Activity and Improved Diastolic Function in Spinal Cord-Injured Subjects. *Med Sci Sport Exerc*. 2014;46(5):887-892.

70. Kim JH, Trilk JL, Smith R, et al. Cardiac Structure and Function in Elite Para-cyclists with Spinal Cord Injury. *Med Sci Sport Exerc*. 48(8):1431-1437.

71. Currie KD, West CR, Stöhr EJ, Krassioukov A V. Left Ventricular Mechanics in Untrained and Trained Males with Tetraplegia. *J Neurotrauma*. 2017;55(8):753-758.

72. Poormasjedi-Meibod M-S, Mansouri M, Fossey M, Squair JW, Mcneill JH, West CR. Experimental Spinal Cord Injury Causes Left-Ventricular Atrophy and Is Associated with an Upregulation of Proteolytic Pathways. *J Neurotrauma*. 2019;36(950):961. doi:10.1089/neu.2017.5624

73. Squair JW, DeVeau KM, Harman KA, et al. Spinal Cord Injury Causes Systolic Dysfunction and Cardiomyocyte Atrophy. *J Neurotrauma*. 2017;434:neu.2017.4984. doi:10.1089/neu.2017.4984

74. Krassioukov A. Autonomic function following cervical spinal cord injury. *Respir Physiol Neurobiol*. 2009;169(2):157-164. doi:10.1016/j.resp.2009.08.003

75. Mathias CJ, Christensen NJ, Corbett JL, Frankel HL, Goodwin TJ, Peart WS. Plasma catecholamines, plasma renin activity and plasma aldosterone in tetraplegic man, horizontal and tilted. *Clin Sci Mol Med*. 1975:291-299.

76. Schmid A, Huonker M, Barturen JM, et al. Catecholamines, heart rate, and oxygen uptake during exercise in persons with spinal cord injury. *J Appl Physiol*. 1998:1195-1200.

77. Levine BD, Zuckerman JH, Pawelcyzk JA. Cardiac atrophy after bed-rest deconditioning. *Circulation*. 1997;96.

78. Grigorean VT, Sandu AM, Popescu M, et al. Cardiac dysfunctions following spinal cord injury. *J Med*

Life. 2009;2(2):133-145.

79. Ditunno JF, Little JW, Tessler A, Burns AS. Spinal shock revisited: A four-phase model. *Spinal Cord*. 2004;42(7):383-395. doi:10.1038/sj.sc.3101603

80. Furlan JC, Fehlings MG, Shannon P, Norenberg MD, Krassioukov A V. Descending vasomotor pathways in humans: Correlation between axonal preservation and cardiovascular dysfunction after spinal cord injury. *J Neurotrauma*. 2003;20:1351-1363.

81. Wecht JM, de Meersman RE, Weir JP, Bauman WA, Grimm DR. Effects of autonomic disruption and inactivity on venous vascular function. *Am J Physiol - Hear Circ Physiol*. 2000;278(2):515-520.

82. Mathias C, Christensen NJ, Corbett JL, Frankel HL. Plasma catecholamines during paroxysmal neurogenic hypertension in quadriplegic man. *Circ Res*. 1976;39(2):204-208.

83. Blackmer J. Orthostatic Hypotension in Spinal Cord Injured Patients. *J Spinal Cord Med*. 1997;20(2):212-217. doi:10.1080/10790268.1997.11719471

84. Faghri PD, Yount J. Electrically induced and voluntary activation of physiologic muscle pump : a comparison between spinal cord-injured and able-bodied individuals. *Clin Rehabil*. 2002;16(8):878-885.

85. West CR, Alyahya A, Laher I, Krassioukov A V. Peripheral vascular function in spinal cord injury: a systematic review. *Spinal Cord*. 2013:10-19.

86. Hopman MTE, Oeseburg B, Binkhorst RA. The effect of an anti-G suit on cardiovascular responses to exercise in persons with paraplegia. *Med Sci Sport Exerc*. 1992;24(9):984-990.

87. Hopman MTE, Oeseburg B, Binkhorst RA. Cardiovascular responses in paraplegic subjects during arm exercise. *Eur J Appl Physiol Occup Physiol*. 1992;65(1):73-78. doi:10.1007/BF01466277

88. Hopman MTE, Oeseburg B, Binkhorst RA. Cardiovascular responses in persons with paraplegia to prolonged arm exercise and thermal stress. *Med Sci Sport Exerc*. 1993;25(5):577-583.

89. Davis GM, Servedio FJ, Glaser RM, Gupta SC, Suryaprasad AG. Cardiovascular responses to arm cranking and FNS-induced leg exercise in paraplegics. *J Appl Physiol*. 1990;69(2):671-677.

90. Figoni SF. Exercise responses and quadriplegia. *Med Sci Sports Exerc*. 1993;25(4):433-441.

91. Sawka MN, Gonzalez RR, Drolet LL, Pandoff KB. Temperature regulation during upper body exercise: able-bodied and spinal cord injured. *Med Sci Sport Exerc*. 1989;21:72-80.

92. Lujan HL, DiCarlo SE. Increasing venous return as a strategy to prevent or reverse cardiac dysfunction following spinal cord injury. *J Physiol*. 2014:1727-1728.

93. Phillips AA, Krassioukov A V. Contemporary cardiovascular concerns after spinal cord injury: Mechanisms, maladaptations, and management. *J Neurotrauma*. 2015;32(24):1927-1942. doi:10.1089/neu.2015.3903

94. Houtman S, Oeseburg B, Hopman MT. Blood volume and hemoglobin after spinal cord injury. *Am J Phys Med Rehabil*. 2000;79(3):260-265. doi:10/1097/00002060-200005000-00008

95. Yoshida T, Tabony AM, Galvez S, et al. Molecular mechanisms and signaling pathways of angiotensin II-induced muscle wasting: Potential therapeutic targets for cardiac cachexia. *Int J Biochem Cell Biol*. 2013;45(10):2322-2332. doi:10.1016/j.biocel.2013.05.035

96. Porrello ER, Delbridge LMD. Cardiomyocyte autophagy is regulated by angiotensin II type 1 and type 2 receptors. *Autophagy*. 2009;5(8):1215-1216. doi:10.4161/auto.5.8.10153

97. Phillips WT, Kiratli BJ, Sarkarati M, et al. Effect of spinal cord injury on the heart and cardiovascular fitness. *Curr Probl Cardiol*. 1998:641-716.

98. Schnee JM, Hsueh WA. Angiotensin II and Cardiac Fibrosis. *Cardiovasc Res*. 2000;46:264-268.

99. Squair JW, Liu J, Tetzlaff W, Krassioukov A V., West CR. Spinal cord injury-induced cardiomyocyte atrophy and impaired cardiac function are severity dependent. *Exp Physiol*. 2018;103(2):179-189. doi:10.1113/EP086549

100. Eysmann SB, Douglas PS, Katz SE, Sarkarati M, Wei JY. Left ventricular mass and diastolic filling patterns in quadriplegia and implications for effects of normal aging on the heart. *Am J Cardiol*. 1995;75(2):201-203. doi:10.1016/S0002-9149(00)80082-X

101. Hellerstein HK, Santiago-Stevenson D. Atrophy of the Heart : A Correlative Study of Eighty-Five Proved Cases. *Circulation*. 1950;1:93-126.

102. Zaglia T, Milan G, Franzoso M, et al. Cardiac sympathetic neurons provide trophic signal to the heart via β2-adrenoceptor-dependent regulation of proteolysis. *Cardiovasc Res*. 2013;97(2):240-250. doi:10.1093/cvr/cvs320

103. Donohue TM, Osna N a. Intracellular proteolytic systems in alcohol-induced tissue injury. *Alcohol Res Health*. 2003;27(4):317-324.

104. Bonaldo P, Sandri M. Cellular and molecular mechanisms of muscle atrophy. *Dis Model Mech*. 2013;6(1):25-39. doi:10.1242/dmm.010389

105. Schiaffino S, Dyar KA, Ciciliot S, Blaauw B, Sandri M. Mechanisms regulating skeletal muscle growth and atrophy. *FEBS J*. 2013;280(17):4294-4314. doi:10.1111/febs.12253

106. Lee D, Goldberg A. Atrogin1/MAFbx: what atrophy, hypertrophy, and cardiac failure have in common. *Circ Res*. 2011;(109):123-126.

107. Lecker SH, Jagoe TR, Gilbert A, et al. Multiple types of skeletal muscle atrophy involve a common program of changes in gene expression. *FASEB J*. 2004;18:39-51.

108. Combaret L. USP19 is a ubiquitin-specific protease regulated in rat skeletal muscle during catabolic states. *AJP Endocrinol Metab*. 2004;288(4):E693-E700. doi:10.1152/ajpendo.00281.2004

109. Bodine SC, Latres E, Baumhueter S, et al. Identification of Ubiquitin Ligases Required for Skeletal Muscle Atrophy Linked references are available on JSTOR for this article : Identification of Ubiquitin Ligases Required for Skeletal Muscle Atrophy. 2016:2-7.

110. Tintignac LA, Lagirand J, Batonnet S, Sirri V, Leibovitch MP, Leibovitch SA. Degradation of MyoD mediated by the SCF (MAFbx) ubiquitin ligase. *J Biol Chem*. 2005;280:2847-2856.

111. Csibi A, Cornille K, Leibovitch MP, et al. The translation regulatory subunit eIF3f controls the kinase-dependent mTOR signaling required for muscle differentiation and hypertrophy in mouse. *PLoS One*. 2010;5:e8994.

112. Ucar A, Gupta SK, Fiedler J, et al. The miRNA-212/132 family regulates both cardiac hypertrophy and cardiomyocyte autophagy. *Nat Commun*. 2012;3:1011-1078. doi:10.1038/ncomms2090

113. Fielitz J, Kim MS, Shelton JM, et al. Myosin accumulation and striated muscle myopathy result from the loss of muscle RING finger 1 and 3. *J Clin Invest*. 2007;117:2486-2495.

114. Kedar V, McDonough H, Arya R, Li HH, Rockman HA, Patterson C. Muscle-specific RING finger 1 is a bona fide ubiquitin ligase that degrades cardiac troponin I. *Proc Natl Acad Sci United States*. 2004;(101):18135-18140.

115. Cohen S, Brault JJ, Gygi SP, et al. During muscle atrophy, thick, but not thin, filament components are degraded by MuRF1-dependent ubiquitylation. *J Cell Biol*. 2009;185(1083-1095).

116. Clarke BA, Drujan D, Willis MS, et al. The E3 Ligase MuRF1 degrades myosin heavy chain protein in dexamethasone-treated skeletal muscle. *Cell Metab*. 2007;6:376-385.

117. Polge C, Heng A-E, Jarzaguet M, et al. Muscle actin is polyubiquitinylated in vitro and in vivo and targeted for breakdown by the E3 ligase MuRF1. *FASEB J*. 2011;25(11):3790-3802. doi:10.1096/fj.11-180968

118. Cohen S, Zhai B, Gygi SP, Goldberg AL. Ubiquitylation by Trim32 causes coupled loss of desmin, Z-bands, and thin filaments in muscle atrophy. *J Cell Biol*. 2012;198:575-589.

119. Paul PK, Bhatnagar S, Mishra V, et al. The E3 Ubiquitin Ligase TRAF6 Intercedes in Starvation-Induced Skeletal Muscle Atrophy through Multiple Mechanisms. *Mol Cell Biol*. 2012;32(7):1248-

1259. doi:10.1128/MCB.06351-11

120. Bertaggia E, Coletto L, Sandri M. Posttranslational modifications control FoxO3 activity during denervation. *AJP Cell Physiol*. 2012;302(3):C587-C596. doi:10.1152/ajpcell.00142.2011

121. Sandri M, Sandri C, Gilbert A, Skurk C, Calabria E. Foxo Transcription Factors Induce the Atrophy-Related Ubiquitin Ligase Atrogin-1 and Cause Skeletal Muscle Atrophy. *Cell*. 2004;117:1-2. doi:10.1016/j.jsbmb.2011.07.002.Identification

122. Miyagoe-Suzuki Y, Takeda S. Mechanobiology in Skeletal Muscle: Conversion of Mechanical Information into Molecular Signal. In: Noda M, ed. *Mechanosensing Biology*. ; 2011:51-59.

123. Romanello V, Sandri M. Mitochondrial biogenesis and fragmentation as regulators of muscle protein degradation. *Curr Hypertens Rep*. 2010;12(6):433-439. doi:10.1007/s11906-010-0157-8

124. Greer EL, Oskoui PR, Banko MR, et al. The energy sensor AMP-activated protein kinase directly regulates the mammalian FOXO3 transcription factor. *J Biol Chem*. 2007;282:30107-30119.

125. Greer EL, Dowlatshahi D, Banko MR, et al. An AMPK-FOXO pathway mediates longevity induced by a novel method of dietary restriction in C. elegans. *Curr Biol*. 2007;17:1646-1656.

126. Mendias CL, Gumucio JP, Davis ME, Bromley CW, Davis CS, Brooks S V. Transforming growth factor-beta induces skeletal muscle atrophy and fibrosis through the induction of atrogin-1 and scleraxis. *Muscle and Nerve*. 2012;45(1):55-59. doi:10.1002/mus.22232

127. Narola J, Pandey SN, Glick A, Chen YW. Conditional expression of TGF-β1 in skeletal muscles causes endomysial fibrosis and myofibers atrophy. *PLoS One*. 2013;8(11). doi:10.1371/journal.pone.0079356

128. Semprun-Prieto LC, Sukhanov S, Yoshida T, et al. Angiotensin II induced catabolic effect and muscle atrophy are redox dependent. *Biochem Biophys Res Commun*. 2011;409(2):217-221. doi:10.1016/j.bbrc.2011.04.122

129. Song Y, Rosenthal N, Delafontaine P, et al. Muscle-specific expression of IGF-1 blocks angiotensin II – induced skeletal muscle wasting. *J Clin Invest*. 2005;115(2):451-458. doi:10.1172/JCI200522324.The

130. Sanders PM, Russell ST, Tisdale MJ. Angiotensin II directly induces muscle protein catabolism through the ubiquitin-proteasome proteolytic pathway and may play a role in cancer cachexia. *Br J Cancer*. 2005;93(4):425-434. doi:10.1038/sj.bjc.6602725

131. Levine B, Kroemer G. Autophagy in the Pathogenesis of Disease. *Cell*. 2008;132(1):27-42. doi:10.1016/j.cell.2007.12.018.Autophagy

132. Mizushima N, Levine B, Cuervo AM, Klionsky DJ. Autophagy fights disease through cellular self-digestion. *Nature*. 2008;451(7182):1069-1075. doi:10.1038/nature06639

133. Levine B, Kroemer G. SnapShot: Macroautophagy. *Cell*. 2008;132(1):162.e1-162.e3. doi:10.1016/j.cell.2007.12.026

134. Wu H, Chen S, Ammar A-B, et al. Crosstalk Between Macroautophagy and Chaperone-Mediated Autophagy: Implications for the Treatment of Neurological Diseases. *Mol Neurobiol*. 2015;52(3):1284-1296. doi:10.1007/s12035-014-8933-0

135. Geng J, Klionsky DJ. The Atg8 and Atg12 ubiquitin-like conjugation systems in macroautophagy. 'Protein modifications: beyond the usual suspects' review series. *EMBO Rep*. 2008;9(9):859-864.

136. Komatsu M, Tanida I, Ueno T, Ohsumi M, Ohsumi Y, Kominami E. The C-terminal region of an Apg7p/Cvt2p is required for homodimerization and is essential for its E1 activity and E1-E2 complex formation. *J Biol Chem*. 2001;276(13):9846-9854.

137. Nemoto T, Tanida I, Tanida-Miyake E, et al. The mouse APG10 homologue, an E2-like enzyme for Apg12p conjugation, facilitates MAP-LC3 modification. *J Biol Chem*. 2003;278(41):39517-39526.

138. Kaufmann A, Beier V, Franquelim HG, Wollert T. Molecular mechanism of autophagic membrane-

scaffold as- sembly and disassembly. *Cell*. 2014;156(3):469-481.

139. Hanada T, Noda NN, Satomi Y, et al. The Atg12-Atg5 conjugate has a novel E3-like activity for protein lipidation in autophagy. *J Biol Chem*. 2007;282(52):37298–37302.

140. Tanida I, Yamasaki M, Komatsu M, Ueno T. The FAP motif within human ATG7, an autophagy-related E1-like enzyme, is essential for the E2-substrate reaction of LC3 lipidation. *Autophagy*. 2012;8(1):88-97.

141. Yamada Y, Suzuki NN, Hanada T, et al. The crystal structure of Atg3, an autophagy-related ubiquitin carrier protein (E2) enzyme that mediates Atg8 lipidation. *J Biol Chem*. 2007;2882(11):8036–8043.

142. Harris H, Rubinsztein DC. Control of autophagy as a therapy for neurodegenerative disease. *Nat Rev Neurol*. 2012;8(2):108-117.

143. Rubinsztein DC, Marino G, Kroemer G. Autophagy and aging. *Cell*. 2011;146(5):682-695.

144. Mizushima N, Yamamoto A, Matsui M, Yoshimori T, Ohsumi Y. In vivo analysis of autophagy in response to nutrient starvation using transgenic mice expressing a fluorescent autophagosome marker. *Mol Biol Cell*. 2004;15:1101-1111.

145. Kinoshita M, Takano H, Takaichi S, Taenaka Y, Nakatani T. Influence of prolonged ventricular assistance on myocardial histopathology in intact heart. *Ann Thorac Surg*. 1996;61:640-645.

146. Wang X, Dai Y, Ding Z, Khaidakov M, Mercanti F, Mehta JL. Regulation of autophagy and apoptosis in response to angiotensin II in HL-1 cardiomyocytes. *Biochem Biophys Res Commun*. 2013;440:696-700.

147. Li W, Claypool MD, Friera AM, et al. Noninvasive imaging of in vivo MuRF1 expression during muscle atrophy. *PLoS One*. 2014;9(4):1-14. doi:10.1371/journal.pone.0094032

148. Daiber A, Steven S, Weber A, et al. Targeting vascular (endothelial) dysfunction. *Br J Pharmacol*.

2017;174(12):1591-1619. doi:10.1111/bph.13517

149. Raffaello A, Laveder P, Romualdi C, et al. Denervation in murine fast-twitch muscle: short-term physiological changes and temporal expression profiling. *Physiol Genomics*. 2006;25(1):60-74. doi:10.1152/physiolgenomics.00051.2005

150. Li J, Chan MC, Yu Y, et al. MiR-29b contributes to multiple types of muscle atrophy. *Nat Commun*. 2017;8(May):1-15. doi:10.1038/ncomms15201

151. Chan NC, Salazar AM, Pham AH, et al. Broad activation of the ubiquitin-proteasome system by Parkin is critical for mitophagy. *Hum Mol Genet*. 2011;20(9):1726-1737.

152. O'Leary MFN, Hood DA. Denervation-induced oxidative stress and autophagy signaling in muscle. *Autophagy*. 2009;5(2):230-231.

153. Cao DJ, Jiang N, Blagg A, et al. Mechanical unloading activates FoxO3 to trigger Bnip3-dependent cardiomyocyte atrophy. *J Am Heart Assoc*. 2013;2(2). doi:10.1161/JAHA.113.000016

154. West CR, Crawford MA, Poormasjedi-Meibod MS, et al. Passive hind-limb cycling improves cardiac function and reduces cardiovascular disease risk in experimental spinal cord injury. *J Physiol*. 2014;592(8):1771-1783. doi:10.1113/jphysiol.2013.268367

155. Rosenkranz S. TGF-beta1 and angiotensin networking in cardiac remodeling. *Cardiovasc Res*. 2004;63:423-432.

156. Ramsey JBG, Ramer LM, Inskip JA, Nima A, Ramer MS, Krassioukov A V. Care of Rats with Complete High-Thoracic Spinal Cord Injury. *J Neurotrauma*. 2010;27:1709-1722.

157. DeVeau KM, Harman KA, Squair JW, Krassioukov A V., Magnuson DSK, West CR. A comparison of passive hindlimb cycling and active upper-limb exercise provides new insights into systolic dysfunction after spinal cord injury. *Am J Physiol - Hear Circ Physiol*. 2017;313(5):H861-H870. doi:10.1152/ajpheart.00046.2017

158. James ND, Bartus K, Grist J, Bennett DLH, McMahon SB, Bradbury EJ. Conduction failure following spinal cord injury: Functional and anatomical changes from acute to chronic stages. *J Neurosci*. 2011;31(50):18543-18555. doi:10.1523/JNEUROSCI.4306-11.2011

159. Graham ZA, Siedlik JA, Harlow L, Tawfeek HA, Bauman WA, Cardozo CP. Key Glycolytic Metabolites In Paralyzed Skeletal Muscle Are Altered 7 Days After Spinal Cord Injury In Mice. *Med Sci Sport Exerc*. 2018;50:199. doi:10.1249/01.mss.0000535740.99319.7c

160. Yung A, Mattucci S, Bohnet B, et al. Diffusion tensor imaging shows mechanism-specific differences in injury pattern and progression in rat models of acute spinal cord injury. *Neuroimage*. 2019;186(October 2018):43-55. doi:10.1016/j.neuroimage.2018.10.067

161. Semelka RC, Tomei E, Wagner S, et al. Interstudy reproducibility of dimensional and functional measurements between cine magnetic resonance studies in the morphologically abnormal left ventricle. *Am Heart J*. 1990;119:1367-1373.

162. Bottini PB, Carr AA, Prisant LM, Flickinger FW, Allison JD, Gottdiener JS. Magnetic resonance imaging compared to echocardiography to assess left ventricular mass in the hypertensive patient. *Am J Hypertens*. 1995;8:221-228.

163. Lindsey ML, Kassiri Z, Virag JAI, Bras LE de C, Scherrer-Crosbie M. Guidelines for Measuring Cardiac Physiology in Mice. *Am J Physiol Heart Circ Physiol*. 2018;(January). doi:10.1152/ajpheart.00339.2017

164. Tator CH. Update on the Pathophysiology and Pathology of Acute Spinal Cord Injury. *Brain Pathol*. 1995;5(4):407-413. doi:10.1111/j.1750-3639.1995.tb00619.x

165. Sekhon LH, Fehlings MG. Epidemiology, demographics, and pathophysiology of acute spinal cord injury. *Spine (Phila Pa 1976)*. 2001;26(24 Suppl):S2-12. doi:10.1097/00007632-200112151-00002

166. Tosolini AP, Morris R. Spatial characterization of the motor neuron columns supplying the rat

forelimb. *Neuroscience*. 2011. doi:10.1016/j.neuroscience.2011.10.054

167. Inskip JA, Ramer LM, Ramer MS, Krassioukov A V. Autonomic assessment of animals with spinal cord injury: Tools, techniques and translation. *Spinal Cord*. 2009;47(1):2-35. doi:10.1038/sc.2008.61

168. Strack AM, Sawyer WB, Marubio LM, Loewy AD. Spinal origin of sympathetic preganglionic neurons in the rat. *Brain Res*. 1988;455(1):187-191. doi:10.1016/0006-8993(88)90132-1

169. Alexander MS, Biering-Sorensen F, Bodner D, et al. International standards to document remaining autonomic function after spinal cord injury. *Spinal Cord*. 2009;47(1):36-43. doi:10.1038/sc.2008.121

170. Sotocinal SG, Sorge RE, Zaloum A, et al. The Rat Grimace Scale: A partially automated method for quantifying pain in the laboratory rat via facial expressions. *Mol Pain*. 2011;7:1-10. doi:10.1186/1744-8069-7-55

171. Kramer JLK, Minhas NK, Jutzeler CR, Erskine ELKS, Liu LJW, Ramer MS. Neuropathic pain following traumatic spinal cord injury: Models, measurement, and mechanisms. *J Neurosci Res*. 2017;95(6):1295-1306. doi:10.1002/jnr.23881

172. Kostrominova TY. Application of WGA lectin staining for visualization of the connective tissue in skeletal muscle, bone and ligament/tendon studies. *Microsc Res Tech*. 2011;74(1):18-22.

173. Hagdorn QAJ, Bossers GPL, Koop A-MC, et al. Translational Physiology A novel method optimizing the normalization of cardiac parameters in small animal models : the importance of dimensional indexing. *Am J Physiol - Hear Circ Physiol*. 2019;316(6):H1552-H1557. doi:10.1152/ajpheart.00182.2019

174. Mohan R, Tosolini AP, Morris R. Segmental distribution of the motor neuron columns that supply the rat hindlimb: A muscle/motor neuron tract-tracing analysis targeting the motor end plates.

Neuroscience. 2015;307:98-108. doi:10.1016/j.neuroscience.2015.08.030

175. Lujan HL, Janbaih H, DiCarlo SE. Dynamic interaction between the heart and its sympathetic innervation following T5 spinal cord transection. *J Appl Physiol*. 2012;113(8):1332-1341. doi:10.1152/japplphysiol.00522.2012

176. Antonini-Canterin F, Poli S, Vriz O, Pavan D, Di Bello, Vitantonio Nicolosi GL. The Ventricular-Arterial Coupling: From Basic Pathophysiology to Clinical Application in the Echocardiography Laboratory. *J Cardiovasc Echogr*. 2013;23(4):91-95. doi:10.4103/2211-4122.127408

177. Ae YH, Kim JY, Choi EY, et al. Value of ventricular stiffness index and ventriculoarterial interaction in patients with nonischemic dilated cardiomyopathy. *Circ J*. 2009;73(9):1683-1690. doi:10.1253/circj.CJ-09-0046

178. Weisfeldt ML, Scully HE, Frederiksen J, et al. Hemodynamic dP / dt determinants of maximum negative and periods of diastole. *Am J Physiol*. 1974;227(3):613-621. doi:10.1152/ajplegacy.1974.227.3.613

179. West CR, Squair JW, McCracken L, et al. Cardiac consequences of autonomic dysreflexia in spinal cord injury. *Hypertension*. 2016;68(5):1281-1289. doi:10.1161/HYPERTENSIONAHA.116.07919

180. Xie M, Burchfield JS, Hill JA. Pathological ventricular remodeling: mechanisms: part 1 of 2. *Circulation*. 2013;128(4):388-400. doi:10.1161/CIRCULATIONAHA.113.001878.Pathological

181. Kehat I, Molkentin JD. Molecular pathways underlying cardiac remodeling during pathophysiologic stimulation. *Circulation*. 2010;122(25). doi:doi:10.1161/CIRCULATIONAHA.110.942268.

182. Unger P, Clavel MA, Lindman BR, Mathieu P, Pibarot P. Pathophysiology and management of multivalvular disease. *Nat Rev Cardiol*. 2016;13(7):429-440. doi:10.1038/nrcardio.2016.57

183. Pianca N, Di Bona A, Lazzeri E, et al. Cardiac sympathetic innervation network shapes the myocardium by locally controlling cardiomyocyte size through the cellular proteolytic machinery. *J*

Physiol. 2019;597(14):3639-3656. doi:10.1113/JP276200